Mechanistic Framework for Risk Assessment of Cast Iron Water Main Fractures due to Moisture-Induced Soil Expansion

by

Piyius Raj Singh

A thesis
presented to the University of Waterloo
in fulfillment of the
thesis requirement for the degree of
Doctor of Philosophy
in
Civil Engineering

Waterloo, Ontario, Canada, 2021

Examining Committee Membership

The following served on the Examining Committee for this thesis. The decision of the Examining Committee is by majority vote.

External Examiner:
Ian Donald Moore
Professor and Department Head,
Department of Civil Engineering,
Queen's University

Supervisor:
Sriram Narasimhan
Professor,
Department of Civil and Environmental Engineering,
University of Waterloo

Internal Member:
Dipanjan Basu
Associate Professor,
Department of Civil and Environmental Engineering,
University of Waterloo

Bryan Tolson
Professor,
Department of Civil and Environmental Engineering,
University of Waterloo

Internal-External Member:
Michael Worswick
Professor,
Department of Mechanical and Mechatronics Engineering,
University of Waterloo

Author's Declaration

I hereby declare that I am the sole author of this thesis. This is a true copy of the thesis, including any required final revisions, as accepted by my examiners.

I understand that my thesis may be made electronically available to the public.

Abstract

North American water distribution networks are at significant risk of failure due to aging cast iron pipes. For instance, of the 650,000 kilometers of cast-iron pipes in active service in the United States and Canada, more than 80% are beyond their intended service life. These aging and deteriorated pipes are failing at an alarming rate (22 breaks per 100 km per year), resulting in significant disruption to drinking and emergency water supply. The capital investment gap to replace this inventory is too large and will likely take several decades to bridge at the current replacement rate of the order of 0.8% per year. Meanwhile, infrastructure managers rely on managing this gap through simplistic replacement prioritization, e.g., the oldest pipes are the most at risk. Such age-based prioritization schemes disregard multiple risk drivers that contribute to pipe failure. Risk-based decision support frameworks that go beyond simple prioritization schemes by considering multiple risk drivers are necessary to identify and prioritize the most at-risk segments of the network, thereby leading to the better management of the aforementioned gap. Previous studies showed that localized corrosion flaws, also known as pitting corrosion, on the external surface are primarily responsible for damage in pipes, and the strength of these deteriorated pipes to withstand loadings constitutes their stress capacity. On the other hand, the stresses caused by different loads on the pipe comprise stress demand. Field failure data indicate that the plausible failure mechanism is flexure which causes "full-circle breaks." In the Central and Northern California region, where expansive soils are prevalent, a majority of these beaks (~ 60%) occurred during the months of high rainfall. This suggests that the plausible loading mechanism is moisture-induced differential soil expansion/contraction.

Despite that, studies focused on flexural failures driven by differential soil expansion and the overall reliability of pipes situated in environments where potential for moisture-induced differential soil expansion/contraction exists have not been studied well. In this thesis, a probabilistic framework is developed for the assessment of pipe-soil systems vulnerable to fracture caused by a combination of pitting corrosion and moisture-induced soil expansion. The main objectives of this thesis are twofold. First, a physics-based approach is employed to develop an analytical soil-pipe interaction model that can predict full-circle breaks given a range of parameters,

such as pipe configuration, soil conditions, and triggering factors (soil expansion). The model is based on classical solutions for beams on elastic foundations that are enriched to reflect material nonlinearities in the soil medium. The model development and comparision are supported by a suite of continuum finite-element simulations that simulate detailed interactions between the pipe and soil. The proposed analytical model demonstrated that it is able to reproduce flexural stresses in a range of pipe configurations with good accuracy and in a fraction of the computational time compared to detailed finite-element models. Next, a risk-based assessment methodology is developed which builds upon this pipe-soil interaction model along with corrosion equations estimating pitting damage in the pipe wall. The sources of uncertainty (uncertainties in various input parameters and the model itself) in all the components are rigorously analyzed and characterized. Subsequently, stochastic simulations employing Monte Carlo procedure is implemented to synthesize various uncertainties into a probabilistic estimate of the failure of a pipe segment, defined by its configurational parameters and age. The prospective use of this is outlined in the context of decision-support frameworks to prioritize replacement.

In summary, this thesis presents a physics-based approach to help identify the most at-risk cast iron main pipes given a combination of configurational, locational, and seasonal factors. The outcome of the research is (1) a computationally inexpensive pipe-soil interaction model for pipes experiencing moisture-induced differential soil expansion loading and (2) a vulnerability assessment framework for a pipe segment given its various characteristics and environmental/loading factors. This approach may be conveniently used by utility operators within a decision support framework for asset management and the prioritization of replacement.

Acknowledgements

I would like to take this opportunity to express my sincere gratitude to all those who have provided me with guidance and support in various ways through my journey as a Doctoral student.

First and foremost, I would like to express my deepest gratitude to my advisor, Professor Sriram Narasimhan for giving me the chance to pursue doctoral studies at the University of Waterloo. I will always appreciate the valuable and inspiring discussions and his excellent support during the research and preparation of this thesis. I am grateful for his steadfast optimism and personal encouragement in addition to his considerable multi-disciplinary technical expertise.

I would like to thank my co-advisor Professor Amit Kanvinde from the University California, Davis. This thesis would not have been possible without his guidance. His consistently constructive and insightful suggestions have encouraged me to overcome many difficulties I faced during this research work. Most importantly, he helped me understand how to approach research and I greatly appreciate his invaluable guidance throughout my thesis work.

I am grateful to my committee members Professors Ian Moore, Bryan Tolson, Dipanjan Basu, and Michael Worswick for agreeing to serve on my thesis committee.

I am fortunate to have a circle of friends whose support and encouragement I cherished through the UW life. I thank Rakesh, Harish, Indranil, and Wanis for sharing long discussions, lunches, and course works. I am grateful to Pampa for influencing me with her undaunted optimism and being a warm and caring friend; Marshal for his simplicity and friendship; Jinane for her deep observations on life and data science; Rajdeep for savvy and helpful suggestions, both on professional and personal issues. And in the end, I am grateful to all those who helped me finish this journey knowingly and unknowingly.

Last but not the least, I would like to thank my parents for their unconditional love from across the world. They have always trusted and encouraged me in my endeavors. Thank you to my wife, Shilpi, for her love, understanding, and encouragement, and my son, Priyansh, for having sacrificed his affectionate attention during my studies.

Dedication

To my son, Priyansh.

Table of Contents

List of Figures

List of Tables

List of Publications

The following is a list of journal publications and conference papers resulting from the work contained in this thesis:

Publications

1. **Singh, P. R.**, Pericoli V., Kanvinde, A., and Narasimhan, S. (2020). "Framework for analyzing cast iron water main fractures due to moisture-induced soil expansion." *Journal of Pipeline Systems Engineering and Practice*, ASCE, DOI: 10.1061/(ASCE)PS.1949-530 1204.0000460.
2. **Singh, P. R.**, Kanvinde, A., and Narasimhan, S. Forthcoming. "Assessing the fracture risk of corroded cast iron pipes in expansive soils." *Journal of Pipeline Systems Engineering and Practice*, ASCE, *in press*.

Conference Proceedings

1. **Singh, P. R.**, Kanvinde, A., and Narasimhan, S. (2020). "Mechanistic framework for analyzing cast iron water main fractures." In Proc., *1st International WDSA / CCWI 2018 Joint Conference*, Kingston, Ontario, Canada – July 23-25, 2018

Chapter 1
Introduction

North America's water infrastructure is in decline, and the signs of distress surface recurrently as water mains break, causing water loss and service disruptions (e.g., Figure 1.1). For transmission and distribution of water, water industries rely on underground pipe networks, which still consist of large proportions of decades-old cast iron pipes. Currently, cast iron water mains constitute approximately 28% (by length) of the water distribution network across the United States and Canada [1]—this corresponds to roughly 600,000 km of pipe length. A majority of these cast-iron mains (>80%) were installed around the 1940s [2], and many are severely deteriorated due to corrosion. The life expectancy data estimated by American Water Works Association [3] suggest that these pipes are beyond their intended service life. For example, the expected life of pipes laid around the 1920s and 1940s are about 100 years and 75 years, respectively [3]—note that the older pipes are expected to last longer because of the overuse of the material. This data suggest that a large majority of these pipes are highly vulnerable to loss-of-service events, such as fracture, in the coming decades.

A comprehensive study by Folkman [1] on water main breaks in the USA and Canada shows that the failure rate is highest in cast-iron pipes. These pipes are failing at an alarming rate (20.8 breaks per 100 km per year in the USA and 30.2 breaks per 100 km per year in Canada), resulting in significant disruption to drinking and emergency water supply. Furthermore, comparing this 2018 survey to the 2012 survey [4], the break rate in cast-iron pipes has increased by over 40%, thus increasing the cost of repair while simultaneously being associated with decreasing water

quality and increasing water loss. Each year, the USA spends around $4.5 billion to operate and maintain water transmission and distribution systems [5]. Meanwhile, a survey conducted by Rajani and McDonald [6] reported that the average annual cost of water main repairs in Canada is more than $80 billion. Apart from the repair cost, water main breaks also incur indirect costs, such as non-revenue water, street flooding, loss of business, damage to public and private properties, and considerable risk of contamination to drinking water.

Figure 1.1: Water main failures[1].

[1] Sources:
https://www.cbc.ca/news/canada/kitchener-waterloo/kitchener-water-main-break-photos-1.5110533
https://www.cbc.ca/news/canada/kitchener-waterloo/waterloo-region-water-main-breaks-potholes-warm-winter-1.5422313
https://www.therecord.com/news/waterloo-region/2015/11/06/water-main-break-floods-ion-construction-site.html
https://www.liherald.com/stories/water-main-break-in-lynbrook-causes-several-issues,111828
https://www.cfpua.org/DocumentCenter/View/941/Kids-Page---Water-Main-Breaks?bidId=

The most direct approach to alleviate this problem is to replace all the worn-out cast-iron pipes from the system. The solution sounds simple enough, but far from being practical. Construction and maintenance of water distribution systems can be a significant burden on the nation's economy, especially pipe networks that can account for 80% of the total expenditure [7]. According to the AWWA report [8] on the water pipe networks in the USA, replacing all existing cast-iron pipes at once will require an estimated $2.1 trillion. Besides, due to lack of proper planning and budgetary constraints, the current replacement rate for water mains is fairly low (~0.8% per year), and at this rate, replacing the entire network would require ~125 years.

Given the condition of pipe networks and capital constraints, it is critical to identify and prioritize the most at-risk pipe segments for replacement because replacing the entire network at once is infeasible. Many cities have embarked on major infrastructure revitalization projects with a focus on cast iron pipe replacement [9]. However, currently, operators utilize a simple prioritization approach; simply replacing pipes in the order they were installed [10] by assuming that the oldest pipes are the most at risk. Field failures of pipes may not necessarily follow this pattern, e.g., as noted by Pericoli et al. [11] in the City of Sacramento, suggesting that factors other than age contribute to the failure process. Such factors include pipe location, soil type, and pipe diameter/thickness, as well as seasonal variations in temperature, precipitation, and soil saturation. Consequently, approaches that consider such factors are required to effectively identify and prioritize the most vulnerable pipe segments for replacement.

Failures of deteriorated water pipes attributed to soil conditions and climate patterns are not well understood. Specifically, as noted by Gould et al. [12], the effect of expansive soils on the failures of underground cast iron pipes has received limited attention in research. Pericoli et al. [11] studied the field failure data of cast iron pipes in the City of Sacramento and observed that a majority (~ 60%) of the "full-circle breaks" (fracture transverse to the pipe axis) coincided with periods of high rainfall. This observation combined with the prevalence of expansive soils in the Sacramento area points towards moisture-induced differential soil expansion/contraction as a key risk driver for such failures. This type of failure is not only limited to the Sacramento area but are

https://bloximages.chicago2.vip.townnews.com/napavalleyregister.com/content/tncms/assets/v3/editorial/8/58/858be80f-2865-5fdc-bcc3-0630d5f33539/4dcac49b16d9e.image.jpg
https://live.staticflickr.com/4620/40540970652_628ccc67ec_b.jpg

prevalent across North America and other locations where expansive soils are prevalent (various locations in the USA– [13]; the Midlands region, England– [14]; Dallas County, Texas– [15]; City of Regina, Saskatchewan– [16]). Despite the prevalence of expansive soils in large parts of North America, studies focused on flexural failures due to differential soil expansion have not received the attention they deserve.

1.1 Research Objectives

The overarching goal of this thesis is to develop a risk-based[2] assessment methodology for pipe-soil system vulnerable to pitting corrosion and moisture-induced soil expansion. The developed framework will rank various regions of a pipe network based on the risk factors or stressors. Along these lines, the proposed research objectives are summarized as follows:

- To develop a physics-based analytical model that will quantify flexural stresses in pipes subjected to moisture-induced soil expansion.
- To develop a probabilistic framework for risk assessment of cast-iron pipes by -soil systems vulnerable to fracture caused by a combination of pitting corrosion and moisture-induced soil expansion.

1.2 Organization of the Thesis

The thesis contains 6 chapters and is organized as follows:

- **Chapter 1** provides a brief introduction and motivation for identifying the most at-risk cast iron pipes given a combination of configurational, locational, and seasonal factors and presents the overarching research goal.
- **Chapter 2** provides background of different mode of water pipe failures and loading conditions. Following this, moisture-induced soil loading is discussed which includes

[2] Note that, in this thesis, the terms "risk" and "reliability" are analogous to the probability of failure and the probability of survival, respectively. In this study, both these terms are used interchangeably to represent the probability of occurrence of an event. The formal definition of "risk", as given in BS 4778 (BS 1991), combines the probability of occurrence and consequence of the occurrence of an event. The consequence of pipe failures is briefly discussed in the appendix with an example.

theory of soil expansion and a review of existing pipe-soil interaction models. Next, a brief review of the literature on risk assessment of deteriorated cast-iron pipes is presented. Finally, research gap areas are identified, and specific research objectives are outlined.

- **Chapter 3** presents a three-dimensional continuum finite element study to investigate the cast-iron pipe response to moisture-induced differential soil expansion. Subsequently, the impact of varying problem geometry and material characteristics on pipe deflection and stresses is assessed.

- **Chapter 4** presents an analytical model to predict pipe flexure stresses due to moisture-induced soil expansion, given a range of parameters that describe pipe configuration and soil conditions. Moreover, a validation of this analytical model against finite element predictions is presented.

- **Chapter 5** presents a probabilistic framework for the assessment of pipe-soil systems vulnerable to fracture caused by a combination of pitting corrosion and moisture-induced soil expansion. The prospective application in decision model aimed at identifying optimum pipe replacement is presented.

- Finally, several conclusions resulting from the presented work are discussed in **Chapter 6**. Several recommendations for future study are also discussed, followed by a summary of the significant contributions of the current work.

Chapter 2
Background

In line with the research objectives proposed in the previous section, this chapter provides the background of the study. The overall reliability assessment process can be considered as a four-step procedure: (1) characterization of pipe failure mechanism which involves identification of key loading conditions experienced by a typical pipe located within the water distribution network, (2) characterization of pipe damage mechanism resulting in capacity estimation of the pipe, (3) formulation of a risk assessment model by combining the results from (1) and (2) which yields the probability of pipe failure, and (4) recommendation for a pipe replacement strategy by extending the results of the pipe segment to the pipe network.

Accordingly, this chapter starts with a discussion of different types of failures in cast iron pipes and loading conditions that are common in pipe networks. The loading due to moisture-induced soil expansion, which is regarded as the plausible failure mechanism responsible for the majority of pipe fractures in North American pipe networks (where expansive soils are prevalent), is then discussed thoroughly. This discussion includes the theory of soil expansion and a review of analogous pipe-soil interaction models developed in other fields, such as pipe crossing faults and tunneling effect on buried pipes. Next, a section is devoted to reviewing studies of modeling cast iron corrosion damage in a soil environment. Next, a brief review of the literature on risk assessment of deteriorated cast-iron pipes is presented. Finally, key research gaps are identified, and specific research goals are outlined.

2.1 Cast-iron Material

Cast iron (particularly gray cast iron) is a legacy material in water pipes throughout the world. According to Cast Iron Pipe Research Association [17], cast-iron pipes were first installed in Europe as early as the 1600s; however, it was the dominant water pipe material from the mid-1800s to the 1950s. While some contemporary cast-iron (i.e., ductile iron) continues to be installed today, in the USA, the oldest cast-iron pipes still in use were installed in the 1880s [2].

Since it was first introduced, cast iron pipe manufacturing techniques have changed significantly. Two primary types of casting methods, pit cast and spun cast, were used to produce cast iron pipes [17]. Pit casting typically involved the use of upright sand molds assembled in pits. Spun casting used horizontal, spinning molds, which were made of sand or metal. The metal molds were water cooled, which promoted more rapid cooling of the pipes. The different casting methods produced profound differences in the metallurgy of the pipe material which affected the mechanical properties [18]. The mechanical properties of exhumed gray cast iron pipes were investigated by Makar and McDonald [19]; Figure 2.1 shows a typical stress-strain curve in tension for pit cast and spun cast iron pipes. Referring to this figure, it is evident that the mechanical behavior of spun cast iron pipes is different from pit cast iron pipes and that pit cast iron pipes exhibit lower elastic modulus and ultimate strengths in tension.

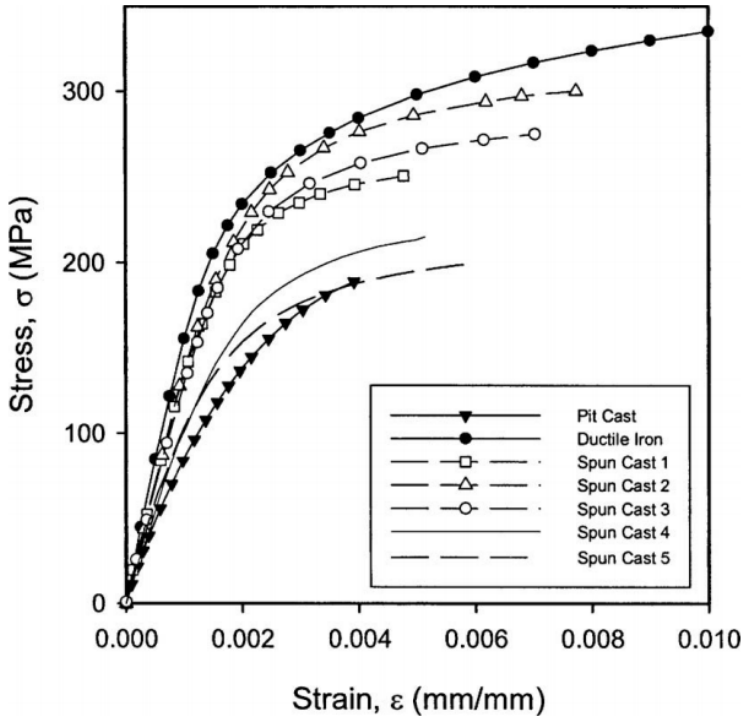

Figure 2.1: Typical tensile stress-strain curves for pit cast, spun cast (different samples) and ductile iron [19].

2.1.1 Cast-iron Pipe Failure Modes

The lifecycle of a typical buried pipe can be described by the "bathtub curve" [20], as shown in Figure 2.2. This consists of three phases: a burn-in phase, an in-usage phase, and a wear-out phase. The burn-in phase describes a period right after installation where breaks occur mainly due to faulty installation or major material defects. Breaks decline over time and enter the in-use phase, where it attains minima and a steady state. However, failure due to unexpected conditions could occur, but they are generally unexpected. The third and the most troublesome phase is the wear-out phase, which is characterized by a higher frequency of failures due to factors related to pipe ageing. Currently, about 28% of all existing water pipes in North American pipe networks which are made out of cast iron are in the wear-out phase [1]. According to AWWA [8], the pipes manufactured at different times in history have different life expectancies due to changing materials and manufacturing techniques. For example, the oldest cast iron pipes dating back to the

late 1800s have an average life expectancy of about 120 years. The pipes laid around the 1920s have an average life expectancy of about 100 years. The more recent piped, laid around 1940s, have the least life expectancy of around 75 years. This information indicates that cast iron pipes have reached their life expectancy in the majority of installations.

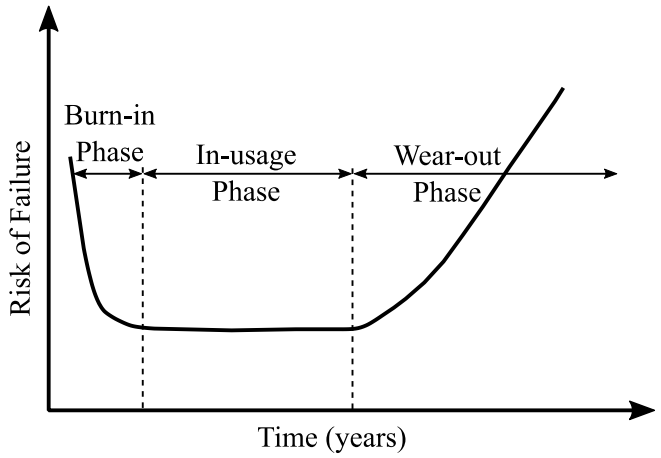

Figure 2.2: Life cycle of a buried pipe [20].

Pipe failures occur due to accumulated damage followed by an associated loading event. In cast-iron pipes, the different modes of pipe fractures, classified by Clark et al. [21], include: (a) longitudinal cracks, (b) circumferential cracks, (c) split bell, and (d) corrosion holes. Examples of failed pipes exhibiting these modes clearly are shown in Figure 2.3.

Figure 2.3: Different modes of failure (a) longitudinal failure (b) circumferential failure (c) split bell (d) corrosion holes (from pipe fracture data, The City of Sacramento).

Excessive circumferential stress probably due to internal water pressure causes longitudinal cracks that are confined to large diameter pipes [22]. On the other hand, circumferential cracks are the most common failure mode in small diameter pipes and are responsible for more than 60% of the failures [6]. Typically, this type of failure occurs due to high longitudinal stresses caused by axial tension and bending which is the result of temperature change, ground movement, soil settlement, traffic load, etc. [23]. Bell splitting is mainly caused by the differential expansion due to the temperature change of filler material (leadite seal) used in the bell and spigot joint [22]. Corrosion holes occur due to the combined effect of pitting corrosion and water pressure inside the pipe, where pitting thins the pipe wall to the point where the water pressure blows out the remaining thickness.

Pericoli et al. [11] studied the field failure data of cast iron pipes in the City of Sacramento and observed that a majority (~ 60%) of failures are circumferential (full-circle breaks transverse to the pipe axis) and they occurred during the months of high rainfall (see Figure 2.4). Furthermore, a moderate increase in failures can be seen in the extreme dry month, which might be associated

with human-induced moisture change in the soil (such as irrigation and watering lawns). This observation combined with the prevalence of expansive soils in the Sacramento area points towards moisture-induced differential soil expansion/contraction as a potential risk driver to explain such failures. This type of failure is not only limited to the Sacramento area but are predominant across North America and other locations where expansive soils are prevalent (various locations in the USA— [13]; the Midlands region, England— [14]; Dallas County, Texas— [15]; City of Regina, Saskatchewan— [16]). Despite such prevalence of expansive soils in large parts of North America, studies focused on flexural failures driven by differential soil expansion and reliability of such systems have not received the attention they deserve. This provided the motivation of this thesis to investigate the flexure failures in cast-iron water pipes caused by soil expansion, which has largely been overlooked in the literature. Expansion in soils can result from two different mechanisms: frost induced expansion (frost heave) and moisture-induced expansion (reactive soils). In this thesis, the investigation is limited to moisture-induced soil expansion; however, the pipe-soil interaction model developed in this thesis can be easily modified to capture the pipe response in frost-induced soil expansion and included in the reliability assessment framework.

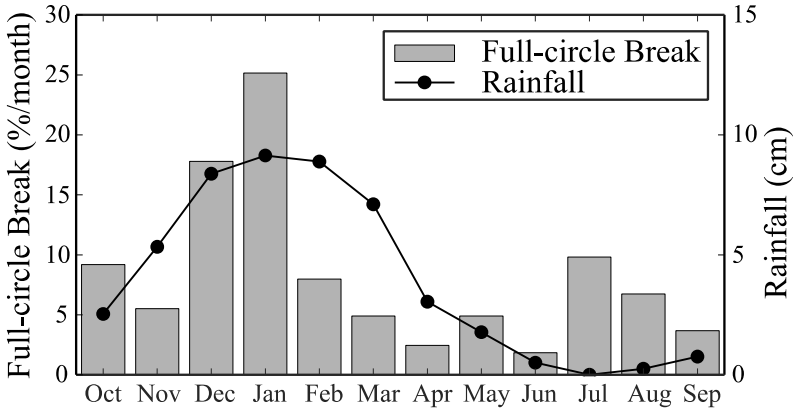

Figure 2.4: Precipitation data and full-circle breaks in the City of Sacramento from 2000 to 2011.

2.1.2 Cast-iron Pipe Failure Criteria

Cast-iron water mains are continuously subjected to deterioration caused by corrosion that undermines their resistance to internal and external loads. Consequently, failure is defined when existing stresses on structurally deteriorated pipes exceed their structural capacity (stress capacity). The structural capacity of a deteriorating pipe diminishes as corrosion pits initiate randomly and subsequently grow over time. Cast iron is a brittle material and typically fails through facture rather than through yielding. Two specific failure criteria are applicable to cast iron, namely, in-plane and bi-axial distortion energy [24]. Based on his experimental work, Mair [25] concluded that the failure criterion in cast iron is best represented by the distortion energy theory given by von Mises. This theory states that failure by fracture occurs when the distortion energy per unit volume at any point in the body becomes equal to that associated with the fracture in a simple tension test [26]. The biaxial failure criterion based on distortion energy theory is given as

$$\sigma_1^2 - \sigma_1\sigma_2 + \sigma_2^2 = \sigma_u^2 \tag{2.1}$$

where σ_1 and σ_2 are biaxial stresses, and σ_u is the ultimate tensile strength.

2.2 Failure Mechanism Associated with Moisture-induced Soil Expansion

2.2.1 Theory of Soil Expansion

Expansive soils (also known as swelling or reactive soils) absorb moisture from available sources (such as rainfall, watering, irrigation, or leakage from water supply pipes or drain) and produce heave. Conversely, they can also contract when dry, resulting in shrinking and cracking of the ground. This heaving-and-shrinking is known as "shrink-swell" behavior [27] . Expansive soils exhibit expansion/contractions primarily due to a high percentage of fine-grained clay particles. Briefly, these clay particles consist of minerals (montmorillonite, elite, and kaolinite) containing sheets of silica tetrahedrons trapping octahedral aluminum hydroxide and other ions (for detailed configuration see [28, 29]). Due to the excess negative charge on these minerals, they absorb water and expand. Similarly, due to evaporation, they lose water and contract.

The severity of the expansive soil is controlled by the amount of moisture variation that the soil experiences. Even though the soil is highly reactive (expansive), no effect would be observed, if the soil moisture is constant throughout the year. On the other hand, areas where the expansive soil experiences consistent moisture fluctuation can be severely affected. The other factor that greatly influences the degree of expansion is the depth of active zone. According to Nelson et al. [30], the depth of active zone may be defined as the depth of soil that experiences moisture fluctuation (see Figure 2.5) and participate in soil expansion. Due to its dependency on various factors such as depth of water table, soil type, vegetation, temperature, and the lack of field measurements, a common practice in the literature is to assume this variable to be between 2 to 3 m [31]. However, discontinuities in the soils (such as the bedding plane, cracks, and fissures) and the presence of tree roots have a significant influence on its values [32]. The depth of active zone has particular importance because the total heave can be estimated by integrating the displacement produced over this depth [27, 33].

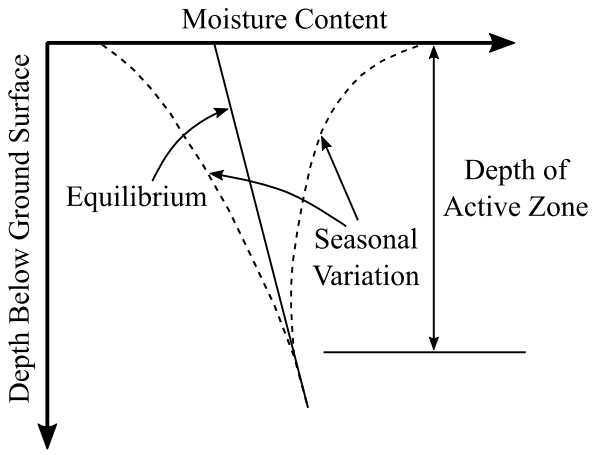

Figure 2.5: Typical water content profile along soil depth.

2.2.2 Heave Prediction Methods

Differential movement of the expansive soil in which a pipe is buried can result in significant pipe deformations due to pipe curvature and bending forces. The pipe deformation and the corresponding stresses/strains depends on the magnitude of soil volume changes (more importantly vertical heaving), which can also be taken as the upper bound of the pipe displacement

[34]. Significant advances have been made in the literature towards the prediction of heave and shrink related volume change behavior of expansive soils. Heave prediction methods were first introduced when researchers were interested in estimating volume change due to settlement in saturated soils [35]. There are several procedures available in geotechnical engineering to estimate the 1-D heave in expansive soils. These procedures can be divided broadly into three main categories: empirical methods, oedometer test methods, and soil suction methods.

The soil classification and Atterberg limits are the basis of empirical methods. Many empirical methods have been suggested to correlate the swelling potential to the soil properties. Table 2.1 presents several proposed relationships between soil classification characteristics and swelling potential. These relationships provide an estimate of 1-D heave, and they were developed through laboratory experiments and field data.

Table 2.1: Summary of empirical methods proposed in literature.

Empirical methods	Reference
$SP = 0.00216 I_P^{2.44}$	Seed et al. [36]
$SP = 0.000413 I_S^{2.67}$	Ranganathan & Satyanarayana [37]
$SP = 1/12\,(0.4LL - w_i + 5.55)$	Vijayvergiva & Ghazzaly [38]
$\log SP = 0.9(I_P/w_i) - 1.19$	Schneider & Poor [39]
$SP = 0.2558 e^{0.08381 I_P}$	Chen [40]
$\Delta H = (SP\%)H$	Dhowian [41]

Where SP is swelling potential, I_P is plasticity index, I_S is shrinkage index, LL is liquid limit, w_i is initial water content, ΔH is total heave and H is soil thickness. Note that these equations are specific to the study test sites.

Oedometer tests are widely used and more common as compared to other methods. The swelling pressure determined from oedometer test methods is one of the key parameters used in the determination of the 1-D heave. The 1-D oedometer tests comprise of loading and unloading sequence on a soil sample to determine the swelling pressure. The index parameters (i.e., swelling index, heave index) can be determined from the Oedometer test, and heave can be calculated with the help of these parameters.

Table 2.2: Heave calculation from Oedometer test methods.

Oedometer test method	**Reference**
$\Delta H = C_s \frac{H}{1+e_0} \log\left\{\frac{P_f}{P'_s}\right\}$	Fredlund [42]
$\Delta H = C_s \frac{H}{1+e_0} \log\left\{\frac{P_s}{P_0}\right\}$	Dhowian [41]
$\Delta H = C_\rho \frac{H}{1+e_0} \log\left\{\frac{\sigma'_f}{\sigma'_{cv}}\right\}$	Nelson & Miller [43]
Where, C_s is swelling index, C_ρ is heave index, e_0 is initial void ration, P_f is final stress state, P'_s corrected swelling pressure, P_s swelling pressure, P_0 is effective overburden pressure, σ'_f is vertical stress at the midpoint of the soil layers and σ'_{cv} is swell pressure from constant volume swell test.	

The soil suction method is more advanced compared to the other two methods in calculating the 1-D heave in expansive soils. It uses the stress state and suction pressure to calculate heave. There are several heave prediction formulations based on soil suction methods available in the literature. The method given by Hamberg & Nelson [44] is widely used because of its simplicity. This method uses the relationship between water content and volume change (between shrinkage limit to liquid limit) which is determined from the COLE (coefficient of linear extensibility) test. The COLE test was developed to calculate the heave of airfield pavements [43]. In this test, the initial moisture content of a resin-coated soil sample is determined by measuring its volume at 33 kPa suction pressure (soil water content at a 33 kPa suction correlate closely with field capacity). To determine the final moisture condition, the oven-dried sample is weighted, and volume measured. A COLE value for the sample is defined as the normal strain that occurs from the moist to the dry condition as shown in Eq.(2.2). COLE values for various locations are outlined in the USDA maps [45]. The COLE represents the free swell capacity of the soil, providing a convenient way to quantify its swell-shrink response [46].

$$COLE = \frac{L_M - L_D}{L_D} = \frac{L_M}{L} - 1 = \left[\frac{\gamma_{dM}}{\gamma_{dD}}\right]^{0.33} - 1 \qquad (2.2)$$

where L_M is the length of moist sample at 33 kPa suction, L_D is the length of oven dried sample, γ_{dM} is the dry density of moist sample at 33 kPa suction and γ_{dD} is the dry density of oven dried sample.

2.3 Pipe-Soil Interaction in an Expansive Soil

A typical situation is shown in Figure 2.6 where a pipe is passes through an expansive soil experiencing moisture fluctuations. In the rainy season, the part of the soil that receives moisture expands and forces the pipe to move upwards. Similarly, in the dry season, the soil shrinks and forces the pipe to move downwards. This up and down movement causes significant bending in the pipe and could lead to circumferential fracture. An early experimental study by Kassiff and Zeitlin [47] showed that the failure in buried pipes is correlated with soil expansion. This study concluded that swelling in expansive soil can damage pipes by introducing cracks in circumferential directions. Another study [48] showed an increased failure rate of pipes in hot and dry seasons (after rainy seasons) and periods of relatively low annual rainfall. Furthermore, Chan [49] and Gould [50] showed that considerably higher percentages of failures occur in reactive soil zones. The number of failures varies with the seasonal climate changes in a consistent pattern.

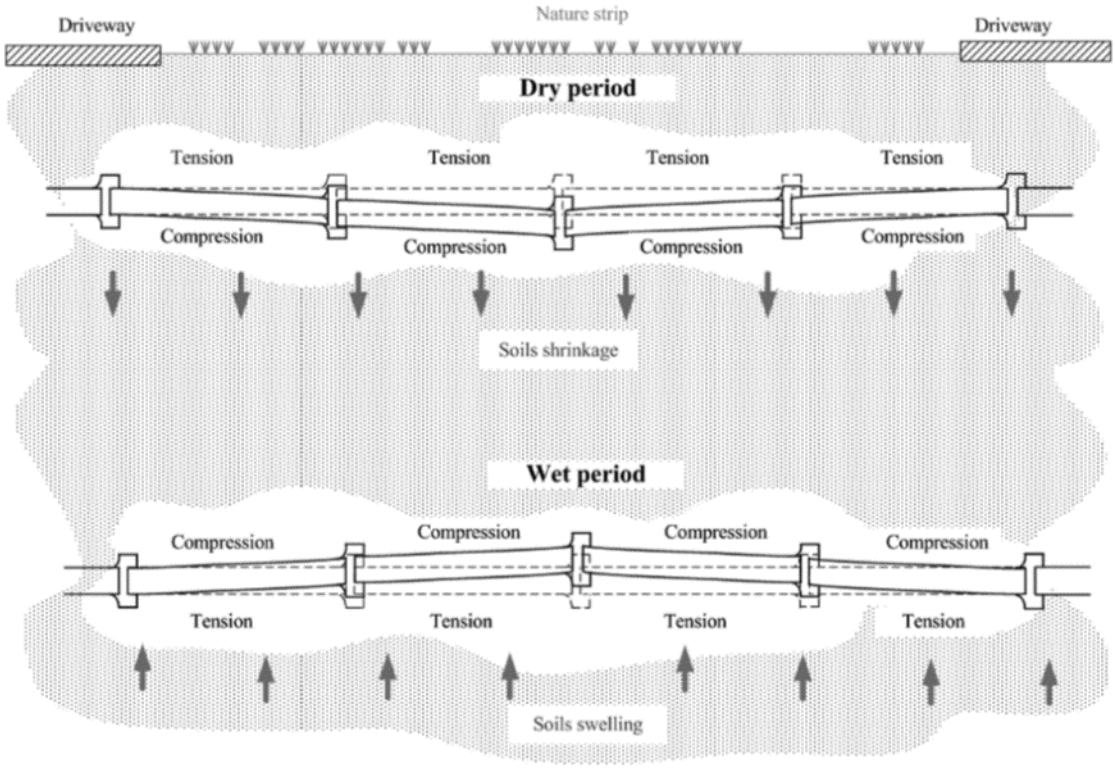

Figure 2.6: Pipe movement due to soil expansion and contraction, Chan at el. [51].

A significant number of circumferential failures and their correlation with moisture change in the soil have led researchers to conclude that the effect of soil expansion is a major reason for pipe failures in the areas where expansive soils are prevalent. The differential movement in the soil causes significant flexural stresses in buried pipes, and when the stresses exceed the strength, failure occurs. Despite this, surprisingly, flexural failures driven by differential soil expansion and reliability of pipes have not received much attention in the literature. The next section is dedicated to exploring the relevant literature in the area of pipe-soil interaction modeling techniques. The discussion is limited to numerical simulations and analytical modeling approaches since there is a lack of experimental studies.

2.3.1 Numerical Simulation of Pipes Buried in Expansive Soil

Literature is very limited for pipes buried in expansive soil subjected to moisture variations. Much of the previous work has been focused on foundations and pavements built on expansive soils.

An earlier work of Sorochan and Kim [52] showed that, due to the differential expansion of expansive soils, objects buried in it can crack. This work did not directly involve pipes; however, provided an understanding of load transfer on buried structures due to soil expansion. Few attempts have since been made to numerically simulate the behavior of pipes in expansive soils. For example, Gould [50] numerically simulated a 20 m long pipe segment buried in an expansive soil using the OpenSEES software package [53]. The soil was simulated using the Winkler foundation approach with two-dimensional linear springs. The elastic properties of the spring were derived from soil shear strength parameters and pipe geometric properties. The pipe-soil interaction was modeled using a beam-on-springs approach. The soil deformation results of this study closely followed the field observations; however, the pipe stresses were overestimated. It is likely that the approximations, such as non-slip boundary condition and soil as linear springs, caused the overestimation of the results.

In another study, Rajeev and Kodikara [54] used FLAC^{3D}, a three-dimensional finite-difference software [55], to model a pipe segment buried in expansive soil. The soil expansive behavior was modeled using a linear relationship between the soil volumetric shrinkage and the water content change, while the mechanical behavior of the soil was modeled using the Mohr-Coulomb failure criterion. Interaction between the pipe and soil was modeled using tied constraints. The study provided reasonable stress and deformation results; however, stated that the results can be improved by introducing slip boundary condition between pipe and soil and finite element analysis.

In a relatively recent work, Weerasinghe et al. [56] numerically simulated the swelling/shrinkage behavior of unsaturated soil and their effect on buried pipes. Major emphasis was given to accurately model the soil expansion rather than to the load transfer (pipe-soil interaction). The soil was modeled as an elastic porous medium with moisture swelling properties. The deformation results were in good agreement with the results of Gould [50]; however, stresses were overestimated. The authors concluded that the inclusion of soil plasticity and experimentally-identified pipe-soil interaction properties can potentially to improve the results.

As discussed above, several assumptions are adopted in the aforementioned studies, even though their effect on the computed pipe stresses are significant. Elasto-plastic behavior of soil

with nonlinear pipe-soil interface is not introduced in the simulations, which may be unavoidable in large ground surface deformations. Another key observation is that these studies emphasize simulating the soil deformation accurately, rather than defining the load transfer mechanism from the soil to the pipe.

2.3.2 Analytical Modeling of Pipes Buried in Expansive Soil

The numerical simulations discussed above may be able to directly simulate the mechanical phenomena (soil expansion and elastoplastic multiaxial soil response, including the effects of confinement and contact/gapping between the soil and pipe) that are relevant to the pipe-soil interaction problem. However, these studies are computationally expensive and challenging to extend to the network level. A simplified analytical model to estimate the pipe responses, such as estimating the deflections, bending moments, and longitudinal stresses, is crucial to assess the reliability at a system level. However, such formulation is not available in order to compute stresses in pipes buried in expansive soils. Several studies exist on the topic of response of buried pipes to extreme loads, e.g., O'Rourke and Trautmann [57]; O'Rourke et al. [58]; Karamitros et al. [59]; O'Rourke et al. [60]; Wang et al. [61]; Vorster et al [62]. Some of these conditions (e.g., the flexural failure of pipes crossing tectonic faults due to fault slip and tunneling effect on buried pipes) can be extended to the problem at hand from a mechanistic standpoint and the analytical formulation under such situations is discussed next.

Tunneling-induced Ground Movements

Figure 2.7 shows a schematic of the pipe deformation caused by tunneling-induced ground movements. In this scenario, due to the excavation of a tunnel under an existing pipe, the soil settles around the pipe causing it to deform. The magnitude of pipe deformation and the corresponding stresses depend on the soil settlement profile at the pipe level and the relative stiffness between the pipe and the surrounding soil. It has been shown that the maximum bending moment occurs above the tunnel centerline which is generally referred to as the sagging moment [61]. Substantial work has been performed to evaluate the pipe response in the tunneling-induced soil deformation [63, 62, 64, 65].

The solution methodology to evaluate the effects of tunneling-induced ground movements on underground pipes requires: (1) characterization of the soil settlement profile and (2) definition for the pipe-soil interaction associated with tunneling-induced soil profile. Following this, several methods have been developed to evaluate the buried pipe response, such as soil-spring based methods [63, 66] and continuum methods [64, 62]. Although these methods are different in many aspects, they share one common assumption, that is, the equation of soil profile due to the tunneling is known, and it does not depend on soil properties. A Gaussian approximation is commonly used to describe the shape of the settlement profile. However, in the case of moisture-induced soil expansion, the ground heave profile is normally not known a priori, and depends on the physicochemical properties of the soil.

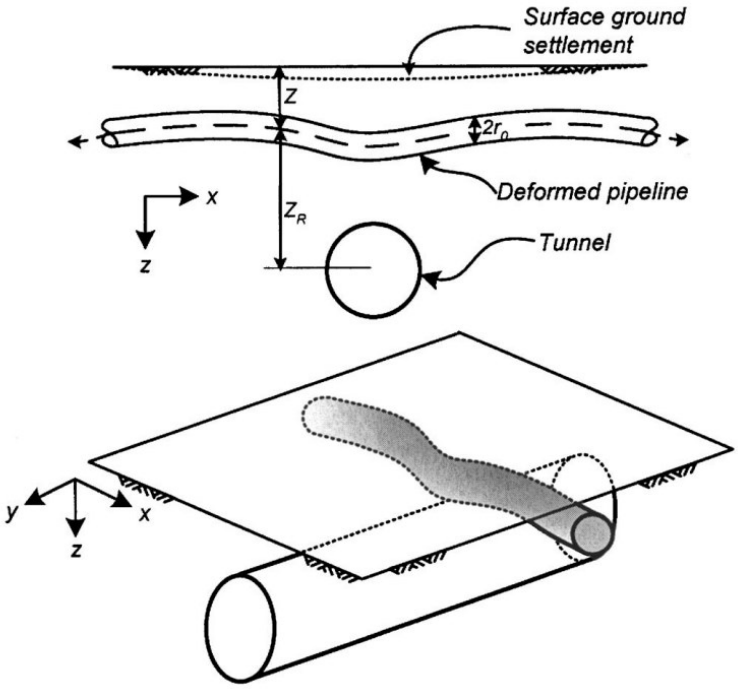

Figure 2.7: Schematic of pipe deformation caused by tunneling-induced ground movements [61].

Flexural Failure of Pipes Crossing Normal Fault

Although less frequent, permanent ground motion poses significant risk to pipes which cross fault planes, as they could impose large axial and flexural strains which lead to failure due to tension or

bending [67]. The earliest methodology for pipe design at fault crossings (strike-slip fault) is proposed by Newmark and Hall [68] which was later improved by Kennedy et al. [69]. An extension of this work that applies to a normal fault (normal to the pipe length) was proposed by Karamitros et al. [70]. Note that the mechanism of pipe-soil interaction in normal fault movement and soil expansion is somewhat similar as shown in Figure 2.8 which shows the 2-D idealization of pipe-soil interaction used by Karamitros et al. [70]. The proposed methodology computed axial and bending stresses along the pipe using the beam-on-elastic-foundation and elastic-beam theories. The pipe-soil interaction in both the axial and the transverse directions were defined using nonlinear springs. The soil was considered nonlinear by assuming a bilinear load-displacement relationship.

The fundamental difference between a pipe crossing a fault and pipe crossing an expansive soil is the magnitude of the soil deformation. Fault movements generally range in meters, but a comparatively small deformation is expected in case of moisture-induced soil expansion. Kourtetzis et al. [71] adopted the solution methodology of pipe crossing normal fault plane to analyzed pipe-soil interaction due to surface settlement/heave without any modification or alteration. Due to various inherent assumptions, this solution methodology may not be suitable for small soil deformations. For example, Kourtetzis et al. [71] assumed that the soil surrounding the pipe will always yield which is not true in the moisture-induced soil expansion case. It is shown later in this thesis that the soil may yield in the bearing condition (when the pipe is pushed towards the soil) and remain elastic in the uplift condition (when the pipe is pulled away from the soil) considering the elastic-perfectly plastic soil response. Moreover, it is also possible that the soil will remain elastic throughout the pipe length. Given the context, the major limitations and assumptions of this work is outlined below.

- Kourtetzis et al. [71] analyzed a 500 mm diameter steel pipe with soil deformation ranging from 0.1 to 1 m. On the contrary, the soil deformation typically ranges from 0 to 0.1 m in the case of moisture-induced soil expansion.
- The elastic soil deformation in the bearing and uplift condition was neglected as it was very small compare to overall soil settlement/heave (see figure Figure 2.8) which may not be true for moisture-induced soil expansion.

- The settlement/heave, considered in this work, does not depend on the soil depth which is true in the case of earth fault movements where the entire soil mass translates. However, in moisture-induced soil expansion, a fixed depth of soil participates in settlement/heave.

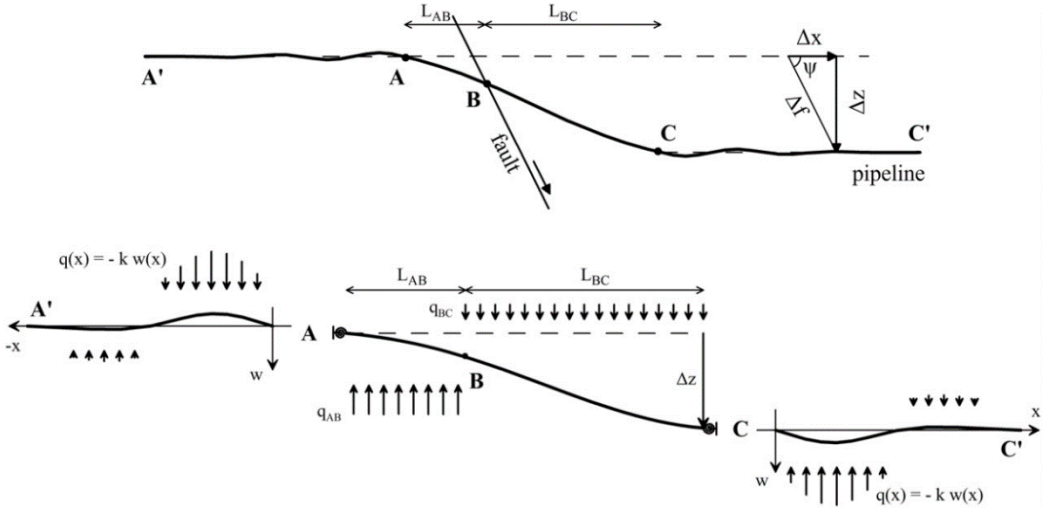

Figure 2.8: Analytical formulation of pipe-soil interaction in normal fault movement [70].

Nonetheless, these aforementioned studies provide a point of reference for the approaches presented in this thesis.

2.4 Cast-iron Pipe Damage Mechanism

As discussed previously, fracture occurs due to accumulated damage (i.e., crack growth) followed by a structural loading (as discussed above). This section describes the possible damage mechanisms for the cast iron water mains, which result in estimations for the structural capacity of the pipe. External corrosion is an obvious source of damage and is widely documented in the literature [3, 72, 73]. Furthermore, fatigue can also be a statistically plausible damage mechanism [9]; however, this study by Pericoli et al. [11] suggests that this may be associated with low probability hence unlikely in most cases, whereas corrosion serves as a dominant risk driver for failure. Besides, the aforementioned study evaluated the fatigue and corrosion damage against the fractographic examination of fracture surfaces which supported the conclusion that corrosion was

the major contributor to damage. In this section, a brief introduction of different corrosion rate models developed for buried pipes is presented.

2.4.1 Corrosion

Corrosion affects cast iron pipes internally from the water supply as well as externally from the interaction with the surrounding soil. The internal surface of cast iron pipes corrodes very rapidly immediately after the start of the water supply; however, the corrosion process subsides after graphitization and mineral deposit [74]. Graphitization is a process in which iron leaches out from the iron-graphite matrix of cast iron leaving behind graphite that naturally inhibits corrosion [75]. Furthermore, the rate of internal corrosion is much slower as compared to external corrosion, specifically pitting corrosion, and hence not a primary concern in underground pipes [76].

On the other hand, corrosion of external surfaces of pipes due to interaction with the soil controls the structural capacity of aging infrastructures [77]. In the specific context of deteriorating water pipes, pitting corrosion on the external surface is most critical [78]. The study of pitting corrosion in buried pipes has a long and substantial history. Early work by Romanoff [72] considered cast-iron pipe corrosion in soils from the basics of corrosion theory and highlighted factors, such as aeration, electrolyte type and concentration, and pH that may affect underground corrosion. Despite this exhaustive study, the proposed corrosion rate model is unviable for field applications due to the large number of input parameters, which are not usually available. A similar problem is encountered with Rossum's corrosion rate model [73] which is based on the principles of electrochemistry. The model is also dependent on factors, such as aeration, electrolyte type, and concentration, and pH, to predict pit growth. A predictive model, provided by the American Water Works Association [3], is commonly used for estimating this pit depth. Due to graphitization, corrosion in cast-iron material is a self-inhibiting process. The AWWA corrosion model simulates the graphitization behavior through the saturation (or limiting) of pitting depth for aged pipes. This model assumes two different corrosion rates – a fast exponential growth at an early age that signifies the availability of iron for corrosion and relatively slow linear growth subsequently to represent corrosion inhibition due to leftover graphite. This model is based on regression fitting to measurements of pit depths from over 43 exhumed pipes that represent a range of soil chemistries (redox potential, resistivity, pH, sulfide, and chloride ion content), ages, and

groundwater level, and seasonal changes. Figure 2.9 illustrates this regression fit as well as the scatter data from which it is generated. Eq. (2.3) indicates the expression for this fit.

$$d_{max} = 0.0125t + 5.85(1 - e^{-0.058t}) \tag{2.3}$$

where, t (year) is the age of the pipe (in years) and d_{max} (mm) is maximum corrosion pit depth.

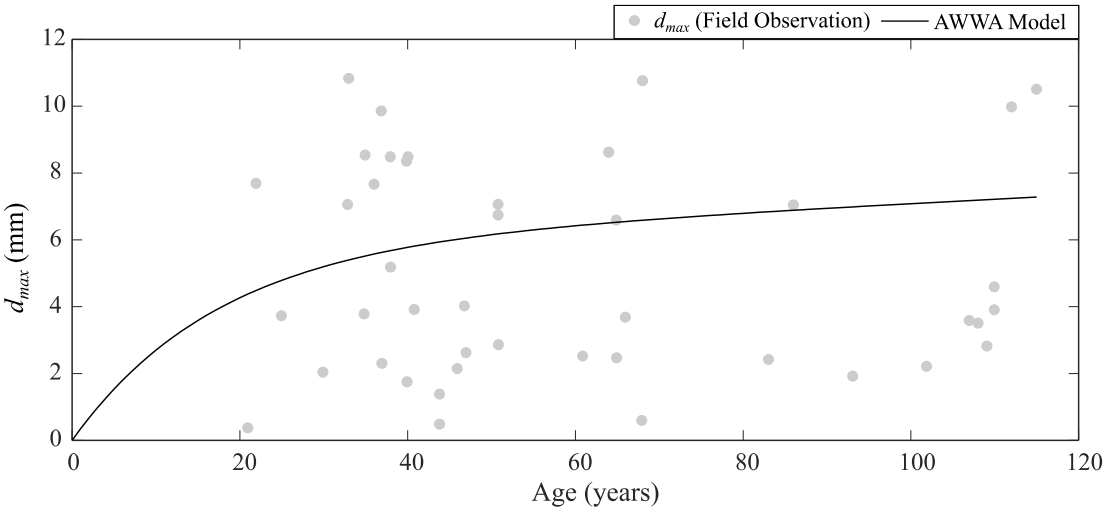

Figure 2.9: AWWA [3] corrosion model for maximum pit depth and the associated observed maximum pit measurements.

2.5 Risk Assessment of Deteriorated Cast-iron Pipes

Probabilistic analysis to predict the failures of degrading systems is well-established [79]. In the specific context of deteriorating water pipes, reliability techniques can be broadly categorized into two groups: statistical and physics-based approaches. A critical review of these approaches is presented by Kleiner and Rajani [7] and Rajani and Kleiner [80], respectively. Statistical approaches rely on identifying failure patterns in historical failure data to predict future failures. The inherent assumption that the future failure will follow the failure pattern derived from past failure data is a major drawback of this approach. This assumption largely disregards changes in the physical conditions of a pipe system over time. On the other hand, a physics-based approach examines loads on a pipe and its capacity to withstand those loads to estimate failure probability. The loads can be divided into two groups: operational loads (such as pressure, temperature, and vehicular)

and environmental loads (such as soil expansion and frost load), and the capacity of the pipe to resist these loads over time depend on the degradation process, manufacturing defects, and improper installation. Failure can be expected when the pipe whose structural capacity has been declined experiences operational and environmental loads.

Most of the existing literature [81, 82, 83, 84, 85, 86] focuses more on operational loads than the loads caused by seasonal and weather effects (environmental loads) specifically moisture-induced soil expansion. However, field failure data of in-service water pipes, e.g., pipe failures in the City of Sacramento trail the rainfall data (see Figure 2.4) which are seasonal and weather related. As can be seen from Figure 2.4, the maximum number of failures is observed in the month of January, which is also the month of the highest rainfall. Furthermore, a moderate increase can also be seen in drier months. This observation indicates that the rate of failure correlates according to the degree of moisture change in the soil. Besides, the correlation between environmental load and annual pipe failure peak has been reported in several previous studies [14, 87, 15, 16, 12]. Despite this common knowledge, moisture-induced soil loading has been largely ignored in the assessment of buried cast iron pipes.

2.6 Research Gaps

The literature review revealed several gaps in existing research related to the risk assessment of water main failures, and these are summarized below:

- Although a plausible failure mechanism responsible for the majority of water main fractures is the flexure of pipes induced by a moisture-induced differential expansion/contraction of expansive soils, this mechanism has received very limited attention thus far in literature.
- From a numerical simulation standpoint, relatively few studies have been reported aimed at understanding pipe behavior in expansive soils. The existing studies adopted several assumptions whose effect on pipe stresses were significant. Furthermore, the focus of these studies is on accurately simulating the soil deformation rather than computing pipe stresses accurately.

- In contrast to analytical models for other mechanisms of failure (e.g., internal water pressure, temperature change, and traffic load) developed and adopted by various researchers [87, 88, 89, 90], analytical formulations for differential-movement-induced flexural stresses in pipes have not been investigated well.
- Despite such prevalence of expansive soils in large parts of North America, reliability studies focused on flexural failures driven differential soil expansion have not received the attention they deserve in literature. The risk assessment requires a probabilistic interpretation of uncertainty present in various inputs (i.e., material and geometric properties and configurational parameters), and the model itself. Currently, the characterization of these uncertainties is not readily available in the literature. Furthermore, the model inputs (and uncertainties thereof) that have the most significant impact on response estimation is not known. Such characterization is important from the standpoint of making targeted investments in data collection, mapping, as well as model development and refinement.

2.7 Specific Objectives

Based on the identified gap areas, the specific research objectives of this thesis are as follows:

1. To simulate moisture-induced soil expansion and pipe response buried in expansive soils numerically. This involves:
    a. modeling swelling behavior of unsaturated soil with moisture migration for pipe stress calculation,
    b. decoupling the soil expansion and pipe stress analysis, and
    c. modeling pipe-soil interaction by applying the net effect, the volumetric expansion of the soil, directly supplied as an input eigenstrain field.
2. To propose a computationally inexpensive approach for evaluating pipe flexural stress due to moisture-induced soil expansion load. This involves:
    a. developing a physics-based analytic solution approach and

b. validating this analytical model against continuum finite-element simulations.

3. To estimate the probability of failure and remaining service life of a pipe segment buried in expansive soil. This involves:
    a. characterizing parameter and model uncertainty of demand and capacity models,
    b. implementing Monte-Carlo procedure to synthesize various uncertainties into a probabilistic estimate of the failure and remaining life of a pipe, and
    c. conducting a sensitivity study to examine the influence of various inputs (and their uncertainties) on the estimated response.
4. To showcase the application of the proposed reliability assessment framework. This involves:
    a. generalizing the reliability results to a pipe crossing multiple boundaries,
    b. computation of network level risk, and
    c. proposing an optimal solution plan using multi-objective optimization.

Chapter 3
Numerical Simulation of Moisture-induced Soil Expansion and Pipe-soil Interaction

This chapter focuses on numerical simulations of moisture-induced soil expansion and its effect on buried cast iron pipes. A three-dimensional continuum finite-element (CFE) study is undertaken to test the hypothesis that the moisture-induced differential soil expansion can produce sufficient flexural stresses to cause fractures in buried water pipes. These simulations are used later to assess the impact of varying problem geometry and material characteristics on pipe deflection and stresses. The observations from this exercise offer insights into the pipe response providing a basis for the development of a simplified analytical model presented in the next chapter. The CFE model simulates critical physical phenomena (pipe-soil interaction) and provides an understanding of the coupled soil-pipe response to various parameters, which are further used as qualitative and quantitative inputs into the analytical model formulation. Additionally, these simulations serve as a testbed against which the analytical approach is refined and validated.

This chapter is organized as follows. The problem formulation is presented first followed by a detailed description of the CFE simulation approach. After that, the results of a parametric study, which examines the pipe and soil material and geometrical factors influencing circumferential fracture, are presented.

3.1 Problem Formulation

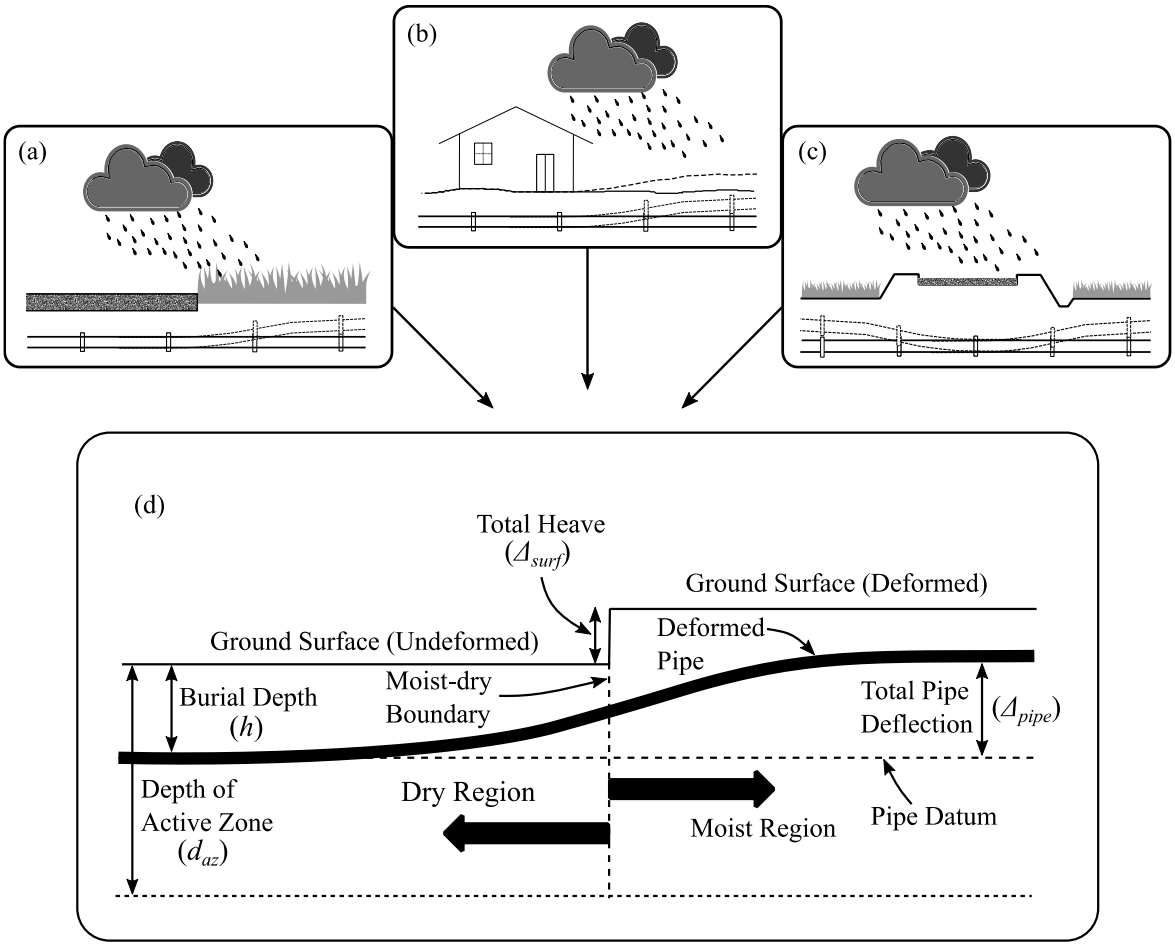

Figure 3.1: Schematic illustration of pipe deformation due to expansive soil: (a) pipe crossing an area where some part of it is covered such as open parking lot, (b) pipe going through a property line, and (c) pipe crossing a road and highway and (d) idealization of these scenarios.

Figure 3.1(a-c) schematically illustrates the problem under study. Referring to this figure, the pipe is assumed to cross a boundary (hereafter referred to as the moist-dry boundary) between soil that expands (or contracts) due to the change in moisture content. These conditions are commonly observed around locations where a portion of the soil is exposed to precipitation, whereas the shaded region remains relatively dry, especially at the onset of such precipitation. For example, the dry-moist boundary is encountered where the entire soil mass is expansive but only a small part

of it receives moisture, e.g., pipe buried under paved and unpaved area [Figure 3.1(a)] and pipe passing through property line [Figure 3.1(b)]). An alternative scenario could be where a portion of the expansive soil is replaced with sandy soil—pipe crossing roads [91] [Figure 3.1(c)]. Such situations are of particular interest in this thesis as they functionally represent physical conditions that may be responsible for a significant proportion of observed fractures. Field failure data reported by Pericoli et al. [11] supports this conclusion, as numerous instances of circular failures are observed at these locations.

Figure 3.1(d) shows an idealized representation of these conditions which forms the basis for the ensuing CFE simulations. In this configuration, a buried pipe (at depth h from the undeformed ground surface) crosses a moist-dry boundary that demarcates the soil region in to two regions, and only the right to the boundary (moist region) is assumed to experience expansion due to the moisture change. This differential expansion of the soil causes the pipe to bend, and the magnitude of bending depends on the total soil heave (Δ_{surf}) and pipe burial depth (h). Note that here h refers to the pipe depth in the undeformed soil condition. The total heave is controlled by various factors including the degree of soil saturation and the properties of the soil such as mineralogical composition, grain size distribution, and cementation. Moisture-induced soil expansion is a mature field of research in itself, and a comprehensive review is provided in Chapter 2. In this study, the main motive is to quantify the pipe responses due to soil expansion. Consequently, the physicochemical processes leading to soil expansion are not modeled; rather the net effect, i.e., the volumetric expansion of the soil, is directly supplied as an input eigenstrain field [92] to the moist region of the soil [Figure 3.1(d)] using a surrogate thermal-structural analysis. The process of computing the eigenstrain using the soil swell capacity is outlined next.

3.1.1 Modelling Approach to Characterize Moisture-Induced Soil Expansion

The scalar magnitude of the eigenstrain field (which is assumed isotropic) is determined as being equal to the coefficient of linear expansion (COLE). The COLE values for US soils are contained in the USDA maps [45]. As described previously, COLE represents the free swell capacity of the soil, providing a convenient way to quantify its swell-shrink response [46]. As a point of reference, the USDA data shows that the City of Sacramento has moderate to high swelling soils with swell capacities ranging from 0% to 9% (see Figure 3.2).

Another parameter necessary to simulate soil expansion is the depth of active zone (d_{az}). Soil swelling is primarily affected by the field degree of saturation of the soil's near-surface zone, the depth of active zone which is also called the zone of seasonal fluctuation, or the depth of wetting [30]. It is the portion of soil (depth) that experiences moisture fluctuations and participates in the expansion process. The depth of active soil zone is of particular importance because the total heave (total expansion) can be simulated by integrating the expansions (computed from an infinitesimally small depth and eigenstrain) over this depth [27, 33]. The depth of the active zone can be computed from the soil suction measurements in the field [40]. However, due to its dependency on various other factors, a common practice in the literature is to assume this variable to be between 2 to 3 m [31]. Discontinuities in the soils such as the bedding plane, cracks and fissures, and tree roots have a significant influence on this parameter. Assuming homogeneous soil condition, the total free deformation (Δ_T) in the moist side of the soil [Figure 3.1(d)] can be computed as follows.

$$\Delta_{surf} = d_{az} \times COLE \tag{3.1}$$

Similarly, the far field pipe deformation (Δ_{pipe}) due to the free swell of the soil, which should be equal to the soil deformation at the pipe level, can be computed as follows.

$$\Delta_{pipe} = (d_{az} - h) \times COLE \tag{3.2}$$

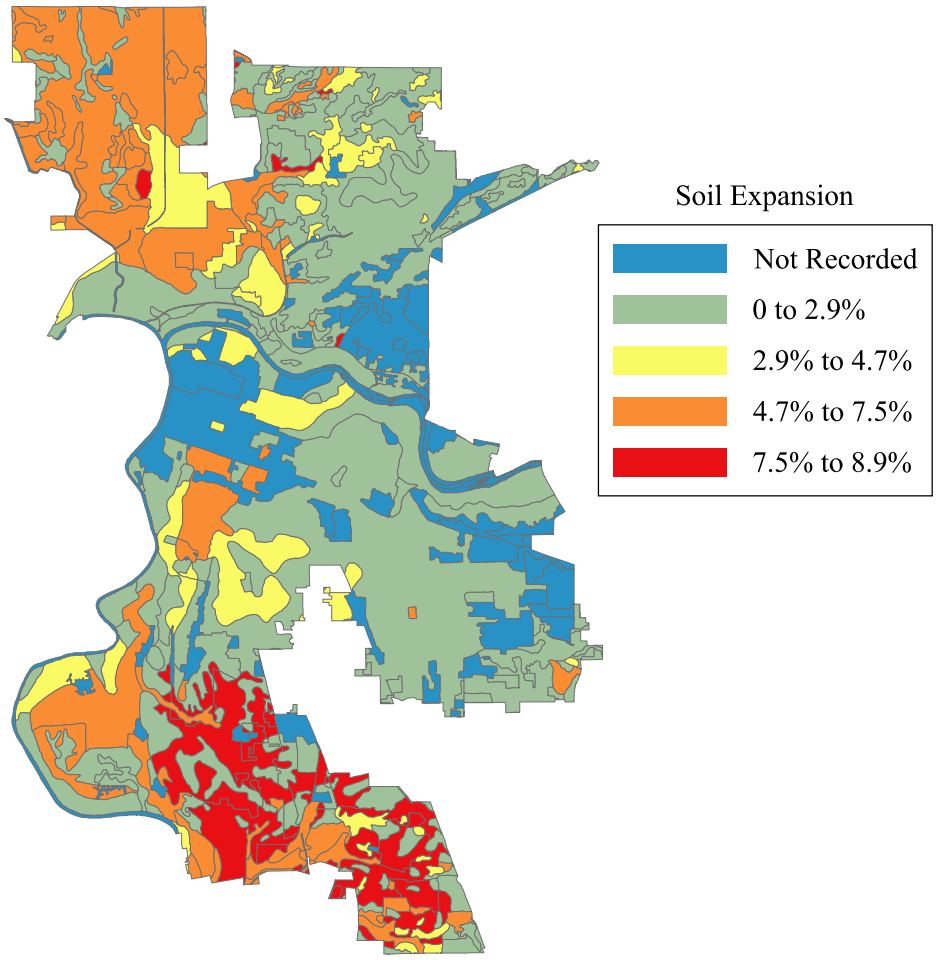

Figure 3.2: Soil linear extensibility records for the City of Sacramento published by USDA ranging from 0 to 8.9%.

Assuming COLE for a region where the pipe is buried is known, a three-dimensional finite element procedure is employed by directly applying the soil expansion as an input eigenstrain field over the soil depth (depth of active zone) to capture the volumetric behavior of the soil. As mentioned previously, the analysis in this thesis does not attempt to model moisture migration and the "soil suction-effective stress-volume change" relation. Instead, the analysis here uses a thermal-structural analysis as a proxy, where the coefficient of thermal expansion is specified such that a 1°C temperature change leads to the desired volume expansion. The 1°C temperature change is selected because in this way the coefficient of thermal expansion would be the same as the COLE value. Any other temperature change can be employed, provided that the coefficient of

thermal expansion is adjusted accordingly to obtain the desired volume increase. The use of the thermal eigenstrain analogy of moisture-induced soil expansion greatly simplifies the CFE analysis. A similar approach of using the eigenstrain for analyzing pipe-soil behavior in frost susceptible soil has been previously employed by Trickey et al. [91]. Note that the impact of moisture change on the soil mechanical properties are not considered.

3.2 Model Description and Parameters

A cast-iron pipe traversing an intersection (moist-dry boundary) is considered, where the geometry (computational domain) of a typical CFE model is illustrated in Figure 3.3. Referring to the figure, the model represents a volume of the soil of 30 m (length) × 2 m (width) × 2 m (height), containing a 30-m long pipe. The dimensions (length and width) of this volume are selected through an iterative process in which a representative model with various geometries is simulated. The model geometry that minimized the effect of edges and boundaries on the response quantities of interest (i.e., peak stresses and deflection) is chosen. The moist-dry boundary divides the models into two sections: expanding (moist side) soil and non-expanding (dry side) soil. The soil transition from non-expanding to expanding soil imposes a nonuniform ground response on the buried pipe which causes longitudinal moments that may induce circumferential fracture.

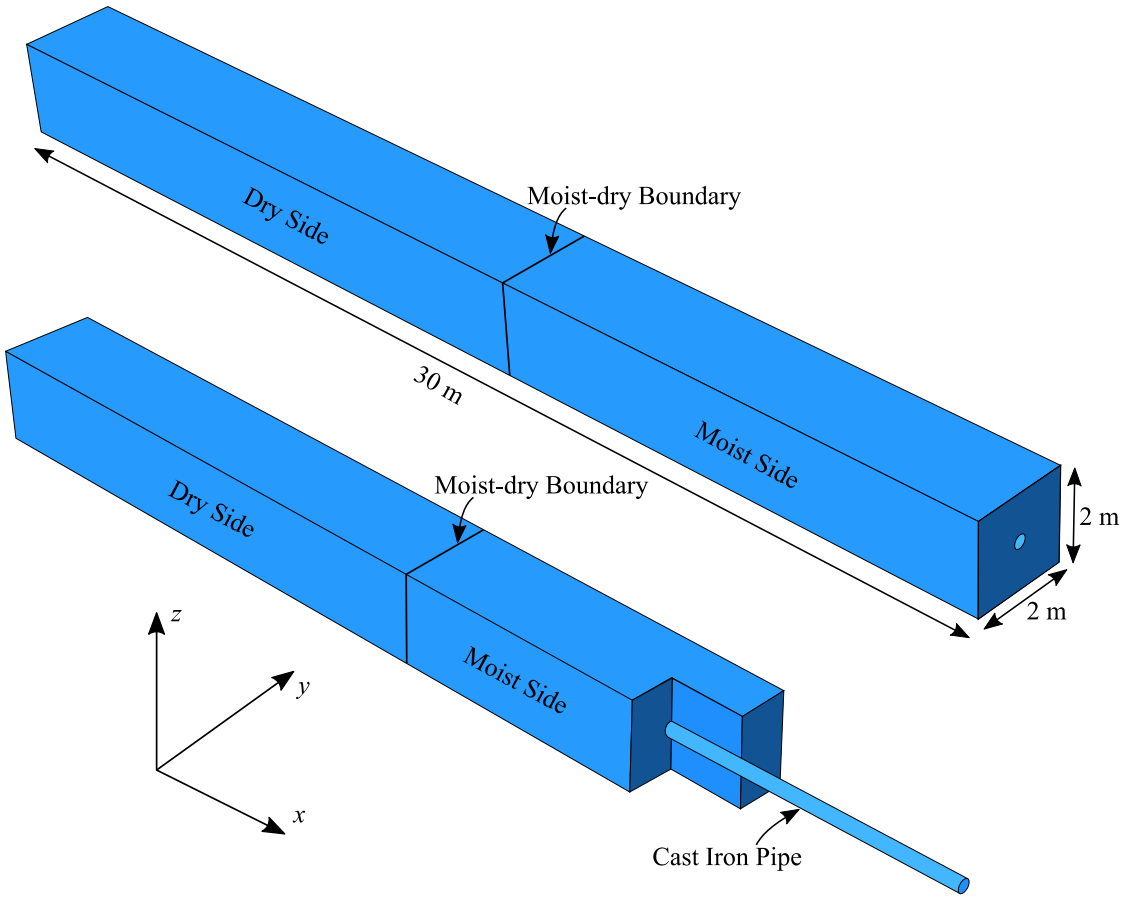

Figure 3.3: Representative CFE model geometry of the pipe-soil interaction model showing soil dimensions and embedded pipe.

The model parameters that are required to quantify the problem are summarized in Table 3.1. These include geometric/configurational parameters as well as material parameters necessary for representing the behaviors of pipe and soil. For example, the elastic response of the pipe is described by two parameters, the Poisson's Ratio (ν_c) and Young's modulus $(E_{SC/PC})$ for cast iron in which the subscripts denote spun cast (SC) or pit cast (PC) pipes. Similarly, the constitutive response of the soil is represented by the parameters of the Drucker Prager model [93]. The parameter values selected in Table 3.1 represent informed estimates of these quantities, encompassing a range of realistic conditions. The final column of the table includes references from which these values are sourced. When considered collectively, these values result in 80 parametric combinations (4 different diameters, 10 levels of soil expansion, and 2 different cast

iron properties). For each of these parametric combinations, CFE simulations are performed to compute longitudinal stresses and deflection.

3.3 CFE Simulations

3.3.1 Element Formulation and Boundary Condition

The pip-soil interaction model is constructed and analyzed using the software platform ABAQUS version 6.14 [94]. Figure 3.4 illustrates the mesh geometry and element type used to simulate various cases with different values of the input variables. Note that in some cases (when the depth of active zone and pipe burial depth is varied), the geometry is changed; however, the element type is unchanged. The bottom surface of the soil is restrained in all three directions $(u_x = u_y = u_z = 0)$, where u_x, u_y, and u_z are displacements in x, y, and z directions, respectively. The sides on the xz-plane are restrained to move in the y-direction $(u_y = 0)$. Similarly, the sides on the yz-plane are restrained to move in the x-direction $(u_x = 0)$. The top surface is left unrestrained.

As shown in Figure 3.4, four-node reduced-integration shell elements (type S4R) were used for modeling the pipe cylindrical profile, whereas eight-node reduced-integration brick elements (C3D8R) are used to simulate the surrounding soil. The CFE model has ~50,000 brick elements for the soil and ~125,000 shell elements for the pipe. The number of elements is estimated from a mesh convergence study which also helped in mesh refinements in areas of high gradients, especially near the moist-dry boundary. In Figure 3.5, the maximum bending stress and the relative error (i.e., $100 \times |\sigma_{n+1} - \sigma_n|/\sigma_n$ where σ is maximum bending stress in step n and $n + 1$) are plotted against the element-size-reduction factor (minimum dimension of the model divided by element size). It can be seen that as the element are factored more (increasing the number of elements), the response and error approach a constant value. After the element-size-reduction factor equals 8, the mesh refinement produces a negligible change in the maximum stress value and the mesh is considered converged.

Table 3.1: Summary of parameters defining the pipe-soil interaction problem.

Parameter Type and Description	Symbol (Unit)	Values Considered	Remark
Geometric			
Pipe Diameter	D (mm)	100, 150, 200, 250	Around 85% of pipes in the Sacramento pipe network lies in this range. (Sacramento pipe network GIS database)
Pipe Thickness	th (mm)	8.9, 9.6, 10.4, 11.2	AWWA historical standards [95, 96]
Pipe Depth	h (m)	1	Based on field data
Material			
Cast Iron			
Modulus of Elasticity	E_{SC} (GPa)	150	Two different cast iron types (due to different manufacturing processes) are present in Sacramento pipe network: Spun cast (SC) and pit cast (PC) [97, 19]
	E_{PC} (GPa)	110	
Poisson's Ratio	ν_c	0.22	
Soil			
Modulus of Elasticity	E_S (MPa)	15	Typical soil properties for clayey soil are taken from Bowles [98]. The Drucker-Prager parameters are evaluated from c and φ. These are also used to characterize the elastic-perfectly plastic spring idealization of soil.
Poisson's Ratio	ν_S	0.4	
Angle of Friction	φ (degree)	30	
Cohesion	c (kPa)	35	
Unit Weight	γ_{soil} (kN/m^3)	19	
Surface Friction Coefficient	μ	0.3	Karamitros et al. [59], McCarron [99]
Swell			
Swell Capacity	s_{exp} (%)	0 to 10	Sacramento Soil Database, USDA
Depth of Active Zone	d_{az} (m)	2	From literature [31, 30]
Others			
Length of Free Bending	L_{free} (m)	Varies	Evaluated after comparison with CFE analysis
Age	*age* (year)	0 to 120	From Sacramento pipe network GIS database

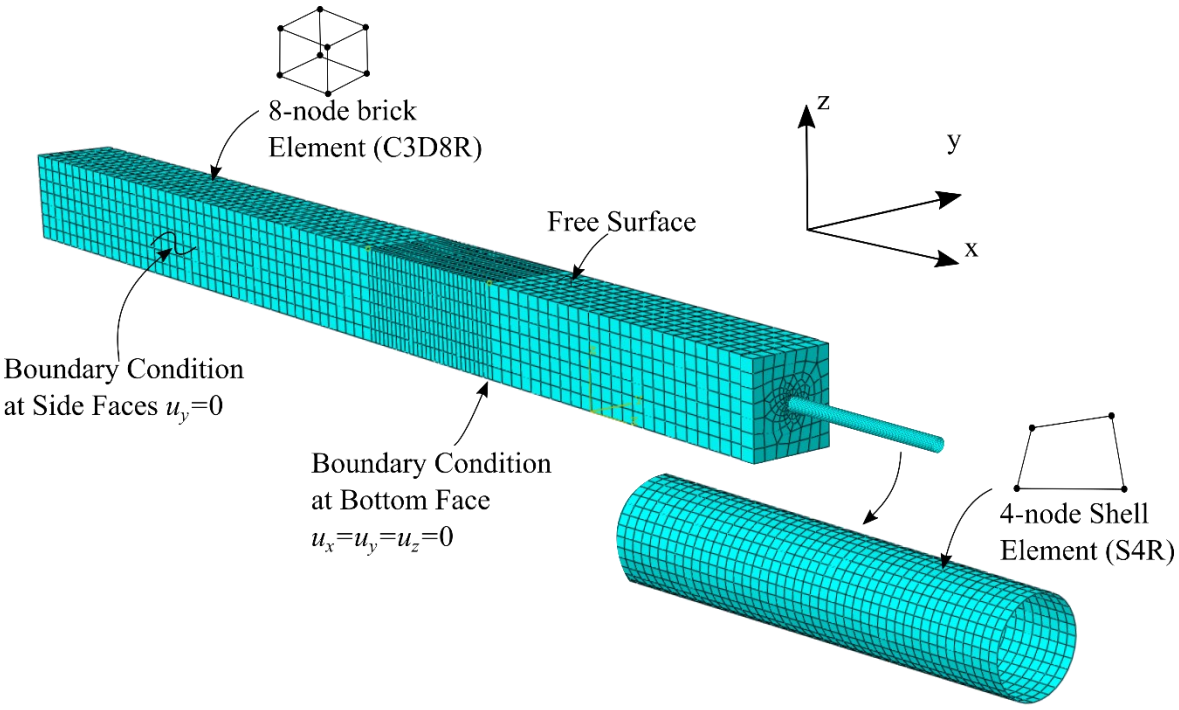

Figure 3.4: Representative CFE model discretization and element type.

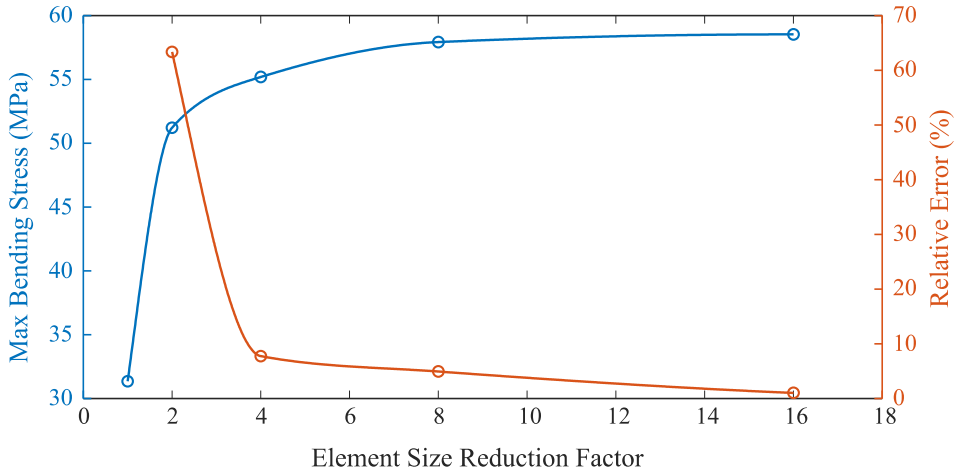

Figure 3.5: Mesh convergence study.

3.3.2 Material Constitutive Relation

The material response of cast iron is assumed linear elastic which can be characterized by two parameters, i.e., the elastic modulus, E, and the Poisson's ratio, ν (assumed to be 0.22). Referring to Table 3.1, two values of the elastic modulus (i.e., E = 110, 150 MPa) are used to reflect observed differences between pit-cast iron and spun-cast iron pipes [97, 19]. The lower E value for the pit-cast iron is due to the manufacturing technique that yields structurally inferior material.

The constitutive response of the soil is represented through the Drucker-Prager yield surface with elastic-perfectly plastic material behavior. The Drucker-Prager yield criterion is a modified version of the von Mises yield criterion that accounts for Coulomb friction [93]. The yield surface, f_y, can be defined as:

$$f_y(\sigma) = \sqrt{J_2} + \alpha I_1 - k \tag{3.3}$$

where I_1 is first stress invariant $(I_1 = \sigma'_1 + \sigma'_2 + \sigma'_3)$; J_2 is the second invariant of deviatoric stress $\left(J_2 = \frac{1}{6}[(\sigma'_1 - \sigma'_2)^2 + (\sigma'_1 - \sigma'_3)^2 + (\sigma'_3 - \sigma'_1)^2]\right)$; and α and k are material parameters. σ'_1, σ'_2, and σ'_3 are the principal effective stresses. The coefficients α and k can be derived from the soil shear strength parameters (cohesion c' and angle of internal friction φ'), which makes the Drucker-Prager yield criterion equivalent to the Mohr-Coulomb yield criterion which is treated as standard failure criteria for soils. The relations between α and k and c' and φ' are shown in Eq. (3.4). The Drucker-Prager yield criterion is preferred here because the Mohr-Coulomb yield surface contains sharp edges (see Figure 3.6), which introduces convergence problems in numerical analysis, especially when contact is modeled. This shortcoming may be overcome by using the Drucker-Prager yield criterion which has a smooth yield surface.

$$\alpha = \frac{2}{\sqrt{3}}\left(\frac{\sin\varphi'}{3 \pm \sin\varphi'}\right)$$
$$k = \frac{2\sqrt{3}\, c' \cos\varphi'}{3 \pm \sin\varphi'} \tag{3.4}$$

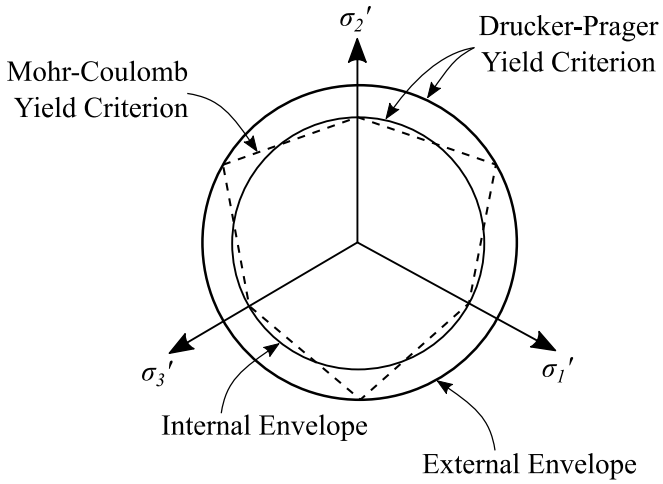

Figure 3.6: Mohr-Coulomb failure envelope with circumscribed and inscribed Drucker-Prager failure envelope drawn in an octahedral stress plane.

3.3.3 Pipe and Soil Interface

A contact algorithm is considered to simulate the interface between the outer surface of the cast iron pipe and the surrounding soil. Contact is a boundary nonlinearity that acts in the tangential as well as in the normal direction to the contact surface. In the tangential direction it is defined such that, due to friction, no relative motion occurs between two surfaces until the tangential force reaches a threshold. Beyond the threshold, sliding occurs without any change in the tangential force. In ABAQUS, the tangential interaction is defined using the penalty method, in which the frictional coefficient (shown in Table 3.1) characterizes the tangential force. On the other hand, in the normal direction, a hard contact pressure-overclosure relationship is defined which minimizes the penetration of two surfaces at the constraint location and specifies zero stress during the tension separation. Among various contact models available in ABAQUS, surface-to-surface interaction (ABAQUS keyword: *CONTACT PAIR) is selected to model the pipe-soil interface. In this model, the user specifies the contact pair between two deformable bodies.

3.3.4 Results

Once the CFE model is constructed, it is loaded in two steps. The first step includes applying a gravity load to simulate the self-weight of the soil above the pipe (ABAQUS GEOSTATIC step). The second step applies a volumetric expansion (specifically, a volumetric expansive strain) to the

soil in the moist region. The representative ABAQUS code is attached in the Appendix. Other input parameter values that represent the City of Sacramento pipe network are shown in Table 3.1. For each of these parametric combinations, CFE simulations are conducted to estimate the deflections and longitudinal stresses which later serve as benchmark solutions to compare the analytical formulation of the same problem.

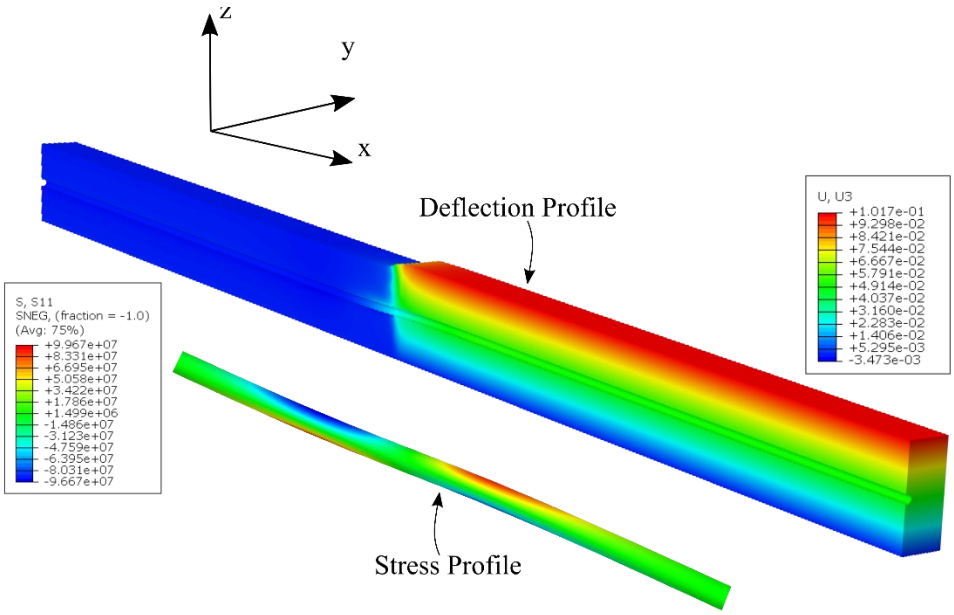

Figure 3.7: Soil deformation $(U3)$ profile in meters for 5% soil expansion and corresponding longitudinal stress $(S11)$ profile in Pa for 200 mm diameter pipe.

Figure 3.7 illustrates a representative output of the CFE simulations, showing the deformation and longitudinal stress distributions for a 200 mm diameter pit cast pipe at 5% soil expansion. Referring to the figure, the CFE simulations capture the relevant aspects of the response well. As expected, for 5% soil expansion and 2 m depth of active zone, the surface heave is theoretically equal to 100 mm $(2000 \times 5/100 = 100)$, and, for this expansion, the longitudinal stress in the pipe is close to 100 MPa. Figure 3.8 shows the maximum longitudinal stresses found in spun cast pipes in various soil expansions. The stress increase with an increase in the soil expansion are deemed sufficient to cause fractures in deteriorated pipes. For example, the maximum longitudinal stress of 150 mm diameter pipe in 4.5% soil expansion (average swell capacity of the City of Sacramento soils) is 135 MPa which is more than its structural strength if more than 40 years old

(Pericoli et al. 2014 reported that the strength of 40 years old 150 mm diameter pipe is 125 MPa). Also, it can be seen from the results that the small diameter pipe is more susceptible to failure. For 5% soil expansion, the maximum stress in 100 mm diameter pipe is 162 MPa which is 25% higher than the stress in 250 mm diameter pipe for the same soil expansion.

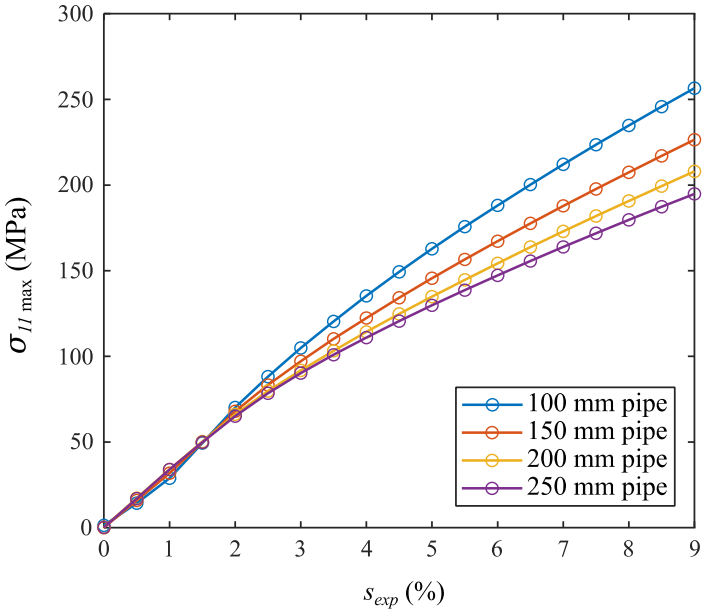

Figure 3.8: Maximum longitudinal stress $(\sigma_{11\,max})$ in different diameter spun pipes due to soil expansion ranging from 0 to 9%.

Figure 3.9(a) shows the equivalent plastic strain $(PEEQ)$ contours on the deformed soil cross-section along its length. Referring to this figure, soil yielding around the moist-dry boundary can be observed clearly. Moreover, it is observed that the $PEEQ$ region is not symmetric about the moist-dry boundary which shows the pipe-soil interaction process is not identical on both sides. Another intriguing observation is that over a small distance (denoted by L_{free}) on either side of the moist-dry interface, the pipe bends freely without bearing stresses either at the top or the bottom as illustrated in Figure 3.9(b). The mismatch between the stiffness of the pipe in bending and the surrounding creates this unsupported segment of the pipe.

The preceding observations provide a basis for the development of a simplified analytical model for characterizing pipe response which is presented in the next chapter.

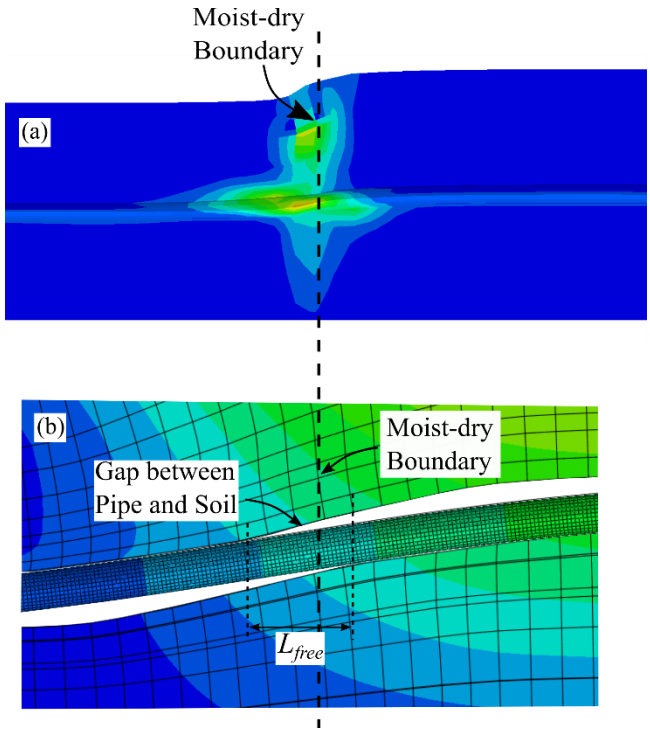

Figure 3.9: (a) Equivalent plastic strain and (b) free bending around the moist-dry boundary.

3.4 Parametric Study

A parametric study is performed to examine the impact of changes in specific geometric and material parameters on the normalized pipe flexural stress $(\sigma_{11}/\sigma_{yield})$, where σ_{11} is longitudinal stress and σ_{yield} is yield stress of cast iron material. The parametric study does not evaluate the factors contributing to either the swell susceptibility of the soil such as grain size, saturation, hydraulic conductivity or moisture availability, or the complexities of climate. Instead, the expansive soil is defined based on the swell capacity, and it is assumed that all the factors contributing to the expansion will be constant. The study examines how other factors (pipe material modulus, soil material modulus, depth of active zone, and pipe burial depth) associated with volume change and pipe-soil interaction influence the response. All the results are shown for 150 mm diameter pit-cast pipe and 5% soil expansion.

Changes in the pipe bending stress are examined as a result of different pipe and soil characteristics:

1. Pipe material: Changes in the pipe's modulus of elasticity are considered to account for different casting methods. As mentioned previously, two different manufacturing processes (pit-cast and spun-cast process) of cast iron pipes were common.
2. Soil properties: Changes in the swell capacity, modulus of elasticity, and depth of active zone are considered to accommodate the spatial variation of soil in large-size pipe networks.
3. Others: Changes in pipe burial depth are considered because pipe may be buried at different depths to meet municipalities' requirements.

3.4.1 Effect of Soil Modulus (E_S)

In this study, the impact of changes in native soil modulus on the maximum pipe flexural stress is monitored by doubling the value of the modulus, while keeping other paraments constant. The original values of the parameters are shown in Table 3.1. The maximum normalized pipe stresses for a 150 mm diameter pipe are shown in Figure 3.10, where the maximum stress increases as soil modulus increases and vice versa. This is to be expected as the decrease in soil modulus leads to a reduction in the pipe curvature, thus reducing the moment and stresses. The change in modulus (by a factor of 2 which is equivalent to 100%) imparted only a 10% change in maximum stress, which leads to the observation that the soil modulus may have a relatively smaller role to play in the maximum pipe stress.

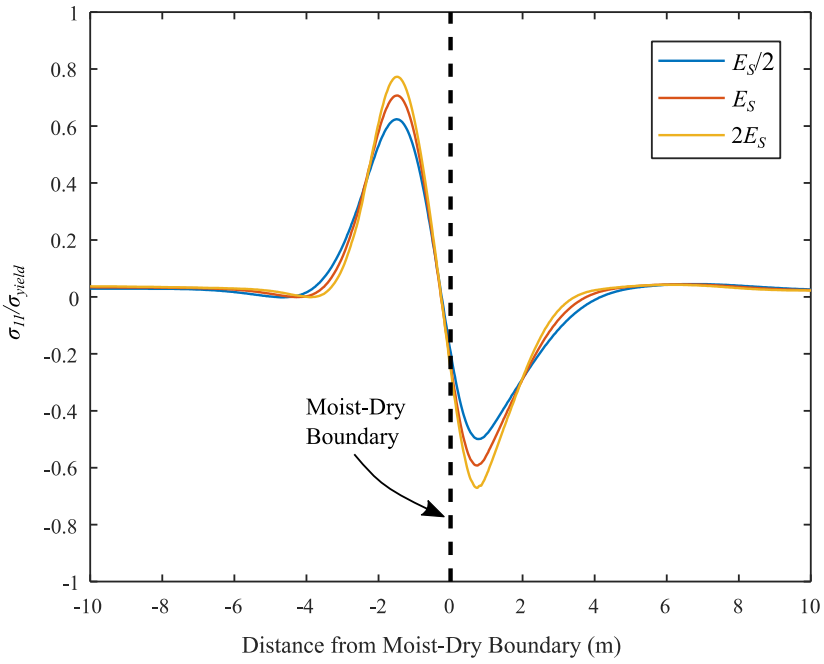

Figure 3.10: Effect of soil modulus on the pipe longitudinal stress observed in 150 mm diameter pit-cast pipe with 5% soil expansion.

3.4.2 Effect of Pipe Modulus ($E_{PC/SC}$)

The second case examined here is the change in pipe modulus and its effect on maximum flexural stress. The pipe modulus value of 110 MPa (pit cast iron) and 150 MPa (spun cast iron) are provided as inputs into the analyses while other parameters are kept constant. Results show that as the pipe modulus increases, the normalized flexural stress increases, as seen in Figure 3.11. This trend is expected because a of larger bending moments associated with a stiff pipe. When the modulus of the pipe is changed by the factor of 1.36 (110 MPa to 150 MPa ~ 36% change), the bending stress increases by approximately 20%. This implies that, unlike the change in soil modulus, the pipe modulus has a significant effect on the maximum bending stress.

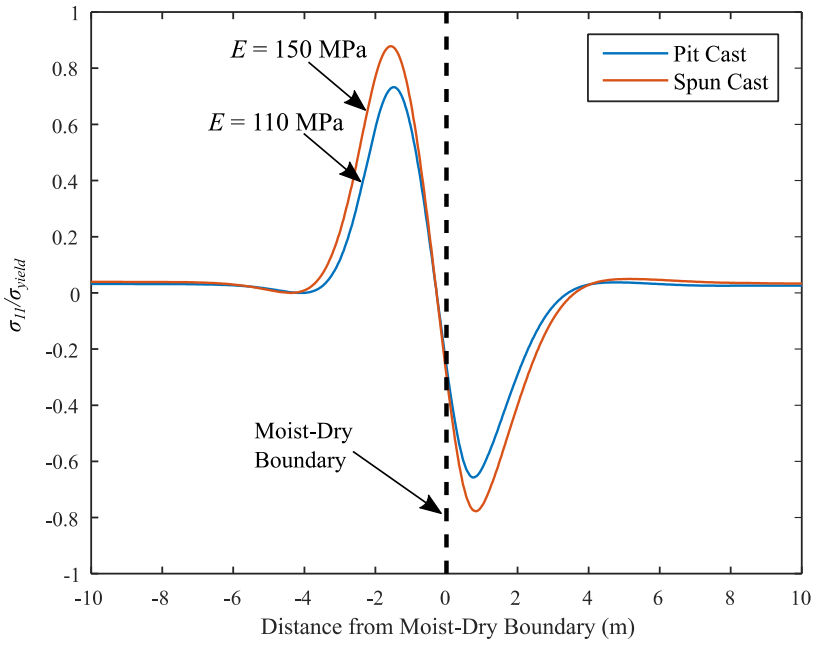

Figure 3.11: Effect of pipe modulus on the longitudinal stress observed in 150 mm diameter pipe with 5% soil expansion.

3.4.3 Effect of Pipe Burial Depth (*h*)

Next, the effect of pipe burial depth on pipe response is examined by modeling two different pipe depths (1 m and 1.5 m) while the depth of active zone is kept constant (2 m). Since the pipe deflection is related to the pipe burial depth, the normalized deflection is also examined along with the maximum bending stress. As shown in Figure 3.12, an increase in pipe burial depth alleviates the effects of soil expansion and decreases both the maximum deflection and the maximum bending stress. The maximum bending stress is reduced by approximately 70% when the pipe is buried 0.5 m deeper. Field experience has also indicated that the burial depth is the easiest way to control pipe stability [89, 91].

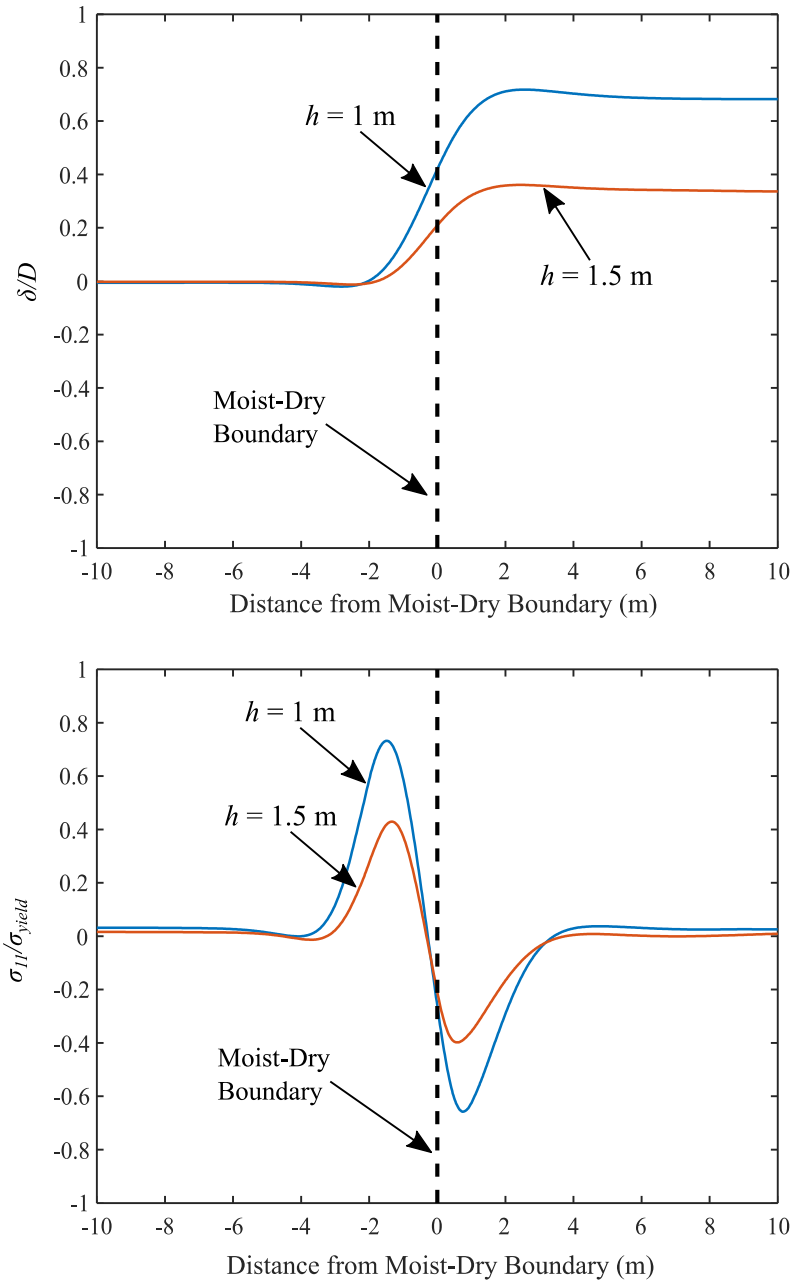

Figure 3.12: Effect of h on pipe deformation and corresponding longitudinal stress observed in 150 mm diameter pit-cast pipe with 5% soil expansion.

3.4.4 Effect of Depth of Active Zone (d_{az})

Finally, the effect of depth of active zone on maximum pipe deflection and bending stress is examined by adopting two different depths of the active zone (2 m and 3 m). Simulation results are shown in Figure 3.12. where as expected, an increase in depth of active zone exacerbates the effects of soil expansion and increases both the maximum pipe deflection and the maximum bending stress. The peak bending stress in the pipe is increased by 60% when the depth of active zone is increased from 2 m to 3 m, which implies that pipes are more susceptible to circumferential failure when buried in soils associated with deeper active zone.

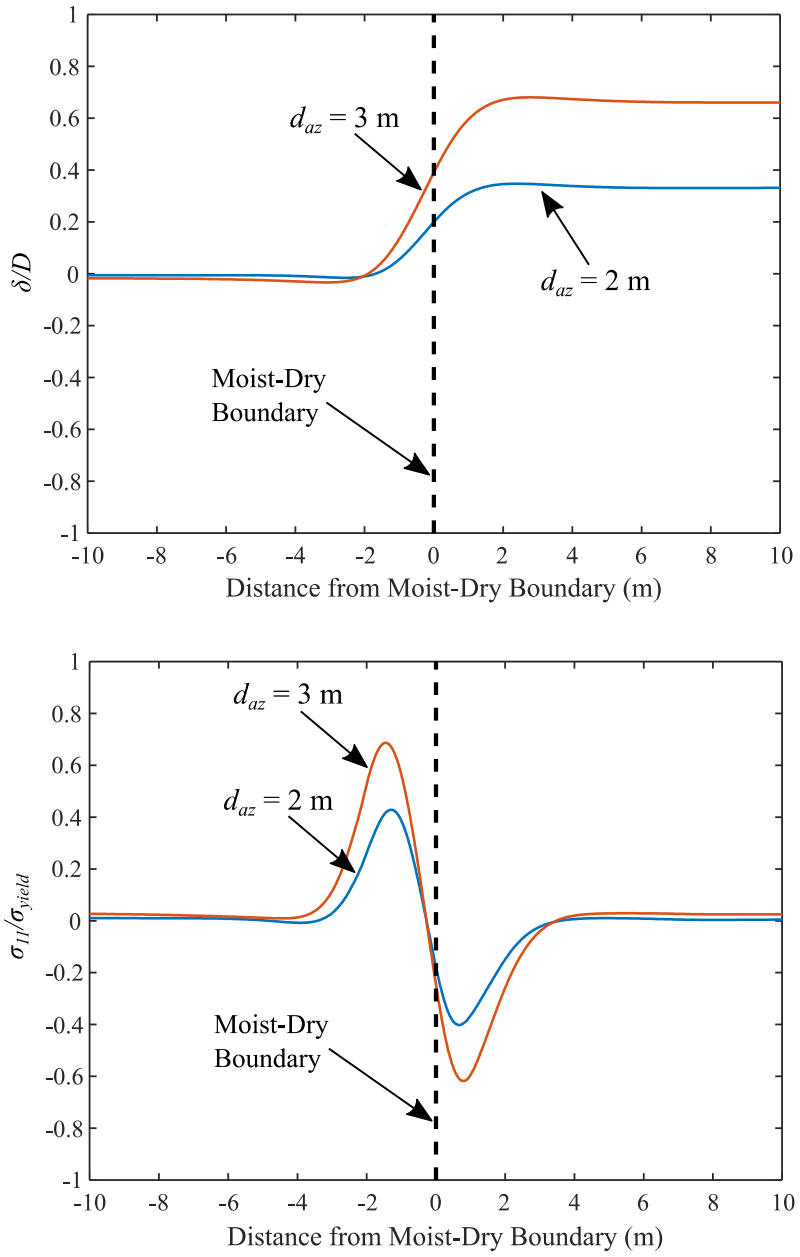

Figure 3.13: Effect of d_{az} on pipe deformation and corresponding longitudinal stress observed in 150 mm diameter pit-cast pipe with 5% soil expansion.

3.5 Summary

In this chapter, 3-D Continuum Finite Element (CFE) analysis of pipe-soil interaction associated with moisture-induced differential soil expansion is performed. CFE simulations of pipe crossing a boundary between soil that expands (or contracts) due to change in moisture content and soil that does not are performed in the software package ABAQUS. These models functionally represent physical conditions that are responsible for a significant proportion of observed water mains fractures. The constitutive response of the soil is represented through the Drucker-Prager yield surface with elastic-perfectly plastic material behavior. The material response of cast iron is assumed linear elastic. Contact properties between the pipe and soil are defined in both the tangential as well as the normal directions using the friction coefficient and hard contact, respectively. The CFE analysis does not capture the physicochemical processes leading to soil expansion; rather the net effect, i.e., the volumetric expansion of the soil, is directly supplied as an input eigenstrain field using a thermal-structural analysis as an artifice. Finally, a parametric study is conducted to investigate the impact of geometric and material conditions.

The analysis demonstrates how differential volume changes due to moisture-induced soil expansion can induce longitudinal stresses sufficient to cause circumferential fractures. A total of 80 simulations are performed and values of the input variables in these simulations are taken from the City of Sacramento pipe network and soil conditions. The purpose of these CFE simulations is to generate benchmark solutions (deflections, bending moments, and stresses) that will inform the development of a simplified analytical model (presented in Chapter 3) as well as serve as a testbed for its validation. The parametric study showed that change in the soil modulus has relatively small effect on the pipe longitudinal stresses; however, change in pipe modulus (which changes pipe bending stiffness) has moderate effect on the pipe longitudinal stress. Moreover, an increase in pipe burial depth from 1 m to 1.5 m decreases deflections as well as stresses, while an increase in the depth of active zone increases pipe deflection and longitudinal stress.

Chapter 4
Analytical Model of Pipe-soil Interaction in Expansive Soil Conditions

4.1 Introduction

The previous chapter detailed Continuum Finite Element (CFE) analyses to simulate the pipe-soil interaction experiencing differential soil expansion. The CFE simulations captured the relevant aspects of the pipe response (such as the deflection profile of the pipe, the bending moment along the length of the pipe, and the longitudinal stresses) well. However, direct simulation of all the mechanical phenomena (such as soil expansion, elastoplastic multiaxial soil response, effects of confinement, and contact/gapping between the soil and pipe) that are essential to the pipe-soil interaction problem is albeit computationally demanding. For example, with a given set of input values, a CFE simulation of a single pipe performed on a sophisticated computer system takes more than four hours to complete. A computationally efficient solution to this problem is needed which can be surrogate to the CFE simulations and can potentially be used for network-scale risk assessment. Along these lines, this chapter proposes a simplified analytical model to estimate pipe responses in a convenient way, without the CFE simulations.

In this chapter, a computationally inexpensive approach for calculating the failure stresses of a pipe segment given its various characteristics and environmental/loading factors is developed. This is achieved by developing a pipe-soil interaction model based on classical solutions of beam

on elastic foundation (abbreviated BEF henceforth) theory with the enrichment of material and interaction nonlinearities. The CFE simulations presented in Chapter 3 are used as benchmark solutions that inform the development of this simplified model as well as serve as a testbed for comparisons.

This chapter is organized as follows. First, the pipe-soil interaction is analyzed using Hetényi [100] solutions of the BEF model, and the results are compared with the results produced by the CFE simulation. This exercise provides a basis for the development of a new simplified analytical model which characterizes pipe response, specifically the stresses and deflections. Next, the methodology of the analytical solution approach considering soil and boundary nonlinearity is outlined. Finally, an assessment of this analytical model against the CFE results is presented.

4.2 Pipe-soil Interaction Model Description

Figure 4.1(a) shows one of the cases of differential soil expansion (other similar cases are discussed in Chapter 3) and their effect on buried pipes. Based on these scenarios, the pipe is assumed to cross a boundary (moist-dry boundary) between soil that expands (or contracts) due to change in moisture content and the soil that does not (soil may be covered to prevent moisture change or replaced with non-expansive soil). Figure 4.1(b) schematically illustrates this idealization. The main idealization is that the boundary between the moist (saturated) and dry (unsaturated) regions is abrupt, such that the boundary between the expanding soil and stationary soil is abrupt as well. In addition to this, the pipe-soil interaction is defined as follows: (1) the constitutive response for the cast iron pipe and the soil; (2) the swell capacity of the soil, which controls volumetric expansion due to moisture change; (3) geometric parameters, including the pipe diameter and wall thickness; and (4) the depth of the active zone (d_{az}) over which the soil is saturated vertically, and the burial depth (h).

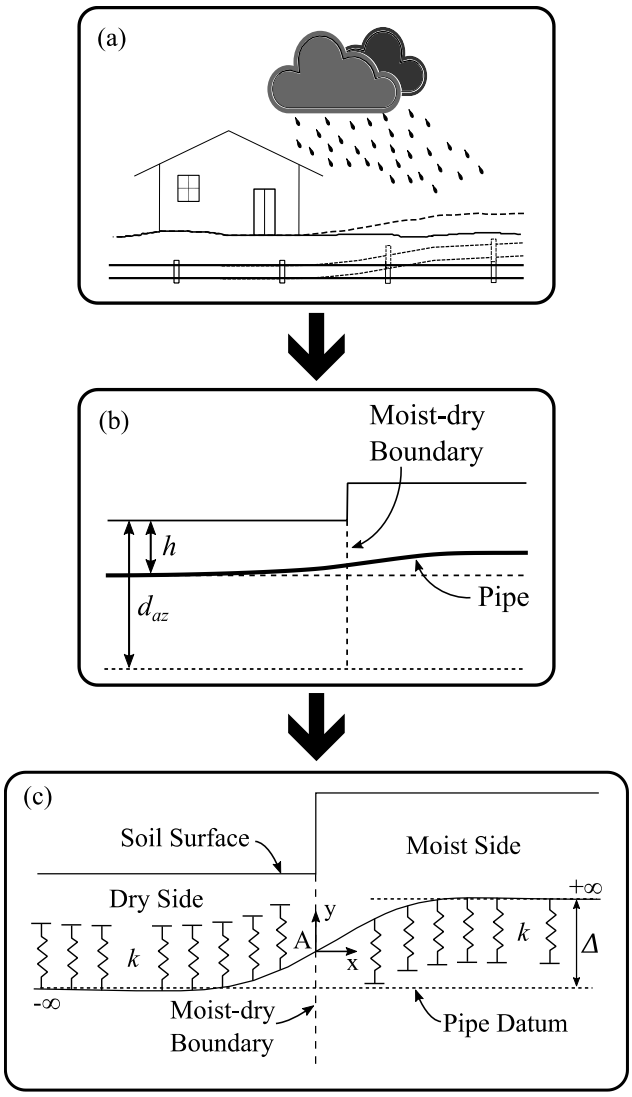

Figure 4.1: (a) Typical uplift caused by soil expansion, (b) idealization of pipe-soil interaction, and (c) schematic representation of the problem using a beam on an elastic foundation.

4.3 Pipe Response using Hetényi solutions

Figure 4.1(c) shows the BEF representation of pipe-soil interaction used the soil as a series of continuously distributed one-dimensional springs (in the vertical direction), whose response is assumed perfectly elastic, and the pipe modeled as a one-dimensional Euler-Bernoulli beam. The governing differential equation for the BEF problem is shown in Eq. (4.1).

$$E_P I_P \frac{d^4 y}{dx^4} = -ky \tag{4.1}$$

where I_P is the moment of inertia of the pipe and E_P is the elastic modulus of the pipe. This equation is based on the Euler-Bernoulli beam theory along with the assumption that the soil is elastic, such that the reactive force between the soil and pipe is linearly proportional to vertical displacement, y, at each point, x. The constant of proportionality, also referred to as the modulus of the subgrade reaction, k, is defined as per the relationship proposed by Vesic [101]. This relationship [Eq. (4.1)] reflects the one-dimensional simplification of soil response [102, 103, 104, 105] (for use within the BEF solution), the latter being the three-dimensional interaction between the soil continuum and the pipe.

$$k = \frac{0.65 E_S}{1 - \nu_S^2} \times \left(\frac{E_S D^4}{E_P I_P} \right)^{\frac{1}{12}} \tag{4.2}$$

where E_S and ν_S are the elastic modulus and Poisson's ratio of the soil, respectively; D and I_P are external diameter and moment of inertia of the pipe, respectively; and E_P is the elastic modulus of pipe material.

Following the Hetényi [100] solution approach, Eq. (4.2) can be solved by subdividing the pipe into two parts at the separation boundary A—one on each side of the moist-dry boundary [see Figure 4.1(c)]. The soil on the moist side experiences heave and exerts an upward force on the pipe, whereas to counteract this motion, the soil on the dry side applies a downward force on the pipe. The unknown internal forces of the one half, which is similar to a semi-infinite beam on elastic foundation with given end displacement and rotation (see Figure 4.2), may be obtained from the solution given by Hetényi [100] as shown in Eq. (4.3).

$$\begin{aligned} y &= y_0 A_{\lambda x} + \frac{1}{\lambda} \theta_0 B_{\lambda x} \\ \theta &= -2\lambda y_0 B_{\lambda x} + \theta_0 C_{\lambda x} \\ M &= 2\lambda EI(\lambda y_0 C_{\lambda x} + \theta_0 D_{\lambda x}) \\ V &= -2\lambda^2 EI(2\lambda y_0 D_{\lambda x} + \theta_0 A_{\lambda x}) \end{aligned} \tag{4.3}$$

where, y_0 and θ_0 are displacement and rotation, respectively; M and V are moment and shear force along the beam; EI is bending stiffness; and $\lambda = \sqrt[4]{k/4EI}$ is called characteristics of the system. $A_{\lambda x}$, $B_{\lambda x}$, $C_{\lambda x}$, and $D_{\lambda x}$ are shape parameters and define as follows:

$$\begin{aligned} A_{\lambda x} &= e^{-\lambda x}(\cos \lambda x + \sin \lambda x) \\ B_{\lambda x} &= e^{-\lambda x} \sin \lambda x \\ C_{\lambda x} &= e^{-\lambda x}(\cos \lambda x - \sin \lambda x) \\ D_{\lambda x} &= e^{-\lambda x} \cos \lambda x \end{aligned} \tag{4.4}$$

After dividing the pipe at A, Eq. (4.3) and Eq. (4.4) may be used to obtain the solution by enforcing continuity and smoothness at the moist-dry boundary. The required boundary conditions are indicated in Eq. (4.5)

$$\begin{aligned} & y|_{A^+} = y|_{A^-} = 0 \\ & \left.\frac{dy}{dx}\right|_{A^+} = \left.\frac{dy}{dx}\right|_{A^-} \\ & y|_{\infty^+} = \frac{\Delta}{2} \\ & y|_{\infty^-} = -\frac{\Delta}{2} \end{aligned} \tag{4.5}$$

where Δ is maximum deformation due to the free swell of the soil, which may be determined as $\Delta = (d_{az} - h) \times COLE$.

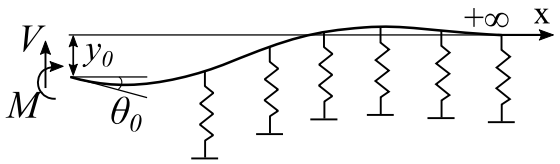

Figure 4.2: Semi-infinite beam on elastic foundation with given end displacement, y_0, and rotation, θ_0.

After applying the boundary condition, the equation of the vertical displacement along the pipe is obtained which is used further to compute the moment and flexural stresses. One of the results (200 mm diameter pit cast pipe for 3% swell capacity) is compared with the corresponding CFE simulation and the error is shown in Figure 4.3(a and b). The relative error in displacement, e_{disp}, computed from the BEF solution is shown in Figure 4.3(a). The error is expressed as a percentage and normalized by the maximum upward displacement in the pipe (i.e., $e_{disp} = 100 \times |u_{BEF} - u_{CFE}|/\Delta$), where u_{BEF} is the displacement computed from BEF solution; u_{CFE} is displacement computed from CFE simulations. A similar comparison between the curvatures obtained from the CFE simulation and the BEF solution is shown in Figure 4.3(b). In both the plots, the horizontal axis is normalized by the characteristic length of the system, $1/\lambda$, which shows the extent to which the BFE solution is accurate. From Figure 4.3(a and b), the following conclusions are made:

- The error in the displacement [Figure 4.3(a)] computed from the BEF solution as compared to CFE simulations is relatively small (the maximum difference is within 10%).
- The error in the curvature [Figure 4.3(b)] computed from the BEF solution compared to the CFE simulation is large (the maximum error is approximately 50%). Note that the curvature is directly related to estimating pipe stresses.
- In both the cases (displacement and curvature), the error is cumulated around the moist-dry boundary and dies out in roughly 3 BEF wavelengths (i.e., $\lambda x \approx 3$).
- Referring to both the figures [Figure 4.3 (a and b)], the error is not symmetric about the moist-dry soil boundary, which indicates that the pipe-soil interaction is not identical on both sides.

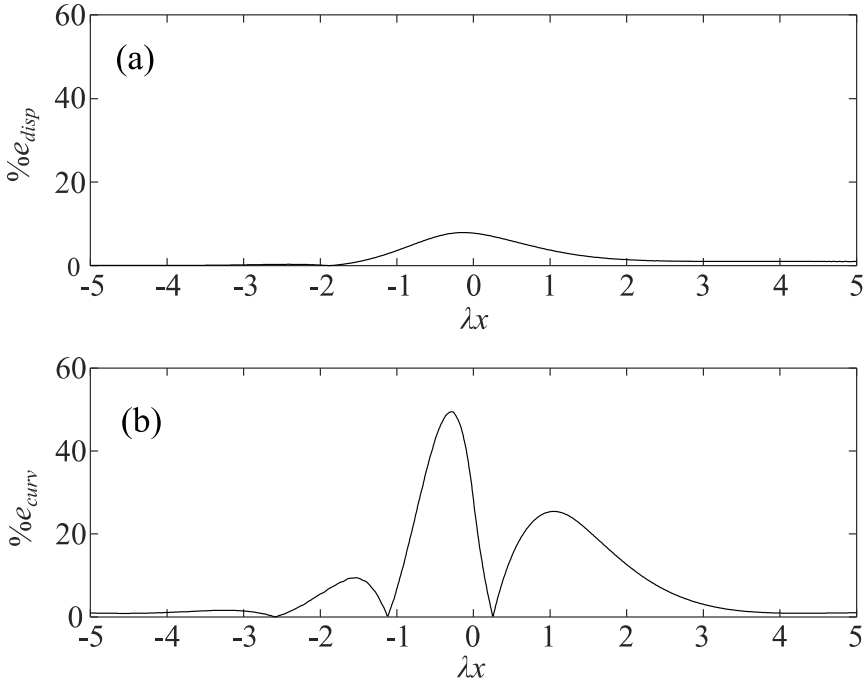

Figure 4.3: Relative error between CFE solution and BEF solution for beam on elastic foundation: (a) vertical displacement; and (b) curvature.

The preceding observations are expected. The BEF formulation is based on two key assumptions which are violated near the moist-dry boundary. The first assumption is the elastic behavior of soil. However, due to the large relative deformation near the moist-dry boundary, soil response is inelastic around the moist-dry boundary. The second assumption is the spring idealization of the soil, which is active in compression as well as in tension, whereas, in reality (and in the CFE), the soil carries only negligible tension. This behavior is captured in the CFE simulations and due to which a small distance on either side of the moist-dry boundary is unsupported (see Figure 4.4). In this region, the pipe transits from the bearing condition to the uplift condition and bends freely with no loading. This free bending occurs due to the mismatch between the stiffness of the pipe in bending and the surrounding soil. The length over which the pipe bends freely is denoted L_{free}; this quantity is used later in the development of the analytical model. The preceding observations offer insights into the pipe response (especially relative to classical solutions, such as the Hetényi solution), providing a basis for the development of a

simplified analytical model for characterizing pipe response, specifically the stresses and deflections. This is the subject of the next section.

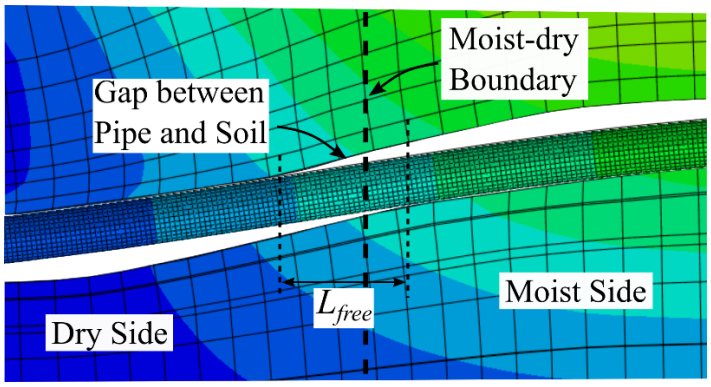

Figure 4.4: Pipe segment, L_{free}, unsupported in the vicinity of moist-dry soil boundary.

4.4 Analytical Model for the Estimation of Pipe Stress

Referring to the foregoing discussion, the analytical BEF solution follows the benchmark CFE response with reasonable accuracy in regions that are distant (i.e., more than 3 BEF wavelengths) from the boundary between moist and dry soil. On the other hand, the BEF solution is compromised in the region immediately surrounding the boundary in which the soil is subjected to plastic deformations. This disagreement can be attributed to three factors: (1) it is unable to incorporate the effect of a nonlinear soil response due to plasticity; (2) it cannot simulate the effect of multiaxial constraint/confinement on soil response; and (3) it is unable to simulate gapping, contact, and friction between the soil and the pipe. Following these observations, the simplified analytical method proposed in this study modifies the Hetenyi solution to simulate these effects.

4.4.1 Model Description

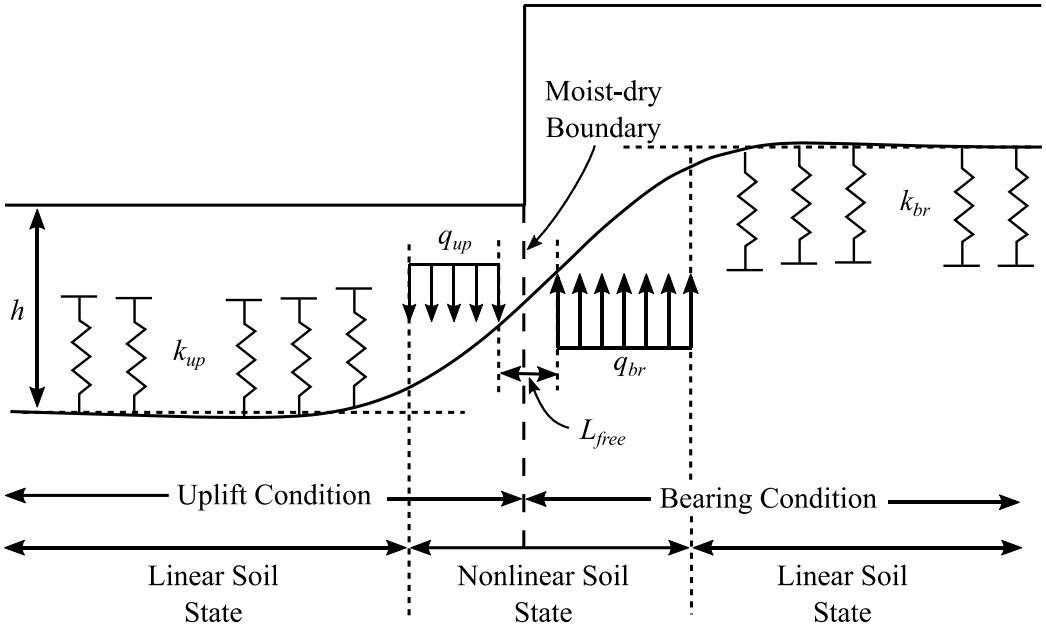

Figure 4.5: Analytical formulation of pipe-soil interaction with one-dimensional soil springs.

As shown in Figure 4.5, a straight continuous pipe is assumed to span across the moist-dry boundary. The moist-dry boundary divides the entire soil domain into two zones; to the right, the expansive soil expands and forces the pipe upwards. In response, the pipe applies a downward force on the soil creating a bearing condition. In the left zone, soil tries to counter the pipe's upward movement by applying a downward force which creates an uplift condition for the soil. Furthermore, the state of the soil (linear or nonlinear) in uplift as well as in bearing is governed by the magnitude of the deflection. The soil segment in the vicinity of the moist-dry boundary in which it changes the direction of loading (from uplift to bearing condition), hereafter referred to as transition zone, behaves nonlinearly. Within this transition zone (depending on the soil properties and magnitude of expansion), the response is assumed to be either constant due to the yielding of the soil or zero due to the free bending of the pipe (see Figure 4.4, shown previously). The response of the soil as nonlinear springs is presented next.

4.4.2 Non-linear Spring representation of soil

The soil is represented as a series of continuously distributed one-dimensional (vertical) springs (Figure 4.5) whose response is elastic-perfectly plastic, as illustrated in Figure 4.6. Referring to this figure, the response of the spring is different in uplift condition and bearing conditions. Although the actual response (force vs. displacement) is elastoplastic, it is simplified to a linearly elastic and perfectly plastic model (shown in dotted line). The spring properties (referring to Figure 4.6) are determined as per the ASCE design guidelines for pipe design [34], as subsequently described.

- In uplift condition (i.e., loading toward the free surface), the yield strength, q_{up}, is determined as

$$q_{up} = cN_{cv}D + \bar{\gamma}_s h N_{qv} D \tag{4.6}$$

  where h is depth of pipe below the ground surface; c is soil cohesion; and D is pipe outer diameter. N_{cv} and N_{qv} are uplift capacity factors that depend on the depth of pipe embedment and the angle of internal friction of soil. These parameters can be estimated from the design charts published by Committee on Gas and Liquid Fuel Lifelines [106] which is shown in Appendix B. The stiffness, k_{up}, may be determined as

$$k_{up} = \frac{q_{up}}{\Delta_{up}} \tag{4.7}$$

  The yield displacement, Δ_{up}, is generally considered independent of the pipe diameter and depends on the depth of the buried pipe [107, 108]. In the present analysis, the depth of buried pipe is a constant (i.e., 1 m). Using this depth, a yield displacement of 5 mm is determined from the aforementioned studies.

- In the similar manner, the spring properties in the bearing condition of the soil is determined. First, the yield strength in bearing, q_{br}, is calculated as follows:

$$q_{br} = cN_c D + \bar{\gamma}_s h N_q D + \frac{1}{2}\gamma_s D^2 N_\gamma \tag{4.8}$$

  where h is depth of pipe below the ground surface; c is soil cohesion; and D is pipe outer diameter. γ_s and $\bar{\gamma}_s$ are total and effective soil unit weight, respectively. N_c, N_q,

and N_γ are Meyerhof's bearing capacity factors for horizontal strip footing [109]. The Meyerhof's bearing capacity design equations are given in Appendix B. Once q_{br} is known, the spring stiffness k_{br} can then be determined as follows:

$$k_{br} = \frac{q_{br}}{\Delta_{br}} \tag{4.9}$$

The yield displacement, Δ_{br}, is generally considered proportional to D (i.e., $0.01D$ to $0.015D$ for both sand and clay) [34].

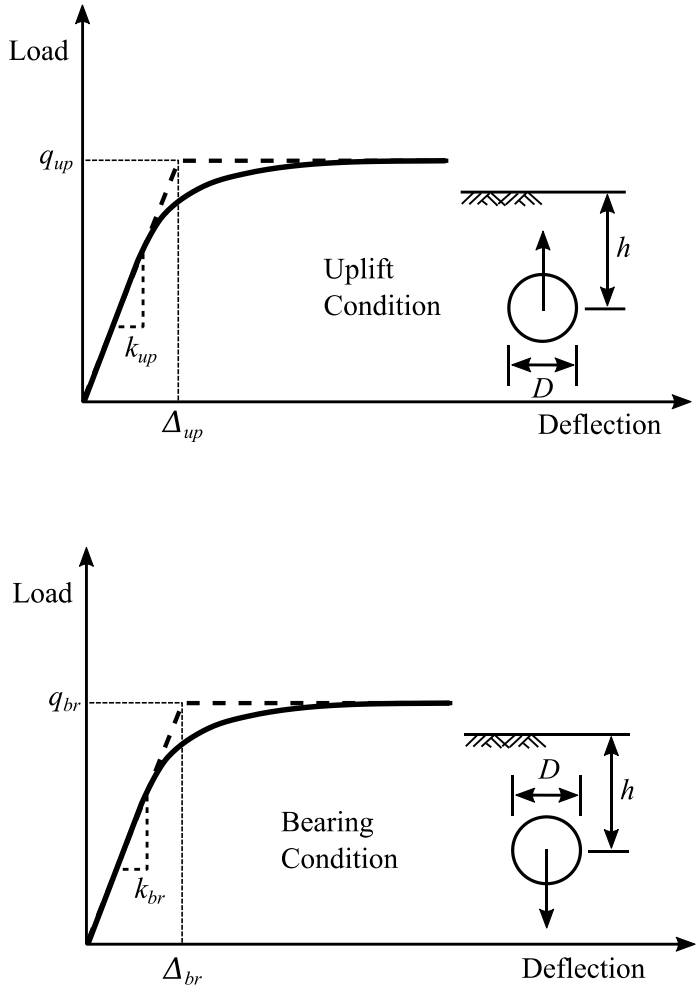

Figure 4.6: Load-displacement relationship of soil springs in uplift and bearing state of soil.

4.4.3 Solution Methodology

The proposed analytical model is a two-dimensional approximation of the three-dimensional pipe-soil interaction problem due to which the formulation of this model requires certain approximations. One of the approximations is idealizing the soil response using one-dimensional springs whose behavior is discussed in the previous section. Besides that, the pipe is represented as an Euler-Bernoulli beam, whose response is linear, with the equivalent cross-sectional area and moment of inertia. Furthermore, the pipe stresses caused by soil overburden are not considered in the analytical formulation. The CFE simulations confirmed that these stresses are very small compared to the stresses caused by soil expansion (around 1%).

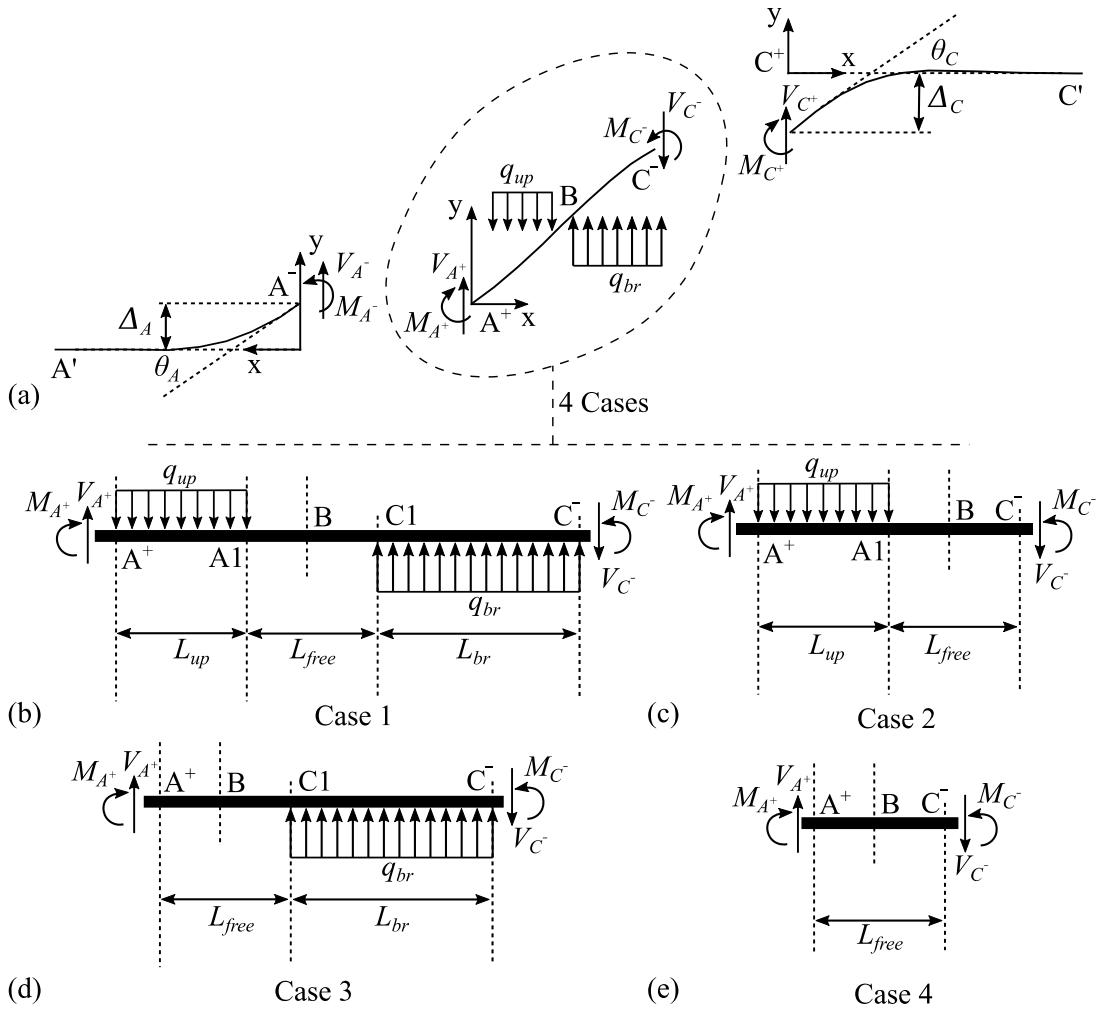

Figure 4.7: (a) Free body diagram of exploded view of two-dimensional idealization; and (b–e) load cases on pipe segment ABC.

Following these idealizations, Figure 4.7(a) illustrates that the pipe may be notionally divided into three segments: the two semi-infinite far-field segments in which the soil behavior is elastic; and the segment in the vicinity of the boundary (transition zone) in which the soil response is plastic. Within this transition zone (depending on the soil properties and magnitude of expansion), the pipe experiences either a constant load due to the plastic behavior of the soil or no load due to the free bending of the pipe (see Figure 4.4, shown previously). The free bending or gapping between pipe and soil occurs in the immediate vicinity of the moist-dry boundary. Figure 4.8

provides a flowchart that schematically illustrates the process for this solution. Key elements are summarized below:

1. Referring to Figure 4.7(a), the segments (A'A^- and C^+C') are equivalent to a semi-infinite beam on elastic foundation (see Figure 4.2) in two different coordinate orientations with given end displacement, $\Delta_{A/C}$, and rotations, $\theta_{A/C}$,. They are solved using Eq. (4.4) and Eq. (4.5) for end unknowns (moment and shear force) at point A and C as a function of Δ and θ. However, the locations of Points A and C (i.e., their distances with respect to the moist-dry interface, Point B) are still unknown.

2. The distances, L_{up} and L_{br}, are evaluated by determining the deformation profile of middle segment ABC (transition zone), and then enforcing continuity and differentiability of the deformation profile at Points A and C.

3. Based on the magnitude of the soil expansion and spring properties, the transition zone may have four types of loading cases [shown schematically in Figure 4.7(b–e)]. These cases are:

    - Case 1 [Figure 4.7(b)]: fully formed plastic zones on both the moist and the dry sides of the interface, surrounding the free bending zone.

    - Case 2 [Figure 4.7(c)]: a fully formed plastic zone only on the dry side of the moist-dry interface. This case is common [34] because the yield strength of soil in the uplift condition (on the dry side in which the soil gets pushed upwards toward the free surface) is lower than that of the bearing condition.

    - Case 3 [Figure 4.7(d)]: fully formed plastic zone only on the moist side of the moist-dry interface; this is an unlikely condition, albeit included in this study for completeness.

    - Case 4 [Figure 4.7(e)]: free bending over the entire length of the transition zone; this is likely to occur for low levels of soil expansion. In this case, the length of the transition zone is exactly equal to L_{free}.

For each of these cases, the deformation profile of the pipe within the transition region is determined using the Euler-Bernoulli beam theory in terms of the unknowns L_{up}, L_{br} (defining the location of Points A and C and the length of the transition zone), and the displacements and rotations at the ends of the transition zone (i.e., Δ_A, Δ_C, θ_A, and θ_C). For each case, this results in a system of six equations (corresponding to the enforcement of equilibrium and continuity/smoothness at each end of the transition zone) and six unknowns (corresponding to deflections, rotations, and length of the transition zone), which may be obtained by solving the equations simultaneously. For a given set of input parameters, the solution must be exclusive, i.e., governed by only one of the cases previously discussed, and should be unique within that case. The definition of each case in Figure 4.7(b–e) imposes physical constraints that may be utilized to solve the system and demonstrate the exclusiveness of the solutions. Specifically, referring to Figure 4.7(b–e), the following is observed:

- In Case 1, the unknown deflections at Points A and C must equal Δ_{up} and Δ_{br}, respectively, and L_{up}, L_{br} must be positive.
- In Case 2, the unknown deflection at Point A must be lower than Δ_{up}, and the deflection at Point C must equal Δ_{br}. Furthermore, L_{up} must equal zero, and L_{br} must be positive.
- In Case 3, the deflection at Point A must equal Δ_{up}, and at Point C, it must be lower than Δ_{br}. Additionally, the unknown L_{up} must be positive while L_{br} must equal zero.
- In Case 4, the unknown deflections at Points A and C must be less than Δ_{up} and Δ_{br}, respectively, and L_{up}, L_{br} must equal zero.

The nonoverlapping domain of the unknowns, as previously explained, ensures that only one case will govern the solution. Further, the uniqueness of the solution within a case, obtained by solving higher order polynomials of unknowns, may be verified using the Descartes' rule of signs [110], which indicates the number of positive real roots of a polynomial. Once the unknowns (L_{up}, L_{br}, Δ_A, Δ_C, θ_A, and θ_C) are determined, the entire deformation profile may be generated. Next, the curvatures may be determined by the differentiation of this deformation profile, ultimately allowing for the calculation of longitudinal stresses in the pipe.

A MATLAB program [111] is developed to solve the pipe response. The solution algorithm and code are provided in Appendix C. This program requires roughly 1/1,000 of the time required to execute the CFE solutions (~8 s per solution) to obtain output quantities that are analytical counterparts to the CFE solutions. Note that the CFE simulations were performed on a Windows server running two Intel Xeon Processor CPU E5-2630 (with a base frequency of 2.2 GHz), and the simulation time for a single case was approximately 4.5 h.

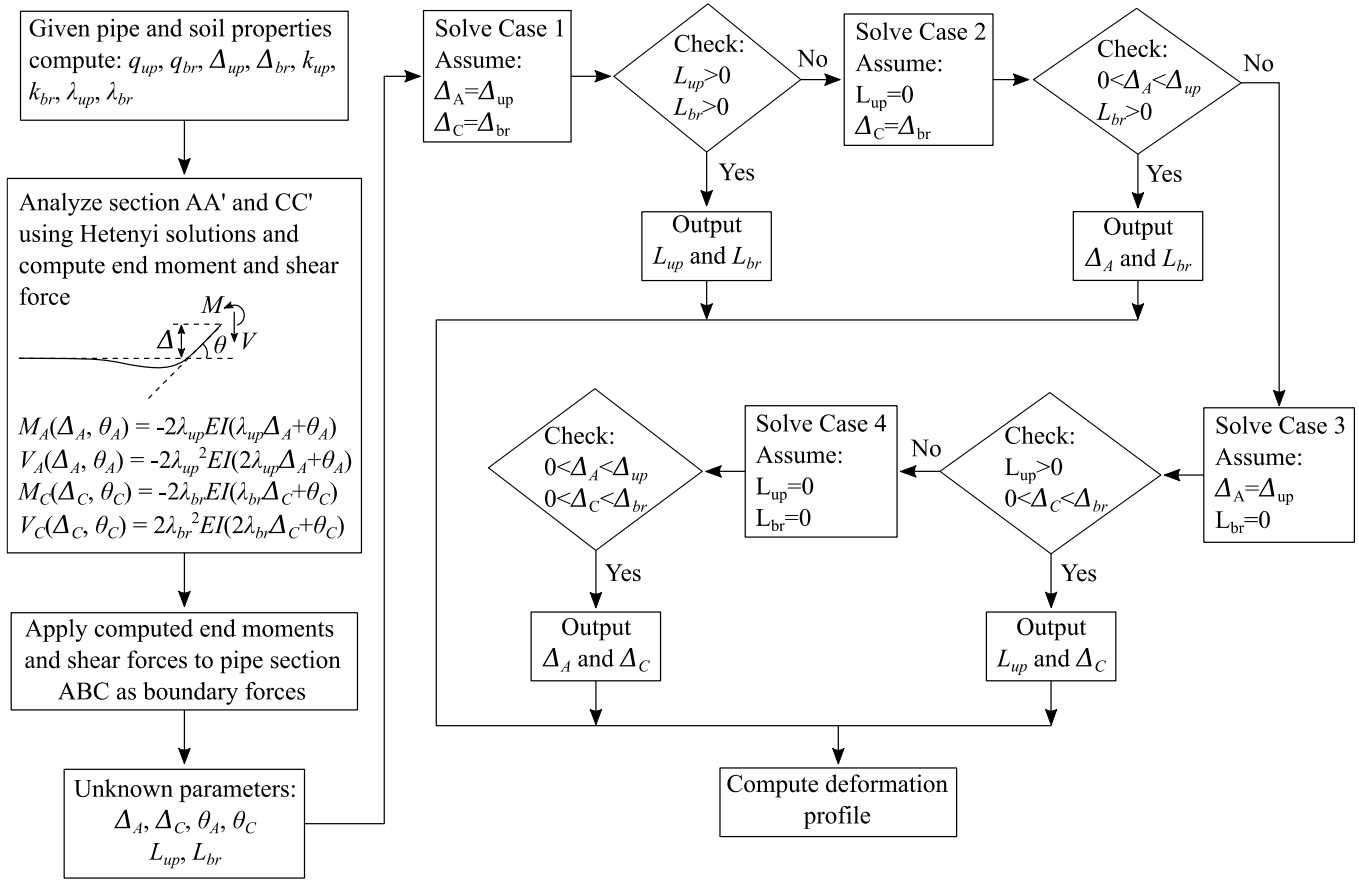

Figure 4.8: Flow chart for solution algorithm.

4.4.4 Characterization of L_{free}

As mentioned earlier, the term L_{free} representing the free bending length of the pipe in the vicinity of the moist-dry interface (Figure 4.4) must be estimated to facilitate the solution process previously outlined. L_{free} is determined from CFE simulations for each of the 80 parameter combinations summarized in Chapter 3. It is observed that L_{free} is strongly correlated with two configurational parameters, i.e., the pipe diameter, D, and the percentage expansion, s_{exp}. The following relationship is proposed to express L_{free} as a function of D and s_{exp}.

$$L_{free} = 0.0403 - 0.23D + 0.082s_{exp} - 0.077Ds_{exp} - 0.004{s_{exp}}^2 \qquad (4.10)$$

This relationship is developed by first estimating (from the CFE model) the values of L_{free} for all the configurational parameters, resulting in a discrete mapping between these parameters and L_{free}. This discrete mapping is used to perform a regression fit (with the coefficient of determination 0.95), shown in Figure 4.9, resulting in the relationship shown in Eq. (4.10).

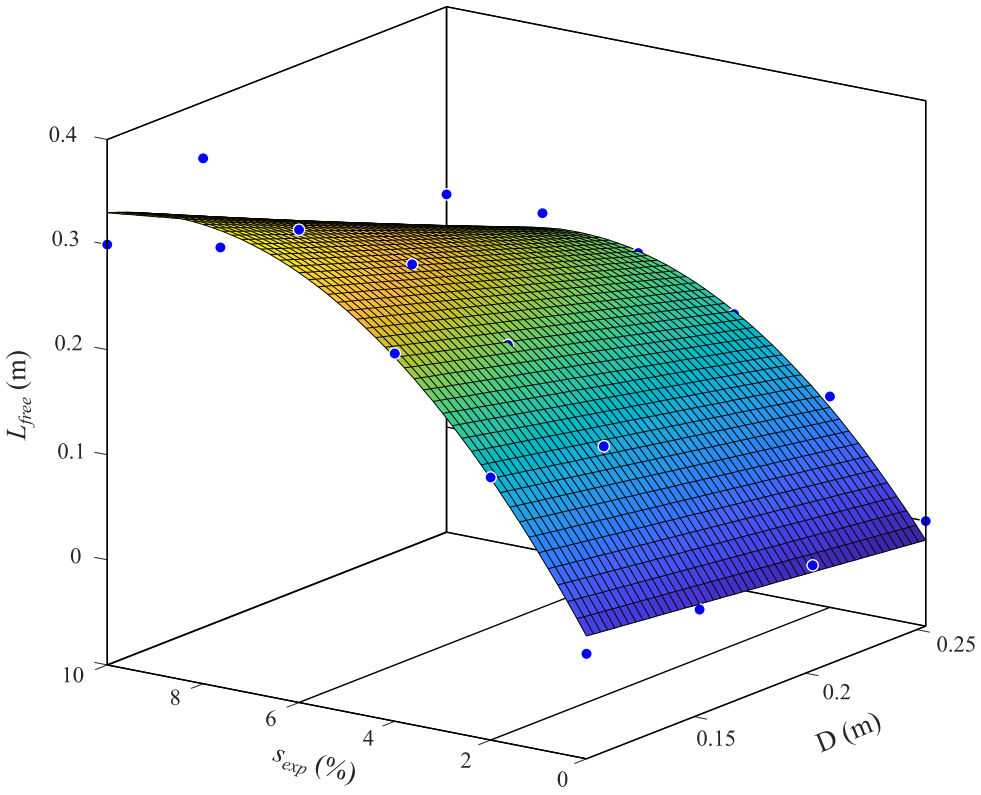

Figure 4.9: Analytical formulation of pipe-soil interaction with one-dimensional soil springs.

4.4.5 Results

Typical results for different diameter of pipes in different soil swell conditions are shown in Figure 4.10. Figure 4.10(a) shows the soil loading on the pipes due to soil expansion. With the increase of soil expansion, the nonlinear region in the vicinity of moist-dry boundary is increasing (0 of the x-axis locates the moist-dry boundary); however, in majority of cases, the bearing side of the soil is predominantly elastic. Figure 4.10(b) plots the deformation profile of the pipes. As expected, the pipe deformation is similar in all the pipes experiencing the same expansion. However, it can be seen that the curvature is significantly different in different diameter pipes (curvature is important from the standpoint of estimating pipe stresses). The bending moment and shear profile of the pipes are shown in Figure 4.10(c) and Figure 4.10(d), respectively. Small diameter pipes are more susceptible to failure because they experience higher bending moment and shear as compared to large diameter pipes, for the same swell.

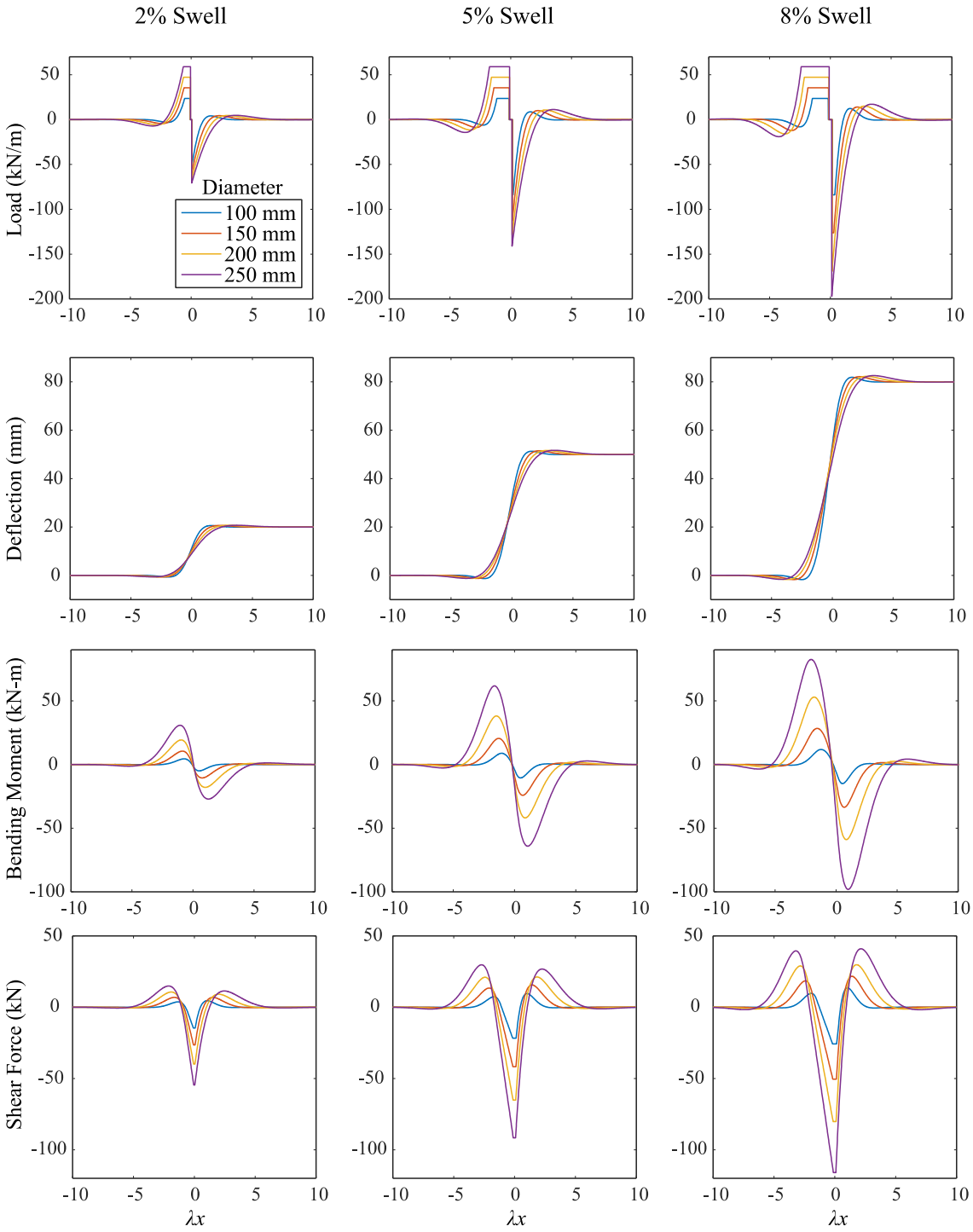

Figure 4.10: Soil loading, displacements, bending moment, and shear force versus normalized pipe axial coordinate x.

4.5 Assessment of the Analytical Model Against the CFE Results

The proposed analytical solution method readily solved the pipe response without involving numerical methods such as CFE simulations; however, several simplifications are adopted. These simplifications significantly reduced the computational need but at the cost of compromised accuracy. To examine that, the proposed methodology is assessed against the results of 3D non-linear CFE simulations presented in Chapter 3. Figure 4.11 and Figure 4.12 show the comparison of the numerical results to the corresponding analytical predictions for 12 of the simulations, spanning a range of pipe diameters and soil expansion magnitudes. Figure 4.11 shows the comparison in terms of the variation, with normalized distance (λx) from the moist-dry boundary, of pipe displacement along its length. A good agreement (test-to-predicted ratio is 1.034) is observed for pipes with various diameters (100mm, 150mm, 200mm, and 250mm) and swell capacity (1%, 5%, and 9%). Figure 4.12 shows the comparisons between the analytical and CFE estimates of pipe curvature for the same pipe diameter and swell capacity. There is good agreement between curvatures which serves as a proxy for pipe longitudinal strain. Referring to these figures, the following observations may be made:

- On average, the displacement and curvature profiles from the analytical solutions agree well with their counterparts from the CFE simulations. Although shown only for 12 cases (a combination of four diameters and three swell capacity), such agreement is observed for all pipe sizes, soil properties, and magnitudes of soil expansion.
- The agreement between analytical and CFE results is noted over the entire length of the pipe, particularly in the region near the moist-dry boundary. This is encouraging when contrasted with the results of the BEF solution (Figure 4.3), which is unable to characterize pipe stresses in this region with similar accuracy.

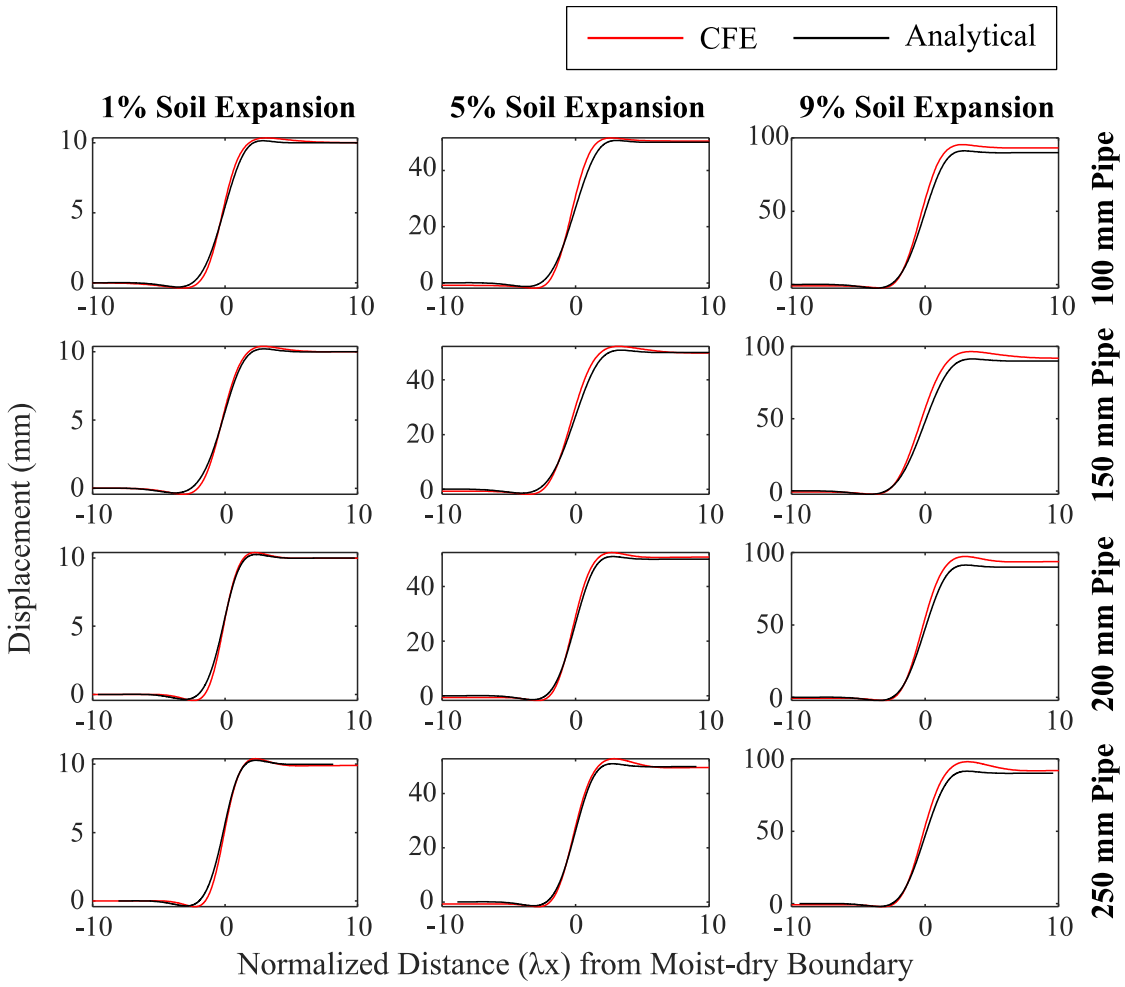

Figure 4.11: Comparison of displacement profiles as determined from the current method with those from the CFE simulations.

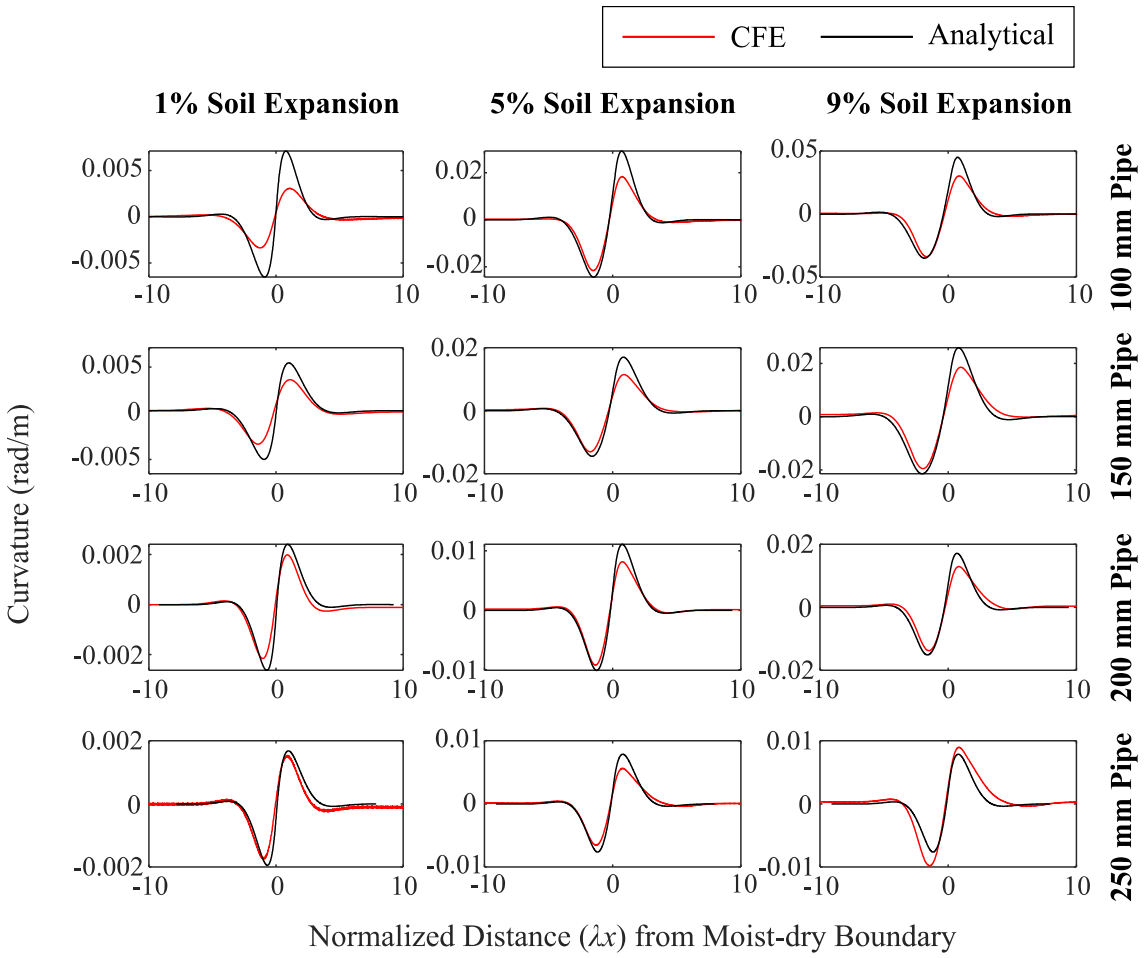

Figure 4.12: Comparison of curvature profiles as determined from the current method with those from the CFE simulations.

Figure 4.13 plots peak longitudinal stress as determined from the analytical model versus their CFE counterparts. In this figure, different diameters of the pipe are identified by different markers, and the color of the marker indicates the relative magnitude of the soil expansion (ranging from 0% to 10%). Referring to the figure, the agreement between the two is remarkable (the majority of the points lie within the 15% error envelope); the average value of $\sigma_{peak\ CFE} = \sigma_{peak\ analytical}$, i.e., the test-to-predicted ratio is 0.96 with a standard deviation of 0.097. No discernible bias in this ratio is observed when subsamples (e.g., pipe diameters and magnitude of soil expansion) are examined. Based on these observations, the analytical model may be used as an effective proxy for CFE simulations for estimating pipe stresses in the idealized problem of a pipe crossing a

moist-dry soil interface. The stresses estimated by this model may be compared to estimates of pipe failure stress to assess the vulnerability of pipe segments within a water distribution network which is the subject of the next chapter.

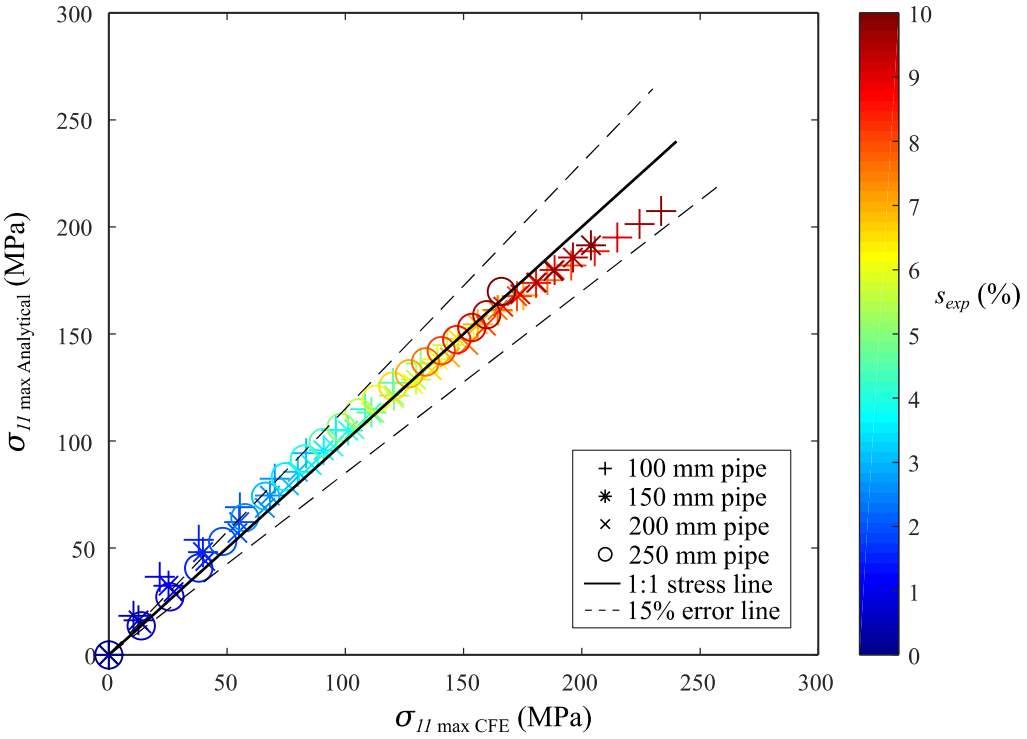

Figure 4.13: Estimated maximum bending stress from the proposed method and the CFE simulations.

4.6 Summary

In this chapter, an analytical formulation to characterize flexural stresses in pipes subjected to moisture-induced soil expansion is presented. The proposed approach involves: (a) examining the pipe-soil interaction using the linear BEF model and the readily available Heténi solution which confirms a large error around moist-dry boundary; (b) development of a simplified analytical model with nonlinear soil response and gapping/contact between the pipe and soil; and (c) validation of this model against CFE simulations.

The proposed analytical model is an adaptation of classical solutions for beams on elastic foundations because these solutions alone are not sufficient to characterize the pipe response in the present context. To prove this, the problem is posed as the BFE model, and the pipe response is obtained using Hetényi solutions with appropriate boundary conditions. The pipe responses are then compared with the corresponding CFE simulations which showed that the BFE approach is not adequate. The solutions exhibited a large error near the moist-dry boundary because the soil nonlinearity and gapping between pipe and soil are not considered. These observations offered insights into the pipe response and provided a basis for the development of an analytical model that can characterize pipe responses accurately. Following this, a simplified analytical model is proposed based on modifications to the Hetenyi solution which include: one dimensional (vertical) springs representation of the soil whose response is elastic-perfectly plastic; different response of these springs in the upward direction (uplift condition), and the downward direction (bearing condition); and inclusion of free bending of the pipe due to gapping. The model is validated against a suite of continuum finite-element simulations, demonstrating that it can reproduce flexural stresses in a range of pipe and soil configurations with good accuracy and in a fraction of the computational time. The final outcome is a computationally inexpensive approach to compute pipe stresses given various pipe and soil characteristics. This approach may be conveniently used within a decision support framework for asset management and the prioritization of replacement of large networks.

The proposed analytical approach however has several limitations that arising from the standpoint of balancing practicality with accuracy; these must be considered in the interpretation and application of this model. The model assumes the boundary between the moist and dry regions (moist-dry boundary) is abrupt (vertical) and the pipe is perpendicular to this boundary. Although this boundary and pipe configuration constitute the most conservative case, a significant reduction in stresses may be possible for other configurations. Furthermore, the model formulation assumes, in the process of expansion, the soil will attain a full saturation. However, the soil may exist in the partially saturated condition which may affect the magnitude of total expansion and consequently overestimate the pipe stresses. Notwithstanding these limitations, the analytical approach outlined in this chapter offers a simplified way to determine the vulnerability of a pipe segment, given its characteristics.

Chapter 5

Fracture Risk of Corroded Cast-iron Pipes in Expansive Soils

In the previous two chapters, an analytical model to predict circumferential fractures in cast iron pipes due to moisture-induced soil expansion was developed (Chapter 4) and validated by a suite of continuum finite-element simulations that simulated detailed interactions between the pipe and soil (Chapter 3). The model combined a classical beams-on-elastic-foundations solution with empirical modifications to capture material and interaction nonlinearity. The model has demonstrated its ability to reproduce flexural stresses in a range of pipe and soil configurations with remarkable accuracy and in a fraction of the computational time compared to those of continuum models.

The main motivation for developing the analytical model is to capture the key quantities of the mechanics of complex pipe-soil interaction in a computationally simple way. This enables the assessment of fracture risk through a probabilistic interpretation which can later be used in a decision support framework at city or regional scales. To start with, this chapter computes the failure probability of a pipe crossing a moist-dry boundary. Later in this chapter, the failure probabilities of a pipe crossing multiple boundaries are combined to compute network risk which is further utilized to develop a decision support framework for pipe replacement using risk-cost optimization. The computation of failure probability needs a rigorous consideration of

uncertainties in various inputs, and the model itself. Besides, the probabilistic interpretation is important for two reasons: (1) to characterize the uncertainty in output/response quantities of interest (e.g., the failure probability of a pipe segment) and perhaps more importantly (2) to assess which model inputs (and uncertainties thereof) have the most significant impact on response estimation. The latter is particularly important from the standpoint of making targeted investments in data collection, mapping, as well as model development and refinement. Currently, water industries rely on simplistic replacement prioritization, e.g., the oldest pipes are the most at risk [10]. The risk-based decision support framework that goes beyond such rudimentary prioritization schemes is necessary to identify and prioritize the most at-risk segments of a network.

In this chapter, a probabilistic framework for the assessment of pipe-soil systems vulnerable to fracture caused by a combination of pitting corrosion and moisture-induced soil expansion is developed. The framework builds upon the previously developed pipe-soil interaction model to characterize the overall risk. The framework has two parts – one pertaining to the characterization of "demand" stresses in the pipe due to soil expansion and pipe flexure, and the other pertaining to "capacity" stresses that deteriorate over time as per a fracture mechanics model based on corrosion. The sources of uncertainty in both these components are rigorously analyzed and characterized. Additionally, the errors in both models—the mechanistic model proposed in the previous chapter and the corrosion model are incorporated into the analysis. The Monte Carlo procedure is implemented to synthesize various uncertainties into a probabilistic estimate of the failure of a pipe segment, defined by its configurational parameters and age. In the end, a sensitivity analysis is performed to examine the influence of various inputs (and their uncertainties) on the estimated response.

The chapter is organized as follows. First, the pipe strength capacity is characterized which includes corrosion rate models and the application of these models to characterize pipe strength using linear fracture mechanics. Next, the various uncertainties present in the demand and capacity models are characterized. The vulnerability of a pipe segment is then determined rigorously by formulating a limit state function and then calculating the probability of failure through Monte Carlo simulation. Finally, the results are discussed with a specific emphasis on the sensitivity of the results due to various uncertainties. The limitations of this work are outlined.

5.1 Degradation Model and Pipe Stress Capacity

5.1.1 Damage Mechanism: Corrosion

Corrosion of the pipe wall in cast iron pipes is the primary deterioration mechanism, leading to the lowering of its load-carrying capacity over time, eventually leading to failure. Pipes corrode externally as well internally; however, the rate of external corrosion, specifically pitting corrosion, is faster and hence of primary concern in underground pipes [76]. Furthermore, pitting corrosion in cast iron is a self-inhibiting process that slows down over time. This is commonly referred to as graphitization in which iron leaches out from the iron-graphite matrix of cast iron leaving behind graphite that naturally inhibits corrosion [75]. As discussed in Chapter 2, several models have been proposed to estimate the growth of corrosion pits over time. In this study, two models, AWWA corrosion model [3] and power law model [112], are of particular interest because they are specifically developed for cast iron pipes in buried conditions.

AWWA corrosion model

AWWA corrosion model is commonly used for estimating pit depths. The model simulates the self-inhibiting nature of the external pitting corrosion due to graphitization through the saturation (or limiting) of pitting depth for aged pipes. This model assumes two different corrosion rates – a fast exponential growth at an early age that signifies the availability of iron for corrosion and relatively slow linear growth subsequently to represent corrosion inhibition due to leftover graphite. This model is fitted over measured pit depths from over 43 exhumed pipes that represent a range of soil chemistries (redox potential, resistivity, pH, sulfide, and chloride ion content), ages, groundwater level, and seasonal changes. Figure 2.9 illustrates this regression fit as well as the scatter data from which it is generated. Eq. (2.3) shows the expression for this fit.

$$d_{max} = 3d_{avg} = 0.0125t + 5.85(1 - e^{-0.058t}) \tag{5.1}$$

where, t is the age of the pipe (in years); d_{max} (mm) is maximum corrosion pit depth; and d_{avg} (mm) is average corrosion pit depth.

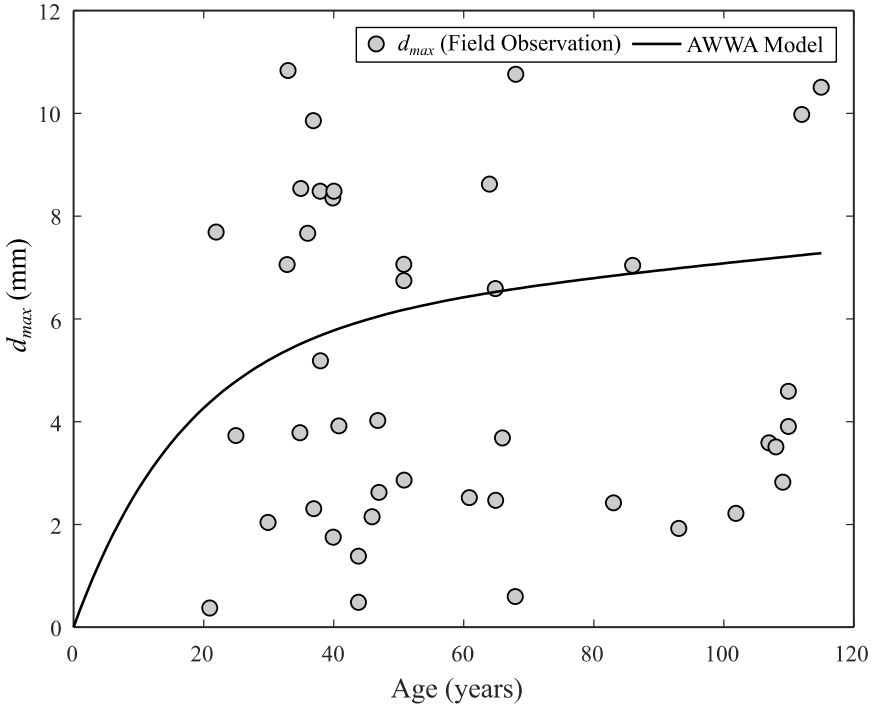

Figure 5.1: AWWA corrosion model for maximum pit depth.

The model is statistically "best-fit" to the average pit depth data, and the maximum pit depth is computed by applying an average "pitting factor" of 3 which is the ratio of the deepest pit depth and the average pit depth obtained from measurements. It is worth noting that the above model does not depend on soil properties and gives an average sense of their influence. However, it is popular due to its simplicity, using age as the sole indicator of pipe deterioration.

Power law corrosion model

The power law model, which was first postulated by Kucera and Mattsson [113], is a widely accepted model of corrosion to measure the depth of corrosion pits in buried structures. The model can be expressed as follows:

$$d_{pit} = kt^n \tag{5.2}$$

where t is the age of the pipe (in years) and d_{pit} (mm) is corrosion pit depth. The factors k and n are pitting proportionality and exponent factors, respectively. Generally, k and n are time-independent and can be determined by data fitting measured corrosion data over exposure time.

It has been observed that these two parameters and strongly correlated with soil properties, specifically with the aeration level of the soil [114]. From Wang et al. [114], the k and n range for different soil condition are shown in Table 5.1.

Table 5.1: k and n values for different soil groups based on aeration.

Soil Group	k	n
Good Aeration	0.759-0.957	0.735-0.795
Fair Aeration	0.746-0.893	0.484-0.560
Poor Aeration	0.762-0.958	0.681-0.755
Very Poor Aeration	0.354-0.392	0.922-0.968

5.1.2 Estimation of Stress Capacity

Using the corrosion model presented above, the failure stress (stress capacity) of a pipe segment can be estimated using linear fracture mechanics [85, 115]. Corrosion pits can be assumed to behave as localized semicircular cracks [86, 116], see Figure 5.2(b), leading to stress concentration at or around the tip of the pit and controls the fracture of the pipe. According to the linear theory of fracture mechanics, when the pipe surface contains a sharp crack (in this case corrosion pit), the stress field ahead of the sharp crack can be defined using a single factor, known as stress intensity factor K_I (see [117]). A fracture occurs when this parameter exceeds a critical value K_{IC}, which is a material constant representing the fracture toughness of the material. The corresponding stress corresponds to the failure stress capacity (σ_{fail}), which is defined as follows:

$$\sigma_{fail} = \frac{K_{IC}}{F}\sqrt{\frac{2.464}{\pi a}} \tag{5.3}$$

where a represents the radius of a semicircular crack which can be assumed to be equal to d_{max}, F is the boundary-correction factor, which is a function of crack radius and pipe diameter and thickness, whose value for a semicircular surface crack (corrosion pit) in pipes subjected to bending was provided by Raju and Newman [118] (see Table 5.2).

Table 5.2: Boundary-correction factors from Raju and Newman [118].

$\frac{r}{th}$	$\frac{a}{th} = 0.2$	$\frac{a}{th} = 0.5$	$\frac{a}{th} = 0.8$
1	1.136	1.162	1.233
2	1.137	1.188	1.287
4	1.133	1.204	1.327
10	1.131	1.212	1.348

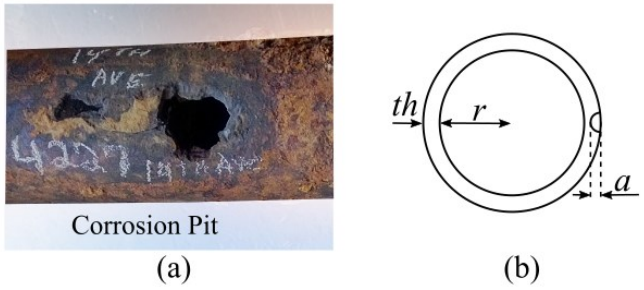

Figure 5.2: (a) Corrosion pit and (b) its idealized representation.

To predict fracture using this method, K_{IC} for cast iron must be determined. AWWA [3] has reported K_{IC} values for North American cast iron pipes using the Charpy Impact Test. This test involves breaking a standardized specimen with a pendulum and measuring the energy released in the fracture. The K_{IC} values for pit cast and spun cast pipes with the 5% and 95% envelope from the AWWA [3] are summarized in Table 5.3.

Table 5.3: Different empirical methods proposed in literature.

Type	K_{IC} (MPa√m)		
	5% bound	Median	95% bound
Pit Cast	7.4	9.7	13.5
Spun Cast	10.7	13.5	15.1

Using the pipe geometry information along with K_{IC} values, pipe capacity stresses as a function of time can be generated as shown in Figure 5.3 and Figure 5.4 for the AWWA corrosion model and power law model. Referring to these figures, as expected, the stress capacity reduces with pipe age as the corrosion pits increase with time; however, the rate of decrease is not similar for both

the corrosion models. The stress capacity computed from the AWWA corrosion model saturates after some time whereas the stress capacity steadily decreases when the power law corrosion model is used. The figures demonstrate stress capacity for median K_{IC} material strength for pit-cast and spun-cast pipe, thus illustrating the strength differences between the materials.

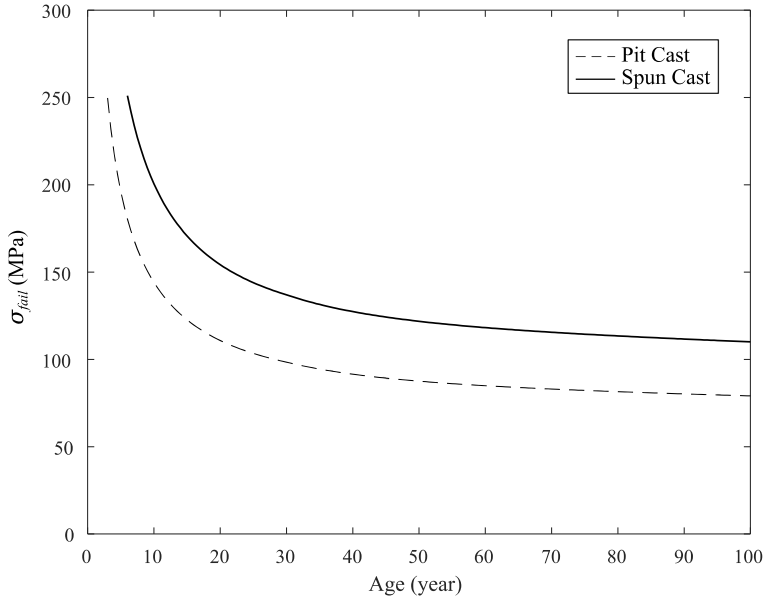

Figure 5.3: Estimated flexural stress capacity of 200 mm pipe, assuming AWWA corrosion model.

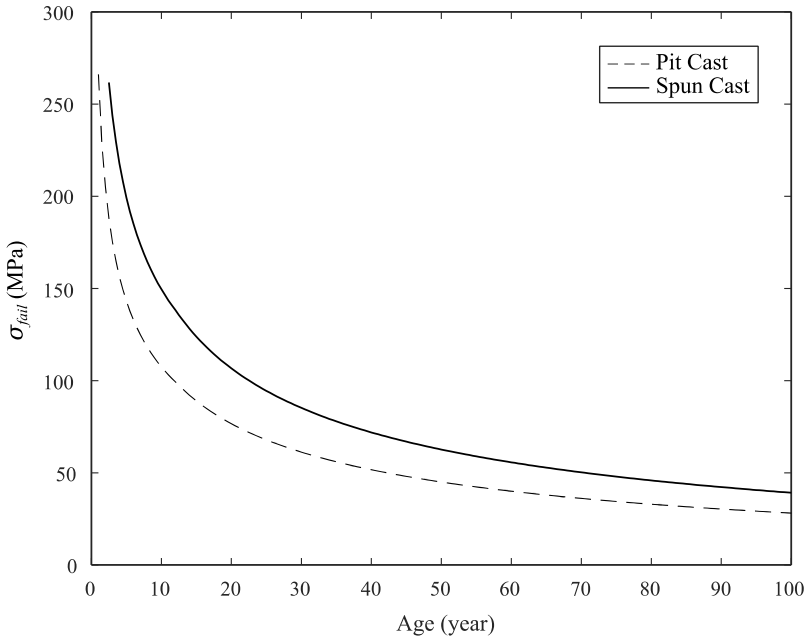

Figure 5.4: Estimated flexural stress capacity of 200 mm pipe in poor aerated soil, assuming power law corrosion model.

5.1.3 Pipe Stress Capacity: Uncertainty Characterization

The previous section effectively estimates the failure stresses in pipes across a range of configurations such as pipe geometry, material, and amount of deterioration as compared to CFE simulations. Once the pipe failure stress (i.e., capacity) is determined, it may be compared to the demand stress (from the analytical model developed in Chapter 4) to estimate the vulnerability of a given pipe segment in terms of the probability of failure. A calculation of this probability requires a characterization of the uncertainty (or probability distributions) that define the capacity; this includes uncertainty in model inputs (i.e., material and geometric properties and deterioration parameters) as well as the uncertainty associated with the model itself. This is presented next.

As discussed previously, the AWWA corrosion model [Eq. (5.1)] is derived from regression fitting to the recorded pit depth data from field failed pipes. The data encompassed various soil chemistries (redox potential, resistivity, pH, sulfide, and chloride ion content), age, groundwater level, and seasonal changes. However, the fitted model [Eq. (5.1)] is associated with large scatter (see Figure 5.1), which translates to large uncertainty in the model predictions. To capture this

uncertainty, pipes are divided into five groups based on their age. For each group, it is assumed that the pit depth is normally distributed with the mean value represented by Eq. (5.1) and co-variance values evaluated from the recorded data. The resulting mean and covariance values are shown in Table 5.4. The distribution of each age-group, as shown in Figure 5.5, is truncated between 0 and pipe thickness to reflect the physical constraints. Note that this formulation inherently assumes that corrosion pits are not time correlated.

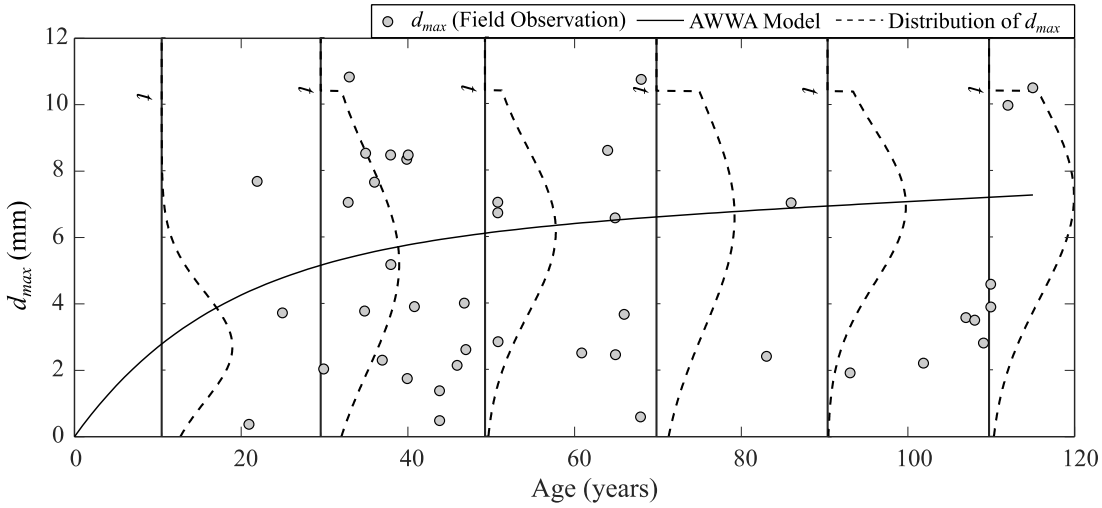

Figure 5.5: Statistical evaluation of AWWA corrosion model.

Table 5.4: Statistical information of parameters of AWWA corrosion model.

	d_{max}	
Pipe Age Group	Mean (mm)	COV (%)
0-20 year	From Eq. (5.1)	61.3
20-40 year		61.3
40-60 year		40.7
60-80 year		51.8
80-100 year		33.2
100-120 year		41.8

Similarly, the pitting proportionality and exponent factors, i.e., k and n, of the power law corrosion model are typically a function of the soil embedment and are modeled as random variables. As pointed out by Wang et al. [116] after statistically analyzing 208 sets of corrosion data that covers a wide range of soil properties, the best-fitted distributions for the proportionality and exponent factors are a 3-parameter (3P) lognormal distribution and Generalized Extreme Value (GEV) distribution, respectively. The distribution parameters are shown in Table 5.5. Furthermore, it was shown that k and n are correlated with the correlation coefficient of (ρ) -0.55. To account for this correlation, rather than assuming k and n as random variables, k is converted in terms of n using the correlation coefficient and probability distribution of n. The relation between two correlated random variables following a distribution can be represented as follows:

$$Y = \rho X + \sqrt{1-\rho^2}X^* \tag{5.4}$$

where X and X^* are independent random variables following the same distribution and Y is another random variable correlated (correlation coefficient ρ) with X [119]. Following Eq. (5.4), k can be written as

$$k = \rho n + \sqrt{1-\rho^2}n^* \qquad [n, n^*: GEV] \tag{5.5}$$

Substituting the Eq. (5.5) in to Eq. (5.2)

$$d_{pit} = \left(\rho n + \sqrt{1-\rho^2}n^*\right) t^n \qquad [n, n^*: GEV] \tag{5.6}$$

The distribution and distribution parameters of k and n are shown in Figure 5.6 and Table 5.5, respectively.

Table 5.5: Statistical information of parameters of power law corrosion model.

		Parameters		
Factors	Distribution	Shape	Scale	Location
n	GEV	0.292	0.620	-0.282
k	3P-Lognormal	0.987	0.711	0.031

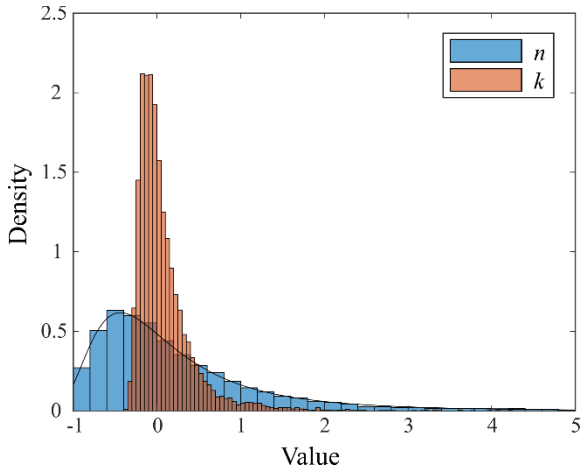

Figure 5.6: Probability distribution of n and k.

Furthermore, the parameters associated with the fracture mechanics idealization of corrosion pitting are also random. The fracture toughness parameter, K_{IC}, depends on the quality control of the material casting process. In several areas (e.g., the City of Sacramento), cast iron pipes are more than 100 years old [2], and CIPRA [17] notes that the two common casting methods—pit cast and spun cast—existed at that time. The probability distribution and its parameters associated with K_{IC} are obtained from the experimental study conducted by AWWA [3] on field recovered pit-cast and spun-cast iron pipe samples. The distribution and its parameters are taken from AWWA [3] and are shown in Table 5.6 and Figure 5.7.

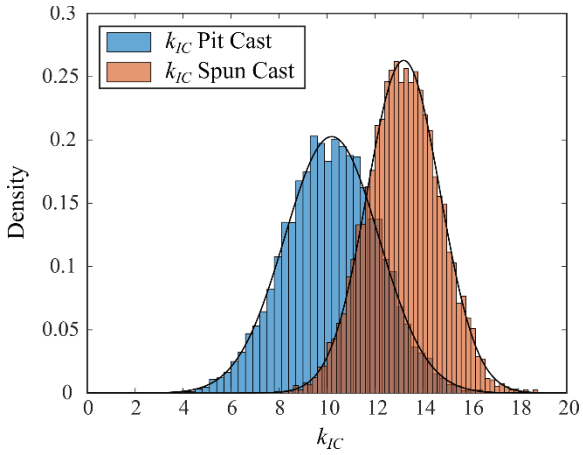

Figure 5.7: Probability distribution of k_{IC}.

Apart from these sources of uncertainty, the fracture mechanics idealization of pitting corrosion may itself be a source of error. This is modeled using a multiplicative random variable α_{cap}, defined as the ratio of model predictions to the true values. The stress demand (σ_{cap}) can then be defined in terms of this random variable (called model uncertainty) as:

$$\sigma_{cap} = \alpha_{cap}\sigma_{fail} \tag{5.7}$$

However, due to the lack of supporting data, it is assumed that α_{cap} is normally distributed with mean 1.0 and COV 10 %. The impact of α_{cap} on failure predictions is assessed later.

Table 5.6: Statistical information of parameters K_{IC}.

	K_{IC} (MPa√m)		
Type	Mean	COV	Distribution
Pit Cast	10.2	19.3	Normal
Spun Cast	13.2	11.5	Normal

5.2 Pipe Demand Stress due to Moisture-induced Soil expansion: Uncertainty Characterization

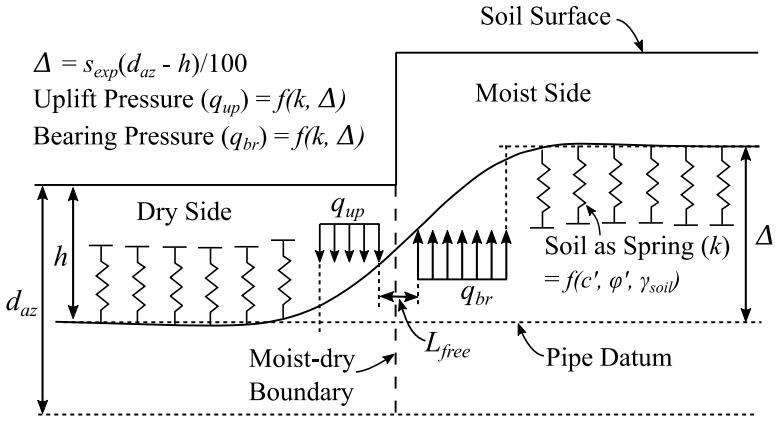

Figure 5.8: Idealized representation of pipe-soil interaction model.

Figure 5.8 shows the idealized representation of the pipe-soil interaction model that is proposed previously. In this idealization, the soil is represented as a series of continuously distributed one-dimensional springs (in the vertical direction), whose response is elastic-perfectly-plastic and the pipe is represented as a one-dimensional Euler-Bernoulli beam. The solution procedure uses an iterative approach to solve the resulting analytical solutions and compute the maximum flexural stress in the pipe for given soil properties. A detailed description has been presented in Chapter 4.

Following this model, the maximum bending stress (σ_{b_max}) produced in the pipe section is a function of various random variables represented as follows:

$$\sigma_{b\_max} = f\left(D, th, c', \varphi', E_{cs}, h, d_{az}, s_{exp}, L_{free}\right) \tag{5.8}$$

where D and th represent the external diameter and the thickness of pipe; c' and φ' represent the soil cohesion and the angle of internal friction; E_{cs} and ν_{cs} are the elastic modulus and the Poisson's ratio of the cast iron pipe material; h is the depth of pipe below the ground surface; d_{az} is the depth of active zone; s_{exp} is the swell capacity of the soil. L_{free}, which is a function of other parameters, represents the free bending length of the pipe around the moist-dry boundary (see section 4.4.4 of Chapter 4). Table 5.7 and Figure 5.9 summarize the probability distributions and

the associated parameters used to represent these random variables. The rationale for arriving at these distributions is summarized next.

Table 5.7: Statistical information of parameters in stress demand model.

Parameter	**Symbol (unit)**	**Mean**	**CoV (%)**	**Distribution**	**Remark**
Pipe Geometry					
Diameter	D (mm)	varies	5	Normal	Sacramento pipe network GIS database
Thickness	th (mm)	varies	5	Normal	
Depth of Burial	h (m)	1	10	Normal	Based on Field Data
Soil					
Cohesion	c' (kPa)	35	30	LogNormal	Baecher and Christian [120]
Angle of Internal Friction	φ' (degree)	30	30	LogNormal	
Unit Weight	γ_{soil} (kN/m^3)	18.64	30	LogNormal	
Cast-iron					
Elastic Modulus	E_{cs} (GPa)	110, 150	10	Normal	Angus [97], Makar and McDonald [19]
Swell					
Swell Capacity	s_{exp} (%)	0 to 10%	20	LogNormal	Based on Field Data (USDA database)
Depth of Active Zone	d_{az} (m)	2	20	LogNormal	

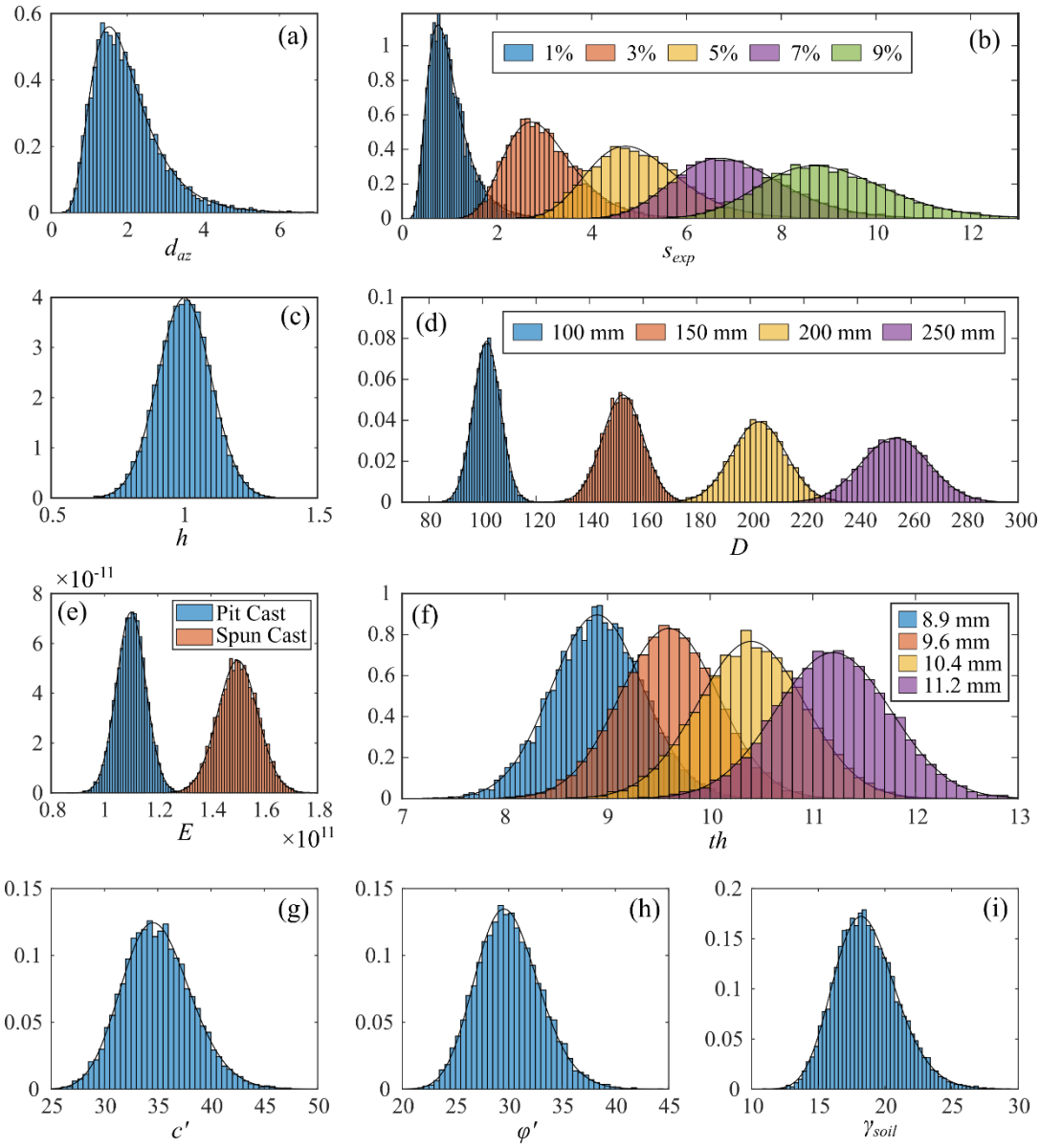

Figure 5.9: Probability distribution of stress demand model parameters (distribution and Monte Carlo samples): (a) depth of active zone, (b) soil swell capacity, (c) pipe burial depth, (d) pipe diameter, (e) pipe material, (f) pipe thickness, (g) soil cohesion, (h) soil angle of friction, and (i) soil density.

5.2.1 Parameter Uncertainty

The randomness associated with pipe geometrical parameters, such as diameter (D) and thickness (th), is a result of geometric imperfections due to manufacturing processes. A normal distribution with small COV (5%) is reported by Ahammed and Melchers [121] for cast iron pipes and adopted here. Pipe material parameters (elastic modulus and Poisson's ratio) depend on the casting methods – the two most common being pit cast and spun cast. Makar et al. [22] previously identified casting flaws, such as porosity and inclusion of foreign material, in both methods. To account for the variability introduced due to flaws, the parameters are assumed to follow a normal distribution, and the distribution parameters are computed from the data published by Makar and McDonald [19]. The uncertainty in the burial depth of the pipe (h) mainly stems from human error and/or improper pipe installation process. Due to limited empirical data to draw upon directly, a judicious estimation is made from the published research [86, 122]. Due to their very nature, the parameters associated with soil, in general, have a relatively large degree of uncertainty. Quantities such as soil shear strength parameters (c', φ') and unit weight (γ_{soil}) are, however, rather well recorded and only subject to variability associated with inhomogeneous soil formation [120]. The coefficients of variation of these parameters are taken from the City of Sacramento soil database and the probabilistic distribution is adopted from Baecher and Christian [120].

Furthermore, the uncertainties associated with the depth of active zone (d_{az}) and swell capacity (s_{exp}) of the soil are not readily quantifiable as these parameters have large spatial variations. The depth of active zone, also called the depth of wetting, is the soil (depth) that experiences moisture fluctuations and participates in the expansion process. Due to its dependency on various factors (such as depth of water table, soil type, vegetation, and temperature) and the lack of field measurements, a common practice in the literature is to assume this variable to be between 2 to 3 m [31]. However, discontinuities in the soils such as the bedding plane, cracks, and fissures have a significant influence on its values. A lognormal distribution with a mean of 2 m and COV of 20% is assumed for the depth of active zone is. The swell capacity, which is the maximum capacity of soil to expand, is also a function of several parameters (such as the soil grain size and distribution, mineral composition, saturation, and soil suction). United States Department of Agriculture (USDA) publishes the Coefficient of Linear Expansion (COLE) data for USA soils

that is similar to swell capacity; however, the resolution of the data is poor. Besides, the data is not available for certain locations, for example, COLE values for urban areas in the City of Sacramento are not available. A lognormal distribution with mean taken from USDA data and 20% COV is assumed to represent the uncertainty in the soil swell capacity.

Additionally, the analytical model of pipe-soil interaction developed previously has several idealizations. For example, the soil is represented as a system of vertical elastic-perfectly plastic springs, no pipe-soil interaction in the longitudinal direction of the pipe, and elastic behavior of pipe material. These idealizations introduce an additional source of uncertainty in the model prediction, which can be modeled using the multiplicative random variable α_{dem}, defined as the ratio of model predictions to the true values. The stress demand (σ_{dem}) can then be defined in terms of this random variable (called model uncertainty) as:

$$\sigma_{dem} = \alpha_{dem}\sigma_{d\_max} \tag{5.9}$$

The model uncertainty (α_{dem}) is evaluated by comparing the results of the analytical model with the finite element simulations. These simulations were performed to replicate the pipe behavior in expansive soil conditions considering material and interaction nonlinearity. It is observed that the error follows a normal distribution with a mean of 0.96 and COV of 10.18% (see Figure 5.10). Although these simulations can accurately reproduce the pipe stresses, if available, field measurements or experimental data are preferred alternatives to quantify α_{dem}.

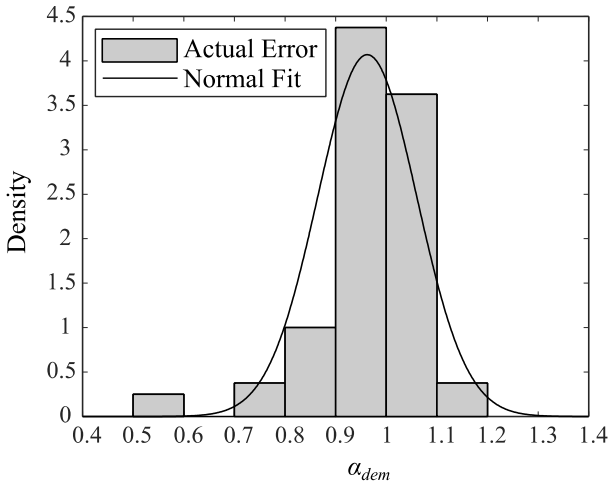

Figure 5.10: Idealized representation of pipe-soil interaction model.

5.3 Reliability Formulation

After characterizing the relevant uncertainties, the next step is to perform the reliability analysis using the aforementioned demand and capacity models. A pipe section is considered safe if the stress caused by the differential soil loading (demand stress, σ_{dem}) does not exceed its structural strength (capacity stress, σ_{cap}). Note that it is assumed that the failure of the pipe in any one location is independent of the pipe failure on any other boundary of that pipe segment. A time-dependent limit state function $\boldsymbol{g(x, y, t)}$ can be defined as follows:

$$g(\boldsymbol{x}, \boldsymbol{y}, t) = \sigma_{cap}(\boldsymbol{x}, t) - \sigma_{dem}(\boldsymbol{y}) \tag{5.10}$$

where, $\boldsymbol{x}$ and $\boldsymbol{y}$ are input variables and $\boldsymbol{t}$ is age. For a given set of input parameters corresponding to a specific age, the pipe is deemed safe when $\boldsymbol{g(x, y, t) > 0}$ and fails when $\boldsymbol{g(x, y, t) \leq 0}$. Using Eq. (5.10), the probability of failure $\boldsymbol{(P_f)}$ may be determined as follows:

$$P_f = P[g(\boldsymbol{x}, \boldsymbol{y}, t) \leq 0] = P[\sigma_{cap}(\boldsymbol{x}, t) \leq \sigma_{dem}(\boldsymbol{y})] \tag{5.11}$$

Due to the nonlinear implicit functional form of the pipe-soil interaction model, the limit state function [Eq. (5.11)] cannot be solved analytically; therefore, the Monte Carlo simulation technique is adopted to calculate the failure probability. In this technique, various values of the

input variables are randomly sampled consistent with their probabilistic distributions. Subsequently, for each set of the sampled values, the limit state function is evaluated using Eq. (5.11). If $g(\boldsymbol{x}, \boldsymbol{y}, t) \leq 0$, then the combination of sampled variables is deemed to be a failure event and a non-failure (reliable) event if $g(\boldsymbol{x}, \boldsymbol{y}, t) > 0$. Using the Law of Large Numbers, the failure probability (P_f) is approximated by the ratio of the number of failure events (N_f), where $g(\boldsymbol{x}, \boldsymbol{y}, t) \leq 0$, to the total number of events (N), which is defined as:

$$P_f = \frac{N_f}{N} \tag{5.12}$$

5.3.1 Random Sampling

In the Monto-Carlo technique, the accuracy of the output variable (in this case, the probability of failure, P_f) depends on the number of input combinations that are sampled from their distributions. Although several methods (see [123]) are available to predetermine the number of samples for a desired level of accuracy, in this case, a simpler approach of performing several trial runs was pursued to examine the effect of sample size on the stability of the results. Figure 5.11 shows one such trial run corresponding to a 50-year-old 200 mm diameter pipe in 5% soil expansion. Referring to Figure 5.11(a), the output variable (P_f) stabilizes after 1000 samples, while Figure 5.11(b) shows that the relative error is less than 0.1% at 1000 samples. Based on these results, a set of 1000 simulation samples are deemed sufficient for this study; results are discussed in the next section.

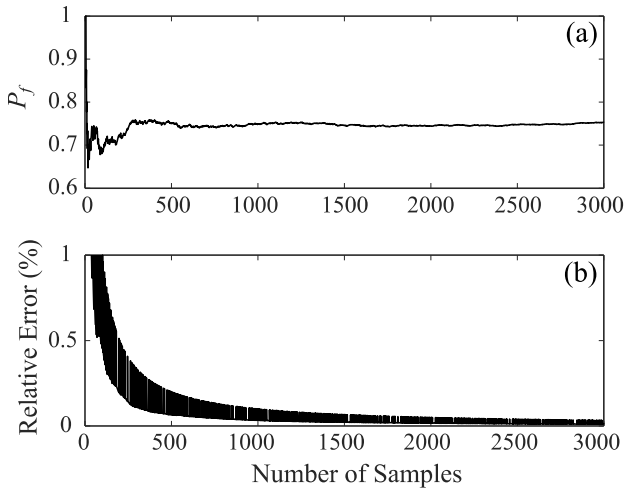

Figure 5.11: Number of samples used in Monte Carlo simulations vs. (a) output (probability of failure) (b) relative error in the output.

5.4 Results and Discussion

Following the reliability formulation for assessment of pipe-soil systems vulnerable to fracture caused by a combination of pitting corrosion and moisture-induced soil expansion, the probabilistic response is discussed in this section. The discussion is centered around two main aspects of the results: (1) failure probability of a pipe segment as a function of the input parameters and age and (2) sensitivity measurements to assess which model inputs have the most significant impact on the estimated response. The failure probability estimates will help decision-makers to prioritize pipe replacement and the sensitivity results may be used to inform areas (model refinement, specific data collection) in which investment may significantly enhance the accuracy of the model response. A detailed discussion of these results is presented next.

5.4.1 Probability of Failure of Pipe Segments

Figure 5.12 shows the failure probability of a range of pipes for three discrete soil swell capacities computed using the AWWA corrosion model and power law corrosion model. As expected, the probability of failure increases with age because the material deterioration overtime time, thereby associated with an increased likelihood of failure. However, the rate of increase varying throughout the pipe service life, with a relatively sharp increase in the probability of failure for young pipes

(less than 30 years old for both the corrosion models) and tapering off beyond that. This observation is consistent with the deterioration model described previously, where the self-inhibiting nature of the corrosion process in cast iron material takes over beyond, say 30 years of age. This indicates that not only should the age difference of two old pipes with similar attributes be considered while replacing old pipes but also other parameters, such as soil swell capacity, depth of active zone and pipe depth, must be accounted for. Also, the observation agrees with the field failure data in the City of Sacramento pipe network, where Pericoli et al. [11] concluded that pipes are not necessarily correlated with their age. Next, comparing the results from both the corrosion models, the probability of failure for all the cases are very similar (see Figure 5.12). Further results are shown for the AWWA corrosion model only.

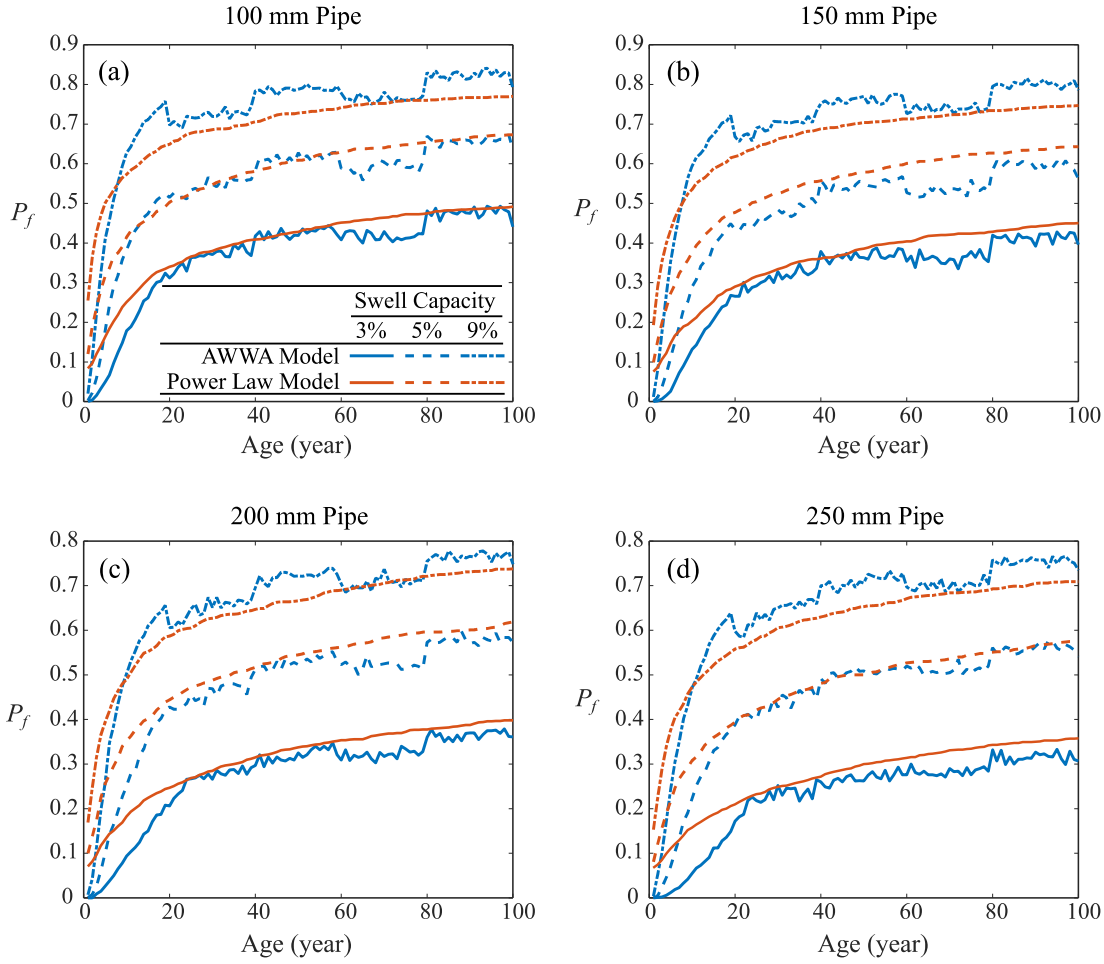

Figure 5.12: Failure probability as a function of pipe age computed using AWWA corrosion model and power law corrosion model for (a) 100 m diameter pipe, (b) 150 mm diameter pipe, (c) 200 mm diameter pipe, and (d) 250 mm diameter pipe in 3%, 5%, and 9% soil swell capacities.

The evolution of failure probability with other parameters is presented in Figure 5.13 for two different age groups (30 years and 100 years old). Results in Figure 5.13(a), which relate the failure probability to the pipe diameter, show that irrespective of the age, the risk of pipe failure is higher in the smaller diameter pipe compared to the large diameter, which is also supported by the field failure data in the City of Sacramento [11]. Results in Figure 5.13(b), which relate the failure probability with soil swell capacity, show that the probability of failure increases with an increase in the swell capacity, which is to be expected since larger bending stresses are associated with

higher swell capacity. Figure 5.13(c) compares the risk of failure of pit cast and spun cast pipes, where the likelihood of failure of pit cast pipes is higher than spun cast pipes. This is because pit cast pipes have inferior material strength, in addition to larger uncertainty in this parameter, compared to spun cast pipes.

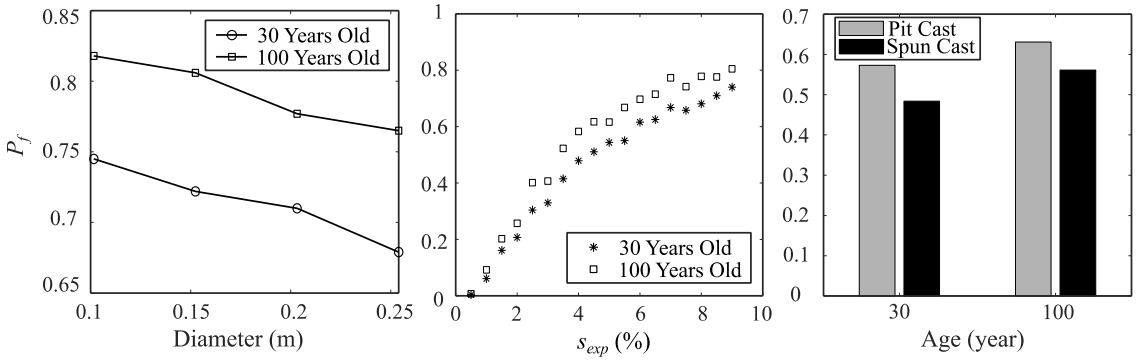

Figure 5.13: Evolution of failure probability with (a) pipe diameter, (b) soil swell capacity, and (c) casting process.

5.4.2 Sensitivity of Demand and Capacity to Input Parameters

The classical "one-at-a-time" sensitivity analysis [124] in which one parameter is varied at a time while holding the other parameters fixed is undertaken next. The sensitivity is determined at the 5th and 95th percentiles of the parameter's distribution and the results are shown in Figure 5.11 and Figure 5.12 using tornado plots. The vertical lines show the "base values" representing the result obtained using all the parameters at their 50th percentile (median value). From these results, the effects of the different input parameters on the demand and the capacity model of a pipe can be easily visualized. As shown in Figure 5.11, the demand model is most sensitive to the depth of active zone, soil swell capacity, and model uncertainty, in that order; however, it is not as influenced by the geometric properties (diameter and thickness) and soil unit weight. Since the capacity model is time-dependent, the results are shown for pipes at different ages (see Figure 5.12). Irrespective of age differences, the pipe stress capacity is most sensitive to the corrosion pit depth. Furthermore, the stress capacity of the pipe is also not as affected by the pipe geometric properties.

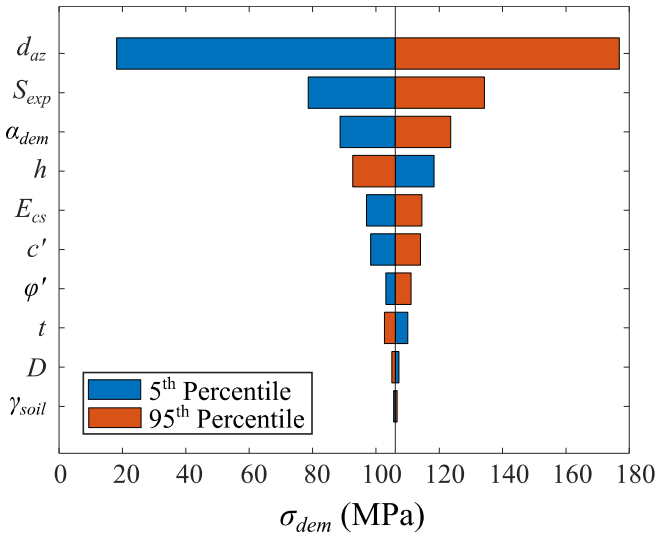

Figure 5.14: Tornado plot showing sensitivity of stress capacity model.

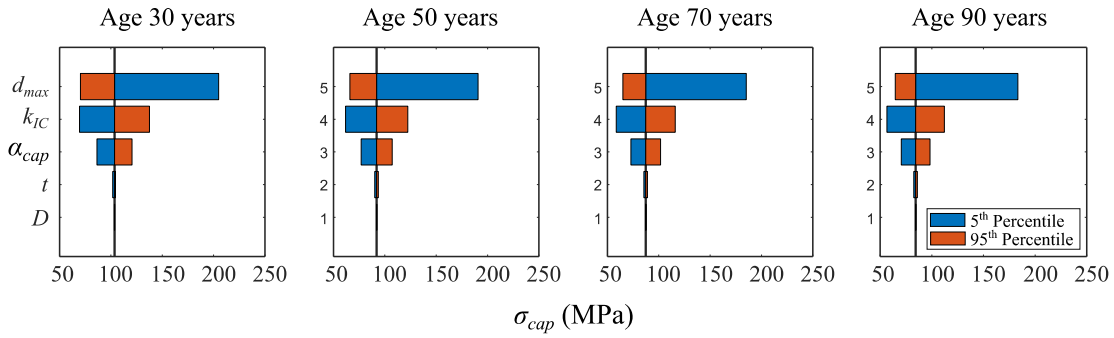

Figure 5.15: Tornado plot showing sensitivity of stress demand model.

5.4.3 Effect of Parameter Accuracy

The magnitude of the accuracy of the influential parameters (corrosion pit depth, critical stress intensity factor, depth of active zone, soil swell capacity, depth of pipe, and modeling uncertainty) is further investigated. The COV values of these parameters are varied and the response on predicted failure probability, shown in Figure 5.16, is observed. Generally, it is expected that the probability of failure will decrease with an increase in the COV [121]; however, this is not always the case. For example, the failure probability increases with the increase in COV of pipe depth

[see Figure 5.16(d)]. It is seen from Figure 5.16(a and d) that, in older pipes, the failure probability is not very sensitive to change in COV of critical stress intensity factor (k_{IC}) and pipe depth (h); only 2% change is detected when the COV value increases from 0 to 50%. The change in the COV of these parameters has no prominent impact on the probability of failure because the capacity and demand models are also not sensitive to these parameters. This implies that the accuracy of these input parameters has relatively little influence on the probability of failure and hence they can be assumed deterministic for the current purposes. Furthermore, the failure probability is moderately sensitive to soil expansion (s_{exp}) and demand model uncertainty (α_{dem}) [Figure 5.16 (e and f)]. Moreover, the failure probability is very sensitive to the corrosion pit depth (d_{max}) and the depth of active zone (d_{az}) [Figure 5.16 (b and c)]. Approximately 40% change is observed when the COV is varied from 0 to 50%. Coincidently, these two parameters are also the most difficult to describe, both deterministically and probabilistically. For example, referring to Figure 5.5, the AWWA [8] corrosion model has an average COV of around 47% which can impart significant uncertainty in the outcome.

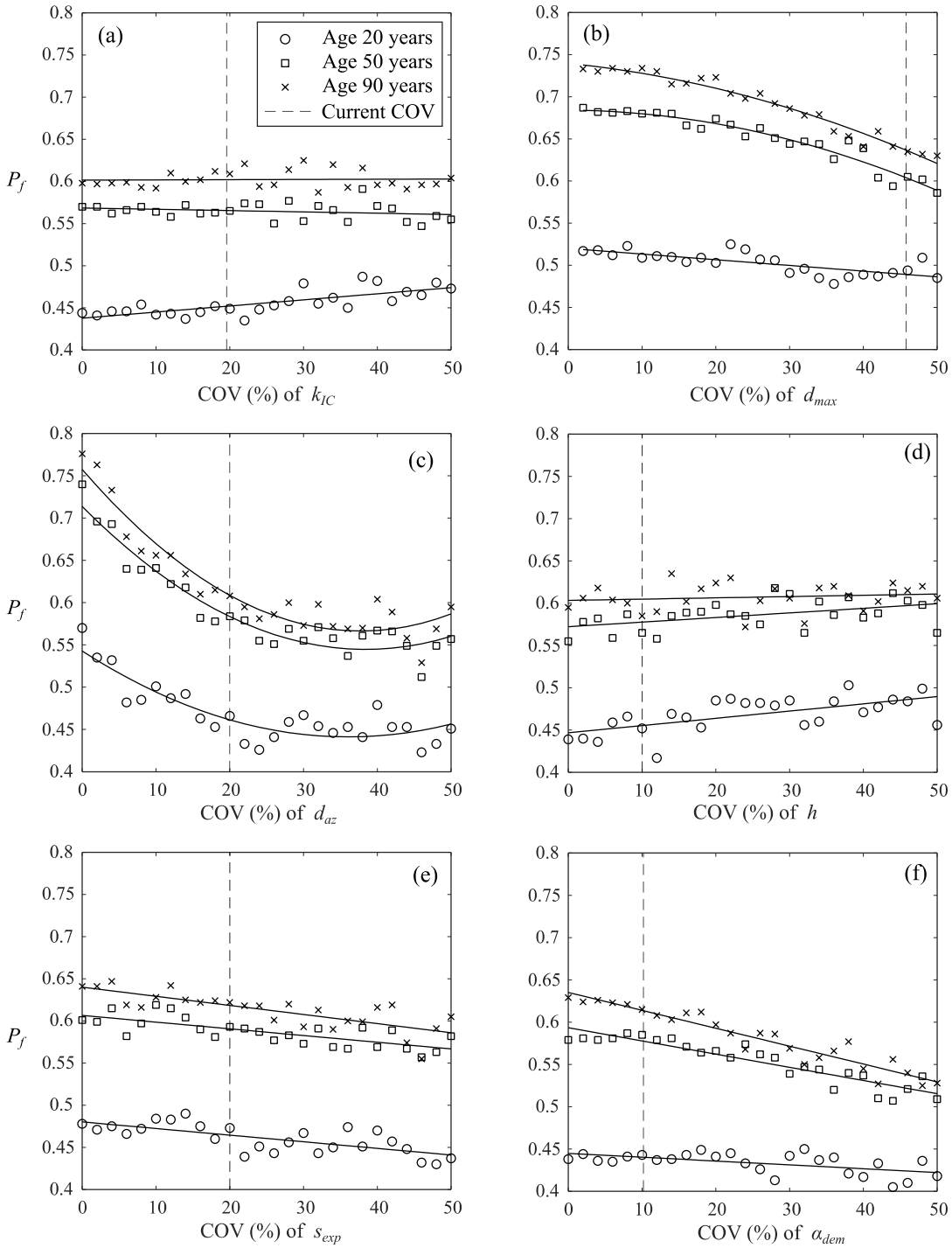

Figure 5.16: Sensitivity of failure probability with COV of (a) k_{IC} (b) d_{pit} (c) d_{az} (d) h (e) s_{exp} (f) α_{dem}.

5.5 Decision Support for Replacement Prioritization in Networks

In this section, the results of the probabilistic interpretation of the analytical model, which is the failure probability of a pipe segment crossing a moist-dry boundary, is used to develop a risk-based decision-support framework to plan pipe replacement at a network level. Figure 5.17 shows an overview of the main components of the methodology developed in formulating this decision-support framework. First, the failure probability for a pipe crossing one boundary is generalized to multiple crossings within a pipe segment. These results are then used to quantify the most at-risk sections of the pipe network. A replacement strategy is formulated by quantifying suitable performance requirements (minimum cost and minimum risk) and incorporating them into a decision model. Once this decision model is formulated, standard optimization algorithms are used to optimize the pipe replacement strategy. These details are explained next.

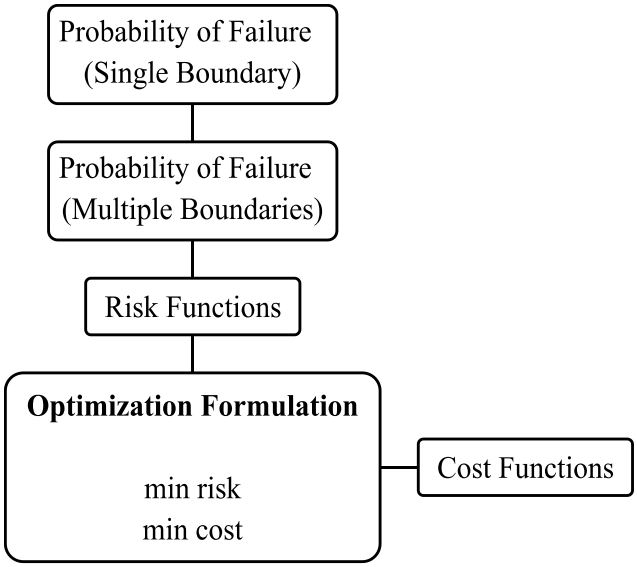

Figure 5.17: Flowchart representation of decision-support framework for pipe replacement.

5.5.1 Model Generalization: Single Boundary to Multiple Boundaries

The failure probability calculation for a pipe crossing a single moist-dry boundary is presented earlier in this chapter, which combined pitting corrosion and moisture-induced soil expansion. By dividing the pipe segments into five groups based on their age (see Figure 5.5), the probability of failure for a range of pipe diameters and soil expansion magnitudes (summarized in Table 3.1) was

generated. These probabilities can be described by their cumulative distribution functions (CDFs) according to their age [125]. For convenience, these CDFs are approximated using known probability distributions through standard curve-fitting techniques. These distributions include Lognormal, Generalized Extreme Value (GEV), and Modified Birnbaum–Saunders distribution (MBS). The MBS distribution is a modified version of the Birnbaum–Saunders distribution [126] in which an additional parameter is introduced as shown below.

$$F(x|\alpha,\beta,\gamma) = \Phi\left[\frac{1}{\alpha}\left(\left(\frac{x}{\beta}\right)^{0.5} - \left(\frac{\beta}{x}\right)^{\gamma}\right)\right] \tag{5.13}$$

where, $\Phi(*)$ is the CDF of the standard normal distribution; α is the shape parameter; β is the scale parameter; γ is the new parameter, called the location parameter. A typical result showing fits with the distribution types using the least square method is presented in Figure 5.18. The CDFs that best fit the failure probability data are selected using a goodness of fit test, i.e., root mean square error (RMSE). The statistics of the goodness of fit $\left(RMSE_{lognormal} = 0.0371,\ RMSE_{GEV} = 0.0221, \text{and } RMSE_{MBS} = 0.0190\right)$ showed that the MBS distribution provides the best fit amongst these distribution types. The parameters of the MBS distribution for various pipe geometric properties and soil swell capacity are determined and shown in Table 5.8 and Table 5.9.

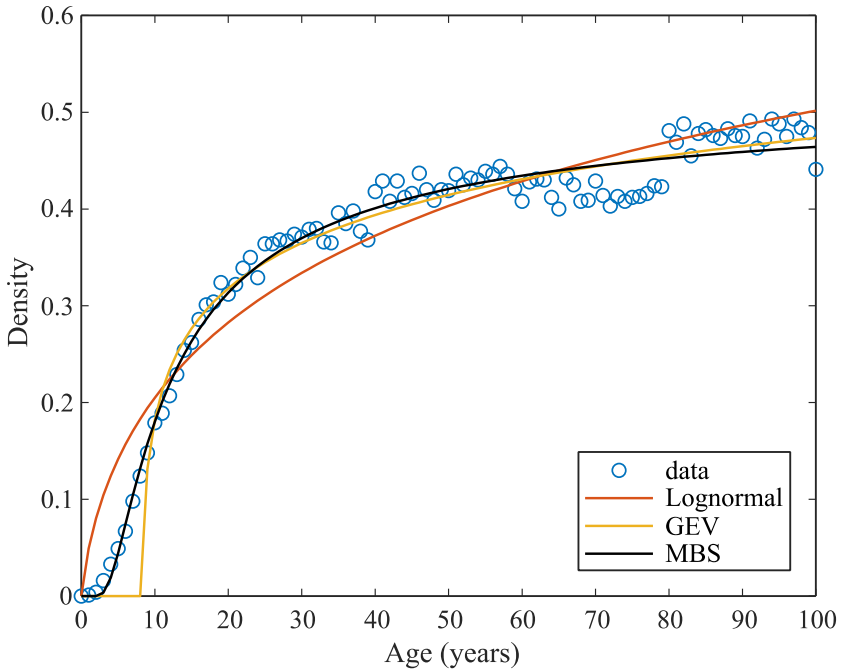

Figure 5.18: Distributions of the predicted failure probability of 100 mm diameter pipe buried in 3% swell capacity soil and the fitted distributions.

Table 5.8: Parameters of MBS distribution for pit-cast iron pipes.

Dia.	100 mm			150 mm			200 mm			250 mm		
Swell Capacity	3%	5%	9%	3%	5%	9%	3%	5%	9%	3%	5%	9%
α	10.5	5.1	4.0	13.1	5.3	4.2	46.4	5.2	4.1	29.6	4.9	4.1
β	96.5	11.6	4.6	204.2	18.9	5.4	1622.1	22.5	6.5	1304.0	31.3	8.0
γ	0.9	1.6	2.2	0.8	1.2	2.0	0.8	1.2	2.0	0.7	1.0	1.8
R^2	0.99	0.98	0.96	0.99	0.99	0.97	0.99	0.99	0.98	0.99	0.99	0.99

Table 5.9: Parameters of MBS distribution fitting for spun-cast iron pipes.

Dia.	100 mm			150 mm			200 mm			250 mm		
Swell Capacity	3%	5%	9%	3%	5%	9%	3%	5%	9%	3%	5%	9%
α	20.1	5.7	4.1	116.3	6.0	4.2	69.1	6.0	4.3	32.2	6.1	4.2
β	269.8	18.7	5.8	11414.2	35.2	6.7	23216.0	41.8	9.4	20403.5	51.0	10.7
γ	0.9	1.3	2.2	0.7	1.1	2.2	0.6	1.0	1.8	0.5	1.0	1.6
R^2	0.99	0.99	0.97	0.99	0.99	0.98	0.99	0.99	0.99	0.98	0.99	0.99

Typically, a pipe segment will encounter multiple moist-dry boundaries, arising from various soil cover types and moisture sources. For example, Figure 5.19 shows a pipe crossing a property line and an in-service road, where two potential locations for differential soil movements to occur are identified. Using the properties of pipe and soil at these boundary locations, the failure probability associated with any one boundary can be calculated using the procedure previously described in this chapter, followed by the analytical form using the curve fitting procedure as outlined above. Note that it is assumed that the failure of the pipe in any one location is independent of the pipe failure on any other boundary of that pipe segment. Next, the failure probability of the i^{th} pipe segment $(P_{f,i})$ due to n boundaries can be calculated according to [127]:

$$P_{f,i} = 1 - \prod_{j=1}^{n} (1 - P_{fb,j}) \tag{5.14}$$

where, $P_{fb,j}$ is the probability of failure due to the j^{th} boundary, and n is the total number of boundaries within the pipe segment.

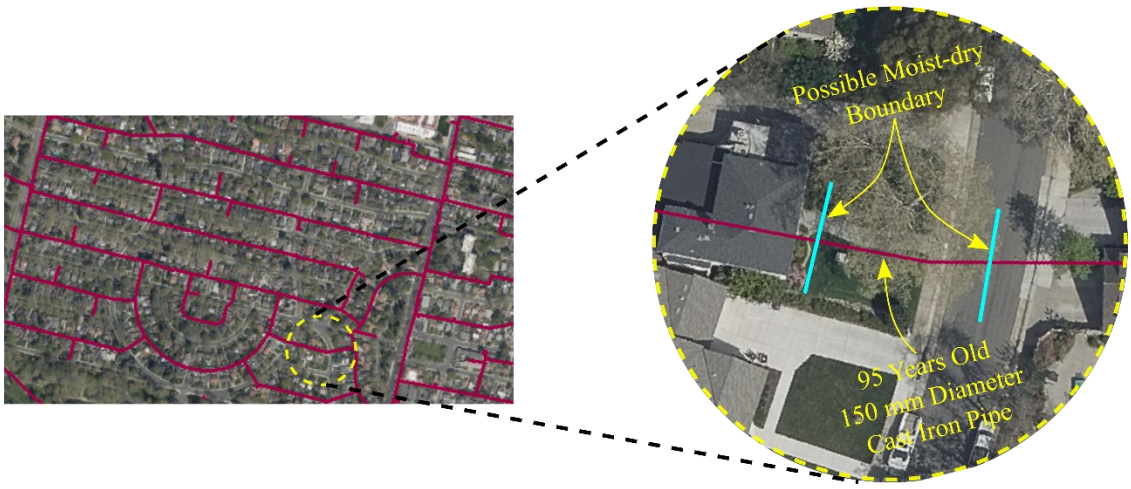

Figure 5.19: A typical example of a pipe crossing multiple moist-dry boundaries extracted from an actual pipe network.

5.5.2 Definition of Risk

In the context of this thesis, the risk associated with a deteriorated cast-iron pipe segment is defined by the product of its probability of failure and the consequence resulting from its failure. The mathematical definition of the expected risk associated with a pipe segment is as follows [128]:

$$R_i = P_{f,i}^{a} \times C_i^{b} \tag{5.15}$$

where, R_i, $P_{f,i}$, and C_i are the risk of failure, the probability of failure, and the consequence of failure of a given pipe i, respectively. a and b are weights representing the relative importance of the probability and the consequence, respectively. The expected total risk, R_{total}, can be then obtained as the summation of the risk of all pipes (N is the number of pipes) using the following formula:

$$R_{total} = \sum_{i}^{N} R_i \tag{5.16}$$

For each pipe segment, the likelihood of failure is calculated using a probability of failure model, described formerly, from the pipe and soil data, and the consequence is calculated using a consequence model which considers service interruption due to failure. When a pipe segment fails,

interruptions could arise, say from: direct service interruption for consumers whose properties directly draw from the pipe segment (local interruption) and the reduction of nodal pressures in a larger area of the network (global interruption). For the purposes of illustrating this decision-support framework, the consequence can be assumed to simply be the number of customers affected through the loss of a pipe segment.

5.5.3 Definition of Cost

The economic cost is the present value of the replacement cost of pipes. For simplicity, it is assumed that pipes will either be replaced with identical ones or be left in place. The total replacement cost is defined as follows:

$$min(C) = \sum_{i}^{N} (RC)_i(d_i) \tag{5.17}$$

where, C is the system cost; $RC_i(d_i)$ is the value of replacement cost of pipe i of diameter d_i; N is the total number of pipes. $RC_i(d_i)$ is defined as

$$(RC)_i(d_i) = R(d_i) \times l_i \tag{5.18}$$

where, $R(d_i)$ is the replacement cost per km of pipe i of diameter d_i, and l_i is the length of the pipe in km.

5.5.4 Optimization and Results of the Example

As formulated above, the optimization problem with two objectives becomes a multi-objective optimization problem defined as [129]:

$$\max f(z) = [f_1(z), f_2(z), f_3(z), \dots, f_n(z)] \qquad z \in Z \tag{5.19}$$

where, $f(z) = [f_1(z), f_2(z), f_3(z), \dots, f_n(z)]$ is a n-dimensional (two, in this example) objective vector. The set of variables (z) is known as the nondominated set or the Pareto optimal front [130]. This set is nondominated in region Z if there exists no other $z' \in Z$ such that $f_i(z') > f_i(z)$ for any $i \in \{1,2,3, \dots, n\}$. In this study, there are two objectives, the system cost, C, and the risk, R_{Total}. Therefore, the problem becomes:

$$\min C \quad \text{and} \quad \min R_{Total} \tag{5.20}$$

The algorithm used in this study to identify the Pareto optimal front is the Non-dominated Sorting Genetic Algorithm II (NSGA-II) from Deb et al. [130]. The details of this algorithm are presented in Appendix A.

The proposed optimization procedure for an optimal replacement strategy is illustrated on a small toy example pipe network consisting of three loops, 10 nodes (marked with ⊙), and 13 pit-cast pipes (marked with ⊡) as shown in Figure 5.20. Table 5.10 presents the pipe data including soil condition and the number of moist-dry boundaries which the pipes are assumed to cross. The pipe replacement cost, which is a function of pipe diameter and length, is assumed from Dandy and Engelhardt [131]. The risk model requires two quantities: failure probability and the number of consumers who will experience interruption. Given the geometric properties, age, and surrounding soil condition (Table 5.10), the failure probability for each pipe segment is calculated using the MBS distribution and the corresponding parameters. As discussed previously, the total number of affected consumers due to a pipe failure could include both local and global interruptions. However, for the sake of illustration and simplicity, the number affected consumers is assumed to be proportional to the area use and varies from a minimum of 3 for rural land use to a maximum of 50 for residential use [131]. Based on this assumption, the number of affected consumers is randomly assigned for each pipe in the example pipe network.

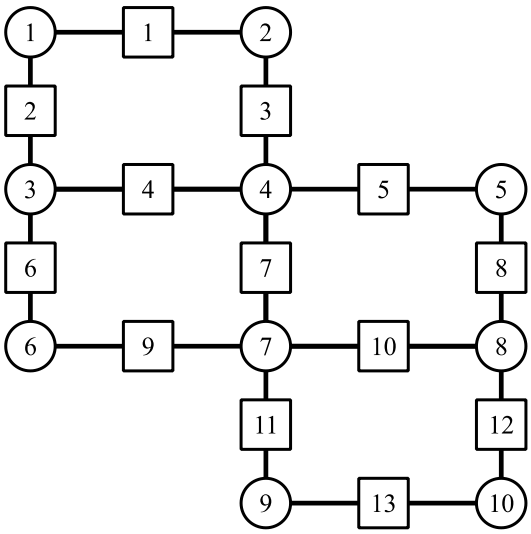

Figure 5.20: Layout of the example network (not to scale).

Table 5.10: Pipes geometrical data and soil condition.

Pipe ID	Diameter (mm)	Thickness (mm)	Length (km)	Age (Year)	s_{exp} (%)	Boundaries crossing
1	100	8.9	4	50	1	1
2	150	9.6	2	68	6	2
3	250	11.2	3	94	2	1
4	100	8.9	6	82	1	2
5	250	11.2	2	95	4	3
6	150	9.6	6	74	2	1
7	150	9.6	7	63	4	1
8	200	10.4	8	91	4	2
9	150	9.6	2	79	6	3
10	250	11.2	1	88	7	4
11	150	9.6	3	84	8	2
12	100	8.9	4	72	3	1
13	100	8.9	5	20	9	3

The example problem at hand is to determine which pipes should be prioritized for replacement under a fixed budget constraint. Figure 5.21 shows the non-dominant solutions by evaluating trade-offs between cost and risk. Each solution point represents the optimal number of pipes that can be replaced without compromising the problem objectives (minimum risk and minimum cost). This curve provides the decision-maker the ability to choose a replacement prioritization plan within the budget constraints and the desired level of service. For example, the optimum pipe replacements for a budget of $10 million (shown in Figure 5.21) corresponds to the replacement of 9 pipes (pipe ID: 1-3, 5, 9-13). These pipes correspond to a total length of 26 km out of the network length which is 53 km. It is important to note here that these pipes are not the oldest ones, which is different from the outcomes of age-based prioritization, e.g., oldest pipes be replaced first. It is worth noting here that this example is intended to illustrate how the analytical model can be used for optimization, an exercise which otherwise would involve significantly more computational effort using the 3D FE model. For example, the toy network considered here to demonstrate the decision support framework needed approximately 13000 cases of pipe-soil interactions to perform. If this analysis had performed using CFE models, it would have taken more than 20,000 hours to run (running on a Windows server with two Intel Xeon Processor CPU E5-2630).

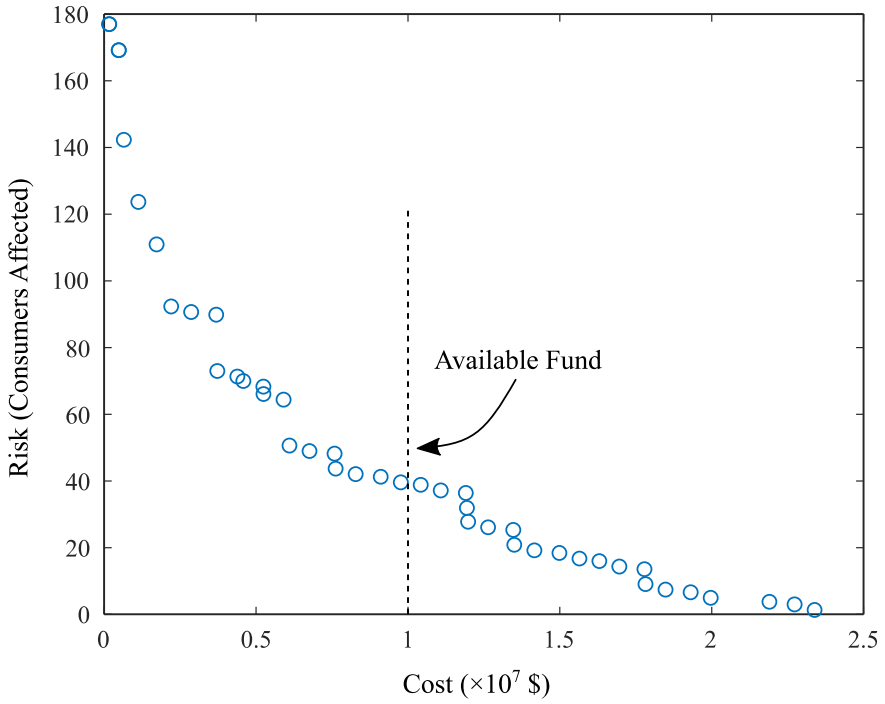

Figure 5.21: Non-dominant optimal solution (Pareto front) of pipe replacement with minimizing cost and risk

5.6 Summary

In this chapter, a reliability analysis to identify the most at-risk cast iron water pipes is presented along with a sensitivity analysis to recognize the parameters that are the primary driver of the risk. A prospective use of the results of this analysis in decision-support to plan pipe replacement is illustrated. The formulation of the proposed risk assessment framework involves: (a) uncertainty characterization of the demand and capacity models which includes uncertainty in model inputs (i.e., material and geometric properties and configurational parameters) as well as the uncertainty associated with the model itself; (b) construction of a limit state function (i.e., capacity stress = demand stress) and then calculating the probability of failure through Monte Carlo simulations; and (c) identification of model inputs (and uncertainties thereof) that have the most significant impact on response estimation.

The framework uses the previously developed pipe-soil interaction model as a loading mechanism and assumes corrosion as the main failure mechanism. Two different corrosion models (the AWWA model and power law model) are adopted. The proposed framework offers a vulnerability assessment of pipe segments in terms of failure probability for a range of pipe and soil configurations representing typical pipe networks. The framework is then extended to assess the role of uncertainty (parameters as well as models themselves) in the computed failure probability using sensitivity analysis. As illustrated using an example, the simplified analytical model allows us to undertake large optimization tasks to optimally prioritize pipe replacements, which otherwise would be prohibitively expensive (from a computational effort standpoint) using 3D CFE models.

Chapter 6
Concluding Remarks

The main contributions of this thesis are: (a) a physics-based analytical model to predict longitudinal stresses in pressurized cast-iron water pipes due to moisture-induced soil expansion; and (b) a reliability framework to identify the most at-risk pipe segments in a pipe network. The prospective use of this framework is presented in the context of decision-support towards pipe replacement prioritization. In this chapter, the significant contributions, key conclusions, limitations, and recommendations for future work are described and highlighted.

6.1 Significant contributions

The key contributions of this research are as follows:

- Focused on the effect of moisture-induced ground deformation on pipes, this thesis proposes a simplified way to perform finite element simulation of pipe-soil interaction using a thermal-structural analysis as an artifice. This method greatly simplifies the simulation process.
- The main contribution of this thesis is the development of an analytical model that provides estimates for longitudinal stresses in cast-iron pipes subjected to a moisture-induced soil expansion given a range of parameters that describe pipe configuration, soil conditions, and triggering factors, such as soil saturation, that leads to expansion. The

model is an improvised classical beams-on-elastic-foundations solution to capture effects, including nonlinear soil response and a gapping/contact between the pipe and soil.

- This thesis presents a vulnerability assessment framework by combining pitting corrosion (pertaining to capacity stresses) and the bespoke moisture-induced soil expansion model (pertaining to demand stresses). The framework calculates the lifetime probability of failure of a given pipe segment by formulating a limit state function and implementing Monte Carlo procedure.
- One of the challenges in performing the reliability analysis is to synthesize various uncertainties present in the system. A sensitivity analysis performed, which examines the influence of various inputs (and their uncertainties) on the estimated response. This is of particular importance from the standpoint of making targeted investments in data collection, mapping, as well as model development and refinement.
- A decision support framework for prioritizing pipe replacement is proposed using the simplified analytical model of pipe-soil interaction in expansive soil conditions. The prioritization framework offers non-dominant pipe replacements solutions by minimizing the overall cost and risk using NSGA-II. With an available budget, water utilities can utilize these solutions while keeping the desired service level.
- Peer-reviewed journal and conference articles that have directly resulted from this work are listed in the front matter.

6.2 Conclusions

The key conclusions resulting from this research are summarized as follows:

- The CFE simulations capture the relevant aspects of the pipe response (such as pipe deflection and longitudinal stresses profile) well and demonstrates that the longitudinal bending may cause pipe fractures.

- The CFE simulations provide a rational explanation of failure distribution among the pipe sizes (diameter) to supplement observed field failure data, whereby smaller diameter pipes have suffered a greater number of fractures. For similar soil conditions, an inverse relationship between the pipe diameter and longitudinal stress was observed from the CFE results.

- The parametric study investigated the effect of parameters such as the modulus of elasticity of soil and pipe material, pipe burial depth, and depth of active zone. From this study, it was concluded that the changes made to the soil modulus had only a small impact on pipe longitudinal stresses, whereas a moderate effect was seen when the pipe modulus was varied. Furthermore, pipe burial depth and depth of active zone clearly had the greatest impact on the pipe response. An increase in depth of active zone exacerbated the effects of moisture expansion by adding more depth of expanding soil and increased both maximum pipe deflection and maximum pipe stress. On the contrary, an increase in pipe burial depth alleviated the effects of soil expansion and decreased both maximum pipe deflection and maximum pipe stress.

- The proposed analytical model is validated against a suite of CFE simulations, demonstrating that it can reproduce flexural stresses in a range of pipe configurations with good accuracy (results lie within the 15% error envelope) and in a fraction of the computational time (requires roughly 1/1,000 of the time required to execute the CFE solutions). Based on these observations, the analytical model may be used as an effective proxy for CFE simulations for estimating pipe stresses in the idealized problem of a pipe crossing a moist-dry soil interface.

- Through reliability analysis, the lifetime probability of failure was estimated for different pipe segments of the City of Sacramento pipe network. It was observed that the likelihood of failure of pipes with similar properties is relatively constant for older pipes. This observation suggests that the simplistic approaches of pipe replacement, e.g., assuming the oldest pipes are the most at risk, may not present an optimum replacement strategy. In addition, the analysis indicated that smaller diameter pit-cast pipes are most

at risk. These results can be helpful in developing a replacement strategy for existing pipes with a view to optimize asset management.

- The study identified the most influential input parameters which affect the pipe response through a sensitivity analysis. It was seen that the pipe demand is controlled by the depth of active zone, soil swell capacity, depth of pipe, and model uncertainty. On the other hand, pipe capacity was governed by the corrosion pit depth and critical stress intensity factor of cast iron. Other parameters, such as pipe geometric properties, soil shear strength parameter, and soil unit weight, had a minor effect on pipe response (bending stress) and they can be considered deterministic.

- Further analysis on the accuracy of the influential parameters revealed that the failure probability is most sensitive to the corrosion pit depth and depth of active zone. Currently, these parameters are associated with large uncertainty due to a lack of empirical data and the use of heavily simplified models. For example, the large scatter (COV of 47%) in the AWWA corrosion model translate to large uncertainty in the estimation of the pit depth. Furthermore, this model is an empirical relation between pit depth and pipe age ignoring surrounding soil properties (moisture content, pH, and corrosivity). A refinement of this relationship is likely to yield significant benefits in the vulnerability assessment. Investment in the accurate measurement of these parameters through sensor networks and other data acquisition will likely offset the costs of uncertainty in repair prioritization of these pipes.

- Finally, a decision-support framework is presented to prioritize pipes to be replaced through trade-offs between economic cost (cost of replacement) and risk of pipe failure. The framework provides optimal replacement solutions using an evolutionary search algorithm by minimizing the risk and cost function. It was seen that the optimal solutions depend on not only pipe age but also other parameters, such as soil swell capacity, depth of active zone and pipe depth. Importantly, the simplified analytical model allows large-scale optimization to be undertaken at a fraction of the computational cost of 3D FE models.

6.3 Limitations of the current study

There are several limitations in this study that must be considered in its application and generalization. These limitations may be refined through further studies. The method considers in this research only one failure mechanism (moisture-induced differential soil expansion). Albeit important in many areas of the USA and Canada, other mechanisms (such as frost heave, soil and water temperature, water pressure, soil surcharge, and vehicular load) may dominate water pipe failures in certain regions. Besides that, pipe failures may also occur due to a combination of several failure mechanisms as well, which is not considered in this thesis.

Even for the moisture-induced soil expansion mechanism, the demand assessment model (proposed analytical pipe-soil interaction model) includes several idealizations that were necessary from the standpoint of balancing practicality with accuracy. This analytical model is limited to pipes perpendicular to the moist-dry boundary only which assumes moisture flow in the vertical direction only (along with the soil depth). Due to this idealization, the boundary between the moist (saturated) and dry (unsaturated) regions is abrupt, such that the boundary between the expanding soil and stationary soil is abrupt as well. Whereas this perpendicular boundary will produce the most conservative estimate of pipe longitudinal stresses, a moist-dry boundary of any arbitrary shape is possible in field conditions. Another limitation of this study is that it assumes the soil depth that is expanding (depth of active zone) is fully saturated. The analytical model proposed here will overestimate pipe stresses for partially saturated soil conditions.

The proposed decision support framework is illustrated on a small pipe network with several simplifications. For example, the consequence of a pipe failure is only measured by the number of customers affected; however, a failed pipe may cause other adverse effects, such as loss of pressure at neighboring nodes and contamination of water. Above all, the example network is intended to demonstrate the use of the simplified analytical model of pipe-soil interaction in a decision support framework. An application of this decision model to an actual pipe network will provide more realistic results, which was not possible during the course of this thesis work.

Notwithstanding these limitations, the approach outlined in this thesis offers significant improvements over currently used approaches for vulnerability assessment and provides the motivation for further study by identifying important weaknesses in the state of the art.

6.4 Recommendations for future study

Based on the research work proposed in this thesis, a couple of research directions can be pursued to extend this work:

- **Generalization of the proposed analytical model:** As discussed above, the proposed pipe-soil interaction model is developed for a vertical moist-dry boundary and fully saturated soil condition, and it offers the most conservative estimate of pipe longitudinal stresses. Generalization of this model for an arbitrary-shaped moist-dry boundary and partially saturated soil may prove useful and present a natural advancement of this work.
- **Data collection and model refinement:** The development of the risk-based decision framework also provided insight into several areas that requires improvement. For example, the study revealed the lack of data (or large uncertainty) in several quantities that mechanistically control pipe fracture. On the demand side, this includes information regarding the soil types, burial depths, depth of the active zone, swell capacity, and soil saturation. Also, at this point, the characterization of the uncertainties present in these parameters is not readily available. A comprehensive data collection and mapping program is needed to validate and improve the proposed methodology. On the capacity side, the key issue is the uncertainty in estimating pitting damage. For example, the large scatter in the AWWA corrosion model results in a severe uncertainty in the estimation of the pit depth; a refinement of this relationship is likely to yield significant benefits in the vulnerability assessment.
- **Real time monitoring system:** In this study, values of the input variables are taken from various sources (such as published and government database); however, field conditions are dynamic and will change these input variables continuously. For example, the ever-changing nature of soil moisture that causes soil expansion as well as aggravating corrosion needs to be accommodated in the analysis. Another critical

parameter for the model which is very sensitive to weather change and human intervention is the depth of active zone. This portion of soil (depth) experiences moisture fluctuations and participates in the expansion process. These parameters require a monitoring system which can inform the risk-based decision support tool regularly for the purposes of capital replacement or maintenance. For real-time (short-term) decision making, the site should be monitored using various sensors such as soil moisture sensors, thermal conductivity sensors, strain gauges, heave transducers, and a weather station.

Bibliography

[1] S. Folkman, "Water main break rates in the USA and Canada: A comprehensive study," Mechanical and Aerospace Engineering Faculty Publications, Utah, 2018.

[2] V. E. Fisher, The history of United States Pipe and Foundry Company : a centennial celebration, Birmingham, Ala: The Company, 1999.

[3] AWWA, Investigation of grey cast iron water mains to develop a methodology for estimating service life, Denver, CO: AWWA Research Foundation and American Water, 2000.

[4] S. Folkman, "Water Main Break Rates in the USA and Canada: A Comprehensive Study," Mechanical and Aerospace Engineering Faculty Publications, Utah, 2012.

[5] G. J. Kirmeyer, W. Richards and C. D. Smith, "An assessment of water distribution systems and associated research needs," American Water Works Association Research Foundation, Denver, 1994.

[6] B. Rajani and S. McDonald, "Water mains break data on different pipe materials for 1992 and 1993," National Research Council of Canada, Ottawa, 1995.

[7] Y. Kleiner and B. Rajani, "Comprehensive review of structural deterioration of water mains: Statistical models," *Urban Water,* vol. 3, pp. 131-150, 2001.

[8] AWWA, "Dawn of the replacement era: Reinvesting in drinking water infrastructure," American Water Works Association, Denver, 2001.

[9] J. P. Bardet, D. Ballantyne, G. E. C. Bell, A. Donnellan, S. Foster, T. S. Fu, J. List, R. G. Little, T. D. O'Rourke and M. C. Palmer, "Expert review of water system pipeline breaks in the City of Los Angeles during summer 2009," University of Southern California, Los Angeles, 2010.

[10] M. E. E. Prosser, V. E. Speight and Y. R. Filion, "Life-cycle energy analysis of performance- versus age-based pipe replacement schedules," *American Water Works Association,* vol. 105, no. 12, pp. E721-E732, 2013.

[11] V. Pericoli, A. Kanvinde, S. Kunnath and B. Younis, "Forensic analysis of cast iron pipe fracture in the City of Sacramento," Department of Civil and Environmental Engineering, University of California, Davis, 2014.

[12] S. J. F. Gould, F. A. Boulaire, S. Burn, X. L. Zhao and J. K. Kodikara, "Analysing underground water-pipe breaks in residual soils," *Water Science & Technology,* vol. 63, no. 11, pp. 2692-2699, 2011.

[13] C. M. Clark, "Expansive-soil effect on buried pipe," *Journal AWWA,* vol. 63, no. 7, pp. 424-427, 1971.

[14] R. Newport, "Factors influencing the occurrence of bursts in iron water mains," *Water Supply and Management,* vol. 3, pp. 274-278, 1981.

[15] P. F. Hudak, B. Sadler and B. A. Hunter, "Analyzing underground water-pipe breaks in residual soils," *Water/Engineering and Management,* vol. 145, no. 12, pp. 15-20, 1998.

[16] Y. Hu and D. W. Hubble, "Factors contributing to the failure of asbestos cement water mains," *Canadian Journal of Civil Engineering,* vol. 34, no. 5, pp. 608-621, 2007.

[17] CIPRA, "Handbook of cast iron pipe for water, gas, sewage and industrial services," Cast Iron Pipe Research Association, Chicago, 1952.

[18] J. M. Makar and B. Rajani, "Gray cast-iron water pipe metallurgy," *Journal of Materials in Civil Engineering,* vol. 12, no. 3, pp. 245-253, 2000.

[19] J. M. Makar and S. E. McDonald, "Mechanical behavior of spun-cast gray iron pipe," *Journal of Materials in Civil Engineering,* vol. 19, no. 10, pp. 826-833, 2007.

[20] B. Rajani and S. Tesfamariam, "Estimating time to failure of cast-iron water mains," *Water Management,* vol. 160, no. 2, pp. 83-88, 2007.

[21] R. M. Clark, J. Q. Adams and R. M. Miltner, "Cost and performance modeling for regulatory decision making," *Water,* vol. 28, no. 1, pp. 20-27, 1987.

[22] J. M. Makar, R. Desnoyers and S. E. McDonald, "Failure modes and mechanisms in grey cast-iron pipes," in *International Conference on Underground Infrastructure Research*, Kitchener, 2001.

[23] A. N. Talbot, "Strength properties of cast iron pipe made by different processes as found by tests," *American Water Works Association,* vol. 16, pp. 1-44, 1926.

[24] S. Tesfamariam, B. Rajani and R. Sadiq, "Possibilistic approach for consideration of uncertainties to estimate structural capacity of ageing cast iron water mains," *Canadian Journal of Civil Engineering,* vol. 33, pp. 1050-1064, 2006.

[25] W. M. Mair, "Fracture criteria for cast iron under biaxial stresses," *Journal of Strain Analysis,* vol. 3, no. 4, pp. 254-263, 1968.

[26] A. C. Ugural and S. K. Fenster, Advanced strength and applied elasticity, New York: Elsevier Science Publishing Co., 1987.

[27] L. D. Jones and I. Jefferson, "Expansive soils," in *Institution of Civil Engineers Manuals series*, ICE, 2011.

[28] B. M. Das, Principles of Geotechnical Engineering, Boston: PWS Publishing Company, 1985.

[29] R. Pusch and R. N. Yong, Microstructure of smectite clays and engineering performance, Oxon: Taylor and Francis, 2006.

[30] J. D. Nelson, D. D. Overton and D. B. Durkee, "Depth of wetting and the active zone," in *Shallow Foundation and Soil Properties Committee Sessions at ASCE Civil Engineering Conference*, Reston, 2001.

[31] CAGE, "Guideline for slab performance risk evaluation and residential basement floor system recommendations," Colorado Association of Geotechnical Engineers, Denver, 1996.

[32] R. Driscoll, "The influence of vegetation on the swelling and shrinking of clay soils in Britain," *Géotechnique,* vol. 33, no. 2, pp. 93-105, 1983.

[33] K. D. Walsh, C. A. Colby, W. N. Houston and S. L. Houston, "Method for evaluation of depth of wetting in residential areas," *Journal of Geotechnical and Geoenvironmental Engineering,* vol. 135, no. 2, pp. 169-176, 2009.

[34] ALA, "Guidelines for the design of buried steel pipe," American Lifeline Alliance, FEMA, Washington, DC, 2001.

[35] K. C. Chao, "Design principles for foundations on expansive soils," Colorado State University, Fort Collins, 2007.

[36] H. B. Seed, R. J. Woodward and R. Lundgren, "Prediction of swelling potential for compacted clay," *Journal of the Soil Mechanics and Foundations Division,* vol. 88, no. 3, pp. 53-87, 1962.

[37] B. V. Ranganathan and B. Satyanarayana, "A rational method of predicting swelling potential for compacted expansive clays," in *6th International Conference on Soil Mechanics and Foundation Engineering, International Society for Soil Mechanics and Geotechnical Engineering*, London, 1965.

[38] V. N. Vijayavergiya and O. I. Ghazzaly, "Prediction of swelling potential for natural clays," in *3rd International Conference on Expansive Soils*, Haifa, Israel, 1973.

[39] G. L. Schneider and A. R. Poor, "The prediction of soil heave and swell pressures developed by an expansive clay," Construction Research Center, University Of Texas, Austin, 1974.

[40] F. H. Chen, Foundations on Expansive Soils, Amsterdam: Elsevier Scientific Pub. Co., 1975.

[41] A. W. Dhowian, "Field performance of expansive shale formation," *Journal of King Abdulaziz University (Engineering Sciences),* vol. 2, pp. 165-182, 1990.

[42] D. G. Fredlund, "Prediction of ground movements in swelling clays," in *31st Annual Soil Mechanics and Found Engineering Conference*, Minneapolis, 1983.

[43] J. D. Nelson and D. J. Miller, Expansive soils: Problems and practice in foundation and pavement engineering, New York: John Wiley & Sons, Inc., 1992.

[44] D. J. Hamberg and J. D. Nelson, "Prediction of floor slab heave," in *5th International Conference on Expansive Soils*, Adelaide, 1984.

[45] USDA, "Web soil survey," USDA, 2018. [Online]. Available: https://websoilsurvey.nrcs.usda.gov/app/WebSoilSurvey.aspx. [Accessed 18 June 2018].

[46] R. Vaught, K. R. Brye and D. M. Miller, "Relationships among coefficient of linear extensibility and clay fractions in expansive, stoney soils," *Soil Science Society of America Journal,* vol. 70, no. 6, pp. 1983-1990, 2006.

[47] G. Kassiff and J. G. Zeitlin, "Behaviour of pipes buried in expansive clays," *Journal of Soil Mechanics and Foundation Division,* vol. 88, no. 2, pp. 132-148, 1962.

[48] S. Gould and J. K. Kodikara, "Exploratory statistical analysis of gas reticulation main failures," Monash University, Melbourne, 2009.

[49] D. C. C. Chan, "Study of pipe-soil-climate interaction of buried water and gas pipes," Monash University, Clayton, 2013.

[50] S. Gould, "A study of the failure of buried reticulation pipes in reactive soils," Monash University, Clayton, 2011.

[51] D. Chan, C. P. K. Gallage, P. Rajeev and J. Kodikara, "Field performance of in-service cast iron water reticulation pipe buried in reactive clay," *Canadian Geotechnical Journal,* vol. 52, no. 11, pp. 1861-1873, 2015.

[52] E. A. Sorochan and M. S. Kim, "Pressure exerted on stationary enclosing structures by expansive soil," *Soil Mechanics and Foundation Engineering,* vol. 31, pp. 52-56, 1994.

[53] F. T. McKenna, "Object-oriented finite element programming: Frameworks for analysis, algorithms and parallel computing," Ph.D. thesis, University of California, Berkeley, CA, 1997.

[54] P. Rajeev and J. Kodikara, "Numerical analysis of an experimental pipe buried in swelling soil," *Computers and Geotechnics,* vol. 38, no. 7, pp. 897-904, 2011.

[55] FLAC3D, "Fast Lagrangian Analysis of Continua in Three-Dimensions," Itasca Consulting Group, Inc, Minneapolis, 2019.

[56] D. R. Weerasinghe, J. Kodikara and H. Bui, "Impact of seasonal swell/shrink behavior of soil on buried water pipe failures," in *International Conference of Geotechnical Engineering*, Colombo, 2015.

[57] T. D. O'Rourke and C. H. Trautmann, "Analytical modeling of buried pipeline response to permanent earthquake displacements," National Science Foundation, Washington, 1980.

[58] M. J. O'Rourke, L. Xuejie and R. Flores-Berrones, "Steel pipe wrinkling due to longitudinal permanent ground deformation," *Journal of Transportation Engineering,* vol. 121, no. 5, pp. 443-451, 1995.

[59] D. K. Karamitros, G. D. Bouckovalas and G. P. Kouretzis, "Stress analysis of buried steel pipelines at strike-slip fault crossings," *Soil Dynamics and Earthquake Engineering,* vol. 27, no. 3, pp. 200-211, 2007.

[60] T. D. O'Rourke, J. K. Jung and A. C, "Underground pipeline response to earthquake-induced ground deformation," *Soil Dynamics and Earthquake Engineering,* vol. 91, pp. 271-283, 2016.

[61] Y. Wang, J. Shi and C. W. W. Ng, "Numerical modeling of tunneling effect on buried pipelines," *Canadian Geotechnical Journal,* vol. 48, no. 7, pp. 1125-1137, 2011.

[62] T. E. B. Vorster, A. Klar, K. Soga and R. J. Mair, "Estimating the effects of tunneling on existing pipelines," *Journal of Geotechnical and Geoenvironmental Engineering,* vol. 131, no. 11, pp. 1399-1410, 2005.

[63] P. Attewell, J. Yeates and A. Selby, Soil movements induced by tunnelling and their effects on pipelines and structures, Glasglow, U.K.: Blackie and Son Ltd, 1986.

[64] A. Klar, T. E. B. Vorster, K. Soga and R. J. Mair, "Soil-pipe interaction due to tunnelling: Comparison between winkler and elastic continuum solutions," *Geotechnique,* vol. 55, no. 6, pp. 461-466, 2005.

[65] A. M. Marshall, A. Klar and R. J. Mair, "Tunneling beneath buried pipes: view of soil strain and its effect on pipeline behavior," *Journal of Geotechnical and Geoenvironmental Engineering,* vol. 136, no. 12, pp. 1664-1172, 2010.

[66] Y. Wang, Q. Wang and K. Y. Zhang, "Tunneling effect on underground pipelines – a closed-form solution," in *Geotechnical Challenges in Megacities*, Moscow, Russia, 2010.

[67] M. J. O'Rourke and X. Liu, "Response of buried pipelines subject to earthquake effects," Multidisciplinary Center for Earthquake Engineering Research (MCEER), New York, 1999.

[68] N. M. Newmark and W. J. Hall, "Pipeline design to resist large fault displacemen," in *U.S. National Conference on Earthquake Engineering*, Ann Arbor, 1975.

[69] R. P. Kennedy, A. W. Chow and R. A. Williamson, "Fault movement effects on buried oil pipeline," *Journal of Transportation Engineering,* vol. 103, pp. 617-633, 1977.

[70] D. K. Karamitros, G. D. Bouckovalas, G. P. Kouretzis and V. Gkesouli, "An analytical method for strength verification of buried steel pipelines at normal fault crossings," *Soil Dynamics and Earthquake Engineering,* vol. 31, pp. 1452-1464, 2011.

[71] G. P. Kouretzis, D. K. Karamitros and S. S. W, "Analysis of buried pipelines subjected to ground surface settlement and heave," *Canadian Geotechnical Journal,* vol. 52, no. 8, pp. 1058-1071, 2015.

[72] M. Romanoff, Underground corrosion, Washington: U.S. Government Publishing Office, 1957.

[73] J. R. Rossum, "Prediction of pitting rates in ferrous metals from soil parameters," *Journal American Water Works Association,* vol. 61, no. 6, pp. 305-310, 1969.

[74] J. E. Singley, H. Sontheimer, A. Kuch, W. Kölle and A. Ahmadi, "Corrosion of Iron and Steel," in *Internal Corrosion of Water Distribution Systems*, Denver, CO, Water Research Foundation, 1985, pp. 33-125.

[75] M. Seica and J. Packer, "Mechanical properties and strength of aged cast iron water pipes," *Journal of Materials in Civil Engineering,* vol. 16, no. 1, pp. 69-77, 2004.

[76] I. S. Cole and D. Marney, "The science of pipe corrosion: A review of the literature on the corrosionof ferrous metals in soils," *Corrosion Science,* vol. 56, pp. 5-16, 2012.

[77] K. Atkinson, J. T. Whiter, P. A. Smith and M. Mulheron, "Failure of small diameter cast iron pipes," *Urban Water,* vol. 4, no. 3, pp. 263-271, 2002.

[78] M. Najafi and S. Gokhale, Trenchless technology, pipeline and utility design, construction, and renewal, New York: McGraw-Hill, 2005.

[79] F. M. Guess and F. Proschan, "Mean residual life: Theory and applications," in *Handbook of statistics 7: Quality control and reliability*, North Holland, Amsterdam, Elsevier Science, 1988, pp. 215-224.

[80] B. Rajani and Y. Kleiner, "Comprehensive review of structural deterioration of water mains: Physically based models," *Urban Water,* vol. 3, pp. 151-164, 2001.

[81] M. Ahammed and R. E. Melchers, "Probabilistic analysis of underground pipelines subject to combined stresses and corrosion," *Engineering Structures,* vol. 19, no. 12, pp. 988-994, 1997.

[82] B. Rajani and J. Makar, "A methodology to estimate remaining service life of grey cast iron water mains," *Canadian Journal of Civil Engineering,* vol. 27, no. 6, pp. 1259-1272, 2000.

[83] F. Caleyo, J. L. Gonzalez and J. M. Hallen, "A study on the reliability assessment methodology for pipelines with active corrosion defects," *International Journal of Pressure Vessels and Piping,* vol. 79, pp. 77-86, 2002.

[84] R. Sadiq, B. Rajani and Y. Kleiner, "Probabilistic risk analysis of corrosion associated failures in cast iron water mains," *Reliability Engineering and System Safety,* vol. 86, no. 1, pp. 1-10, 2004.

[85] C. Q. Li and M. Mahmoodian, "Risk based service life prediction of underground cast iron pipes subjected to corrosion," *Reliability Engineering and System Safety,* vol. 119, pp. 102-108, 2013.

[86] J. Ji, D. J. Robert, C. Zhang, D. Zhang and K. Kodikara, "Probabilistic physical modelling of corroded cast iron pipes for lifetime prediction," *Structural Safety,* vol. 64, pp. 62-75, 2017.

[87] A. Habibian, "Effect of temperature changes on water-main breaks," *Journal of Transportation Engineering,* vol. 120, no. 2, pp. 312-321, 1994.

[88] B. Rajani, C. Zhan and S. Kuraoka, "Pipe–soil interaction analysis of jointed water mains," *Canadian Geotechnical Journal,* vol. 33, pp. 393-404, 1996.

[89] S. A. Trickey and I. D. Moore, "Three-dimensional response of buried pipes under circular surface loading," *Journal of Geotechnical and Geoenvironmental Engineering,* vol. 133, no. 2, pp. 219-223, 2007.

[90] Z. Sun, X. Gong, J. Yu and J. Zhang, "Analysis of the displacement of buried pipelines caused by adjacent surcharge loads," in *International Conference on Pipelines and Trenchless Technology*, Reston, VA, 2013.

[91] S. A. Trickey, I. D. Moore and M. Balkaya, "Parametric study of frost-induced bending moments in buried cast iron water pipes," *Tunnelling and Underground Space Technology,* vol. 51, pp. 291-300, 2016.

[92] T. Mura, Micromechanics of defects in solids, Dordrecht, Netherlands: Martinus Nijhoff, 1987.

[93] D. C. Drucker and W. Prager, "Soil mechanics and plastic analysis or limit design," *Quarterly of Applied Mathematics,* vol. 10, no. 2, pp. 157-165, 1952.

[94] M. Smith, "ABAQUS/Standard user's manual, version 6.14-2," Simulia, Providence, RI, 2014.

[95] AWWA, "American standard specifications for cast iron pipe centrifugally cast in sand-lined molds, for water or other liquids," American Water Works Association, Denver, CO, 1953.

[96] AWWA, "1908 Cast-iron pipe specifications," *Journal American Water Works Association,* vol. 46, no. 7, pp. 701-712, 1954.

[97] H. T. Angus, Cast iron : Physical and engineering properties, London: Butterworth & Co, 1976.

[98] J. E. Bowles, Foundation analysis and design, Singapore: McGraw Hill, 1996.

[99] W. O. McCarron, "Limit analysis and finite element evaluation of lateral pipe–soil interaction resistance," *Canadian Geotechnical Journal,* vol. 53, no. 1, pp. 14-21, 2016.

[100] M. Hetényi, Beams on elastic foundation: Theory with applications in the fields of civil and mechanical engineering, Ann Arbor, MI: The University of Michigan Press, 1946.

[101] A. S. Vesic, "Beams on elastic subgrade and the Winkler's hypothesis," in *5th International Conference on Soil Mechanics and Foundation Engineering*, Paris, 1961.

[102] J. Yin, "Comparative modeling study of reinforced beam on elastic foundation," *Journal of Geotechnical and Geoenvironmental Engineering,* vol. 126, no. 3, pp. 265-271, 2000.

[103] S. M. Elachachi, D. Breysse and A. Denis, "The effects of soil spatial variability on the reliability of rigid buried pipes," *Computers and Geotechnics,* vol. 43, pp. 61-71, 2012.

[104] S. M. Elachachi, D. Breysse and L. Houy, "Longitudinal variability of soils and structural response of sewer networks," *Computers and Geotechnics,* vol. 31, pp. 625-641, 2004.

[105] S. C. Dutta and R. Roy, "A critical review on idealization and modeling for interaction among soil–foundation–structure system," *Computers and Structures,* vol. 80, pp. 1579-1594, 2002.

[106] ASCE, "Guidelines for the seismic design of oil and gas pipeline systems," ASCE TCLEE Committee on Gas and Liquid Fuel Lifelines, Reston, VA, 1984.

[107] A. P. S. Selvadurai, "Enhancement of the uplift capacity of buried pipelines by the use of Geogrids," *Geotechnical Testing Journal,* vol. 12, no. 3, pp. 211-216, 1989.

[108] S. Yimsiri, K. Soga, K. Yoshizaki, G. R. Dasari and T. D. O'Rourke, "Lateral and upward soil-pipeline interactions in sand for deep embedment conditions," *Journal of Geotechnical and Geoenvironmental Engineering,* vol. 130, no. 8, pp. 830-842, 2004.

[109] G. G. Meyerhof, "Influence of roughness of base and ground-water conditions on the ultimate bearing capacity of foundations," *Géotechnique,* vol. 5, no. 3, pp. 227-242, 1995.

[110] L. E. Dickson, Elementary theory of equations, New York: Wiley, 1914.

[111] MathWorks, "MATLAB user's manual (R2018a)," MathWorks, 2018. [Online]. Available: https://www.mathworks.com/help/matlab/. [Accessed 5 March 2018].

[112] P. Marcus, Corrosion mechanisms in theory and practice, Boca Raton, FL: CRC Press, 2011.

[113] V. Kucera and E. Mattsson, "Atmospheric corrosion," in *Corrosion Mechanisms*, New York, Marcel Dekker, 1987, pp. 211-284.

[114] W. Wang, C. Q. Li, D. Robert and A. Zhou, "Experimental investigation on corrosion effect on mechanical properties of buried cast iron pipes," *Journal of Materials in Civil Engineering,* vol. 30, no. 8, p. 04018197, 2018.

[115] G. Ugoh, R. Cunningham, J. Farrow, M. J. Mulheron and D. A. Jesson, "On the residual strength of ageing cast iron wastewater assets: Models for failure," *Materials Science & Engineering A,* vol. 768, p. 138221, 2019.

[116] W. Wang, W. Shi and C. Q. Li, "Time dependent reliability analysis for cast iron pipes subjected to pitting corrosion," *International Journal of Pressure Vessels and Piping,* vol. 175, p. 103935, 2019.

[117] T. L. Anderson, Fracture mechanics: Fundamentals and applications, Boca Raton, FL: CRC Press, 1995.

[118] I. S. Raju and J. C. Newman, "Stress intensity factors for circumferential surface cracks in pipes and rods under tension and bending loads," ASTM, West Conshohocken, PA, 1985.

[119] H. Cramer, Random variables and probability distributions, Cambridge: Cambridge University Press, 2004.

[120] G. B. Baecher and J. T. Christian, Reliability and Statistics in Geotechnical Engineering, West Sussex, England: John Wiley & Sons Ltd., 2003.

[121] M. Ahammed and R. E. Melchers, "Probabilistic analysis of pipelines subjected to pitting corrosion leaks," *Engineering Structures,* vol. 17, no. 2, pp. 74-80, 1995.

[122] R. K. Mazumder, A. M. Salman, Y. Li and X. Yu, "Performance evaluation of water distribution systems and asset management," *Journal of Infrastructure System,* vol. 24, no. 3, p. 03118001, 2018.

[123] G. S. Fishman, Monte Carlo: Concepts, algorithms, and applications, New York: Springer, 1995.

[124] D. M. Hamby, "A review of techniques for parameter sensitivity analysis of environmental models," *Environmental Monitoring & Assessment,* vol. 32, pp. 135-154, 1994.

[125] C. E. Ebeling, An introduction to reliability and maintainability engineering, Long Grove, Illinois: Waveland Press Inc., 2004.

[126] A. Desmond, "Stochastic models of failure in random environments," *The Canadian Journal of Statistics,* vol. 3, pp. 171-183, 1985.

[127] P. Thoft-Christensen and J. D. Sorensen, Structural reliability theory and its applications, Berlin, Heidelberg: Springer-Verlag, 1982.

[128] H. Minagata, K. YOSHIZAKI and Y. Hatsuda, "Risk assessment of gray cast iron pipelines," in *Pipeline Engineering and Construction International Conference*, Baltimore, Maryland, 2003.

[129] A. Goicochea, D. R. Hansen and L. Duckstein, Multi-objective decision analysis with engineering and business applications, New York: J. Wiley and Sons, 1982.

[130] K. Deb, A. Pratap, S. Agarwal and T. Meyarivan, "A fast and elitist multiobjective genetic algorithm: NSGA-II," *IEEE Transactions on Evolutionary Computation,* vol. 6, no. 2, pp. 182-197, 2002.

[131] G. C. Dandy and M. O. Engelhardt, "Multi-objective trade-offs between cost and reliability in the replacement of water mains," *Journal of Water Resources Planning and Management,* vol. 132, no. 2, pp. 79-88, 2006.

[132] R. K. Rowe and E. H. Davis, "The behaviour of anchor plates in sand," *Géotechnique,* vol. 32, no. 1, pp. 25-41, 1982.

[133] R. K. Rowe and E. H. Davis, "The behaviour of anchor plates in clay," *Géotechnique,* vol. 32, no. 1, pp. 9-23, 1982.

[134] C. H. Trautmann and T. D. O'Rourke, "Behavior of pipe in dry sand under lateral and uplift loading," Cornell University, Ithaca, New York, 1983.

[135] A. Ostfeld, "Reliability analysis of water distribution systems," *Journal of Hydroinformatics,* vol. 6, no. 4, pp. 281-294, 2004.

[136] A. Gheisi, M. Forsyth and G. Naser, "Water distribution systems reliability: A review of research literature," *Journal of Water Resources Planning and Management,* vol. 142, no. 11, p. 04016047, 2016.

[137] D. Halhal, G. A. Walters, D. Ouzar and D. A. Savic, "Water network rehabilitation with a structured messy genetic algorithm," *Journal of Water Resources Planning and Management,* vol. 123, no. 3, pp. 137-146, 1997.

[138] Z. Y. Wu and A. R. Simpson, "Optimal rehabilitation of waterdistribution system using a messy genetic algorithm," in *17th AWWA Fed. Convention, Australian Water and Wastewater Association*, Artarmon, NSW, Australia, 1997.

[139] W. de Schaetzen, M. J. Randall-Smith, D. Savic and G. A. Walters, "A genetic algorithm approach for rehabilitation in water supply systems," in *International Conference on Rehabilitation Technology for Water Industry*, 1998.

Appendices

Appendix A
NSGA-II Algorithm

The technique used in this study to identify the Pareto optimal front is the Non-dominated Sorting Genetic Algorithm II (NSGA-II) from Deb et al. [130]. Figure A.1 shows the algorithm flowchart of NSGA-II, and the steps are briefly described below.

1. First step is to generate an initial population. Each element of the population is called a chromosome and values of the design parameters, which are called genes, are embedded into it.
2. The objective functions are evaluated for the population, and they are ranked based on their dominance.
3. From the initial population, parent chromosomes are selected based on their crowding distance and rank (elitism).
4. New offsprings are produced from the parents using the crossover and mutation process. In the crossover process, two parents breed to produce offsprings by interchanging their genes. In the mutation procedure, some values of the genes in each offspring are changed, thus providing the offspring with different genes than their parents.

5. The previous steps are repeated until convergence is reached. In this study, the optimization algorithm is terminated after a fixed number of generations which is selected heuristically.

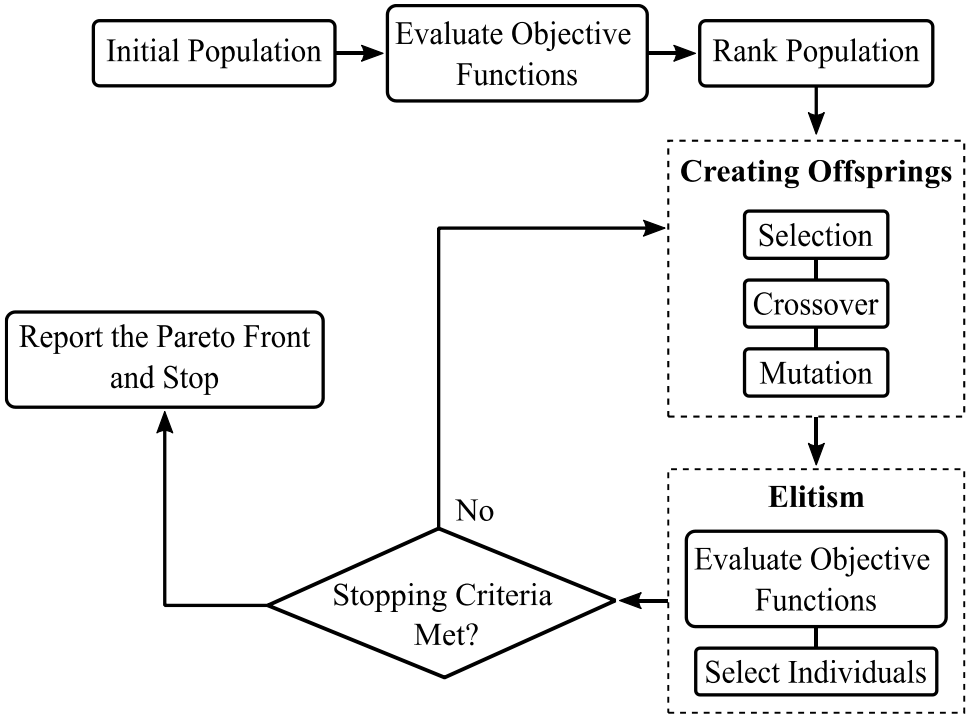

Figure A.1: General flowchart of NSGA-II.

Appendix B
Calculation of Soil Spring Factors

B.1 Vertical Uplift Soil Spring

For the uplift condition of the soil the yield strength q_{up} may be determined as

$$q_{up} = cN_{cv}D + \bar{\gamma}_s h N_{qv} D \tag{B.1}$$

where h is the depth of pipe below the ground surface; c is soil cohesion; and D is pipe outer diameter. N_{cv} and N_{qv} are uplift capacity factors, also known as the vertical uplift factor, that depend on the depth of pipe embedment and diameter. For a range of h/D, the values of these factors are experimentally obtained by Rowe and Davis [132, 133] which is also adopted by ASCE guidelines for the seismic design of oil and gas pipes [106]. The design charts are shown in Figure B.1. Since the design charts are developed using small-scale laboratory tests and theoretical models, their application is limited to relatively shallow burial depths $(h/D \leq 10)$. For higher h/D ratios, case-specific geotechnical guidance may be required.

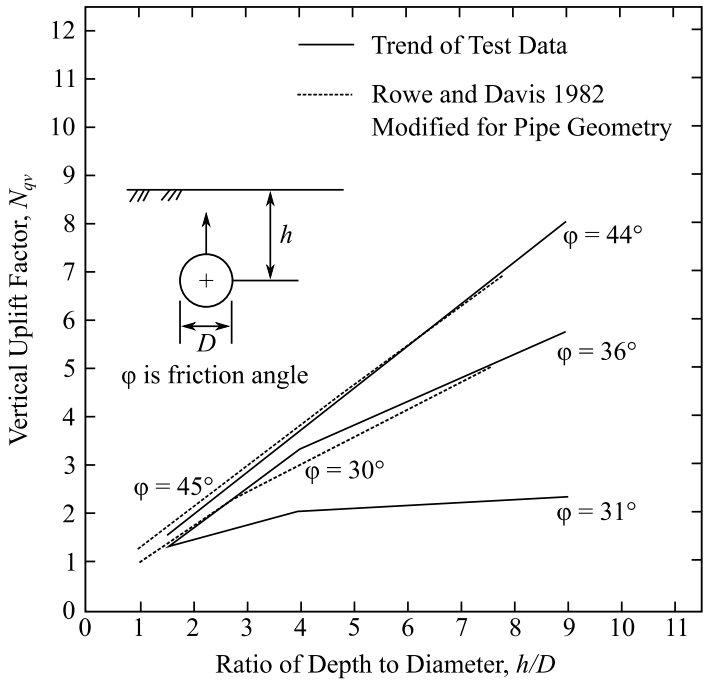

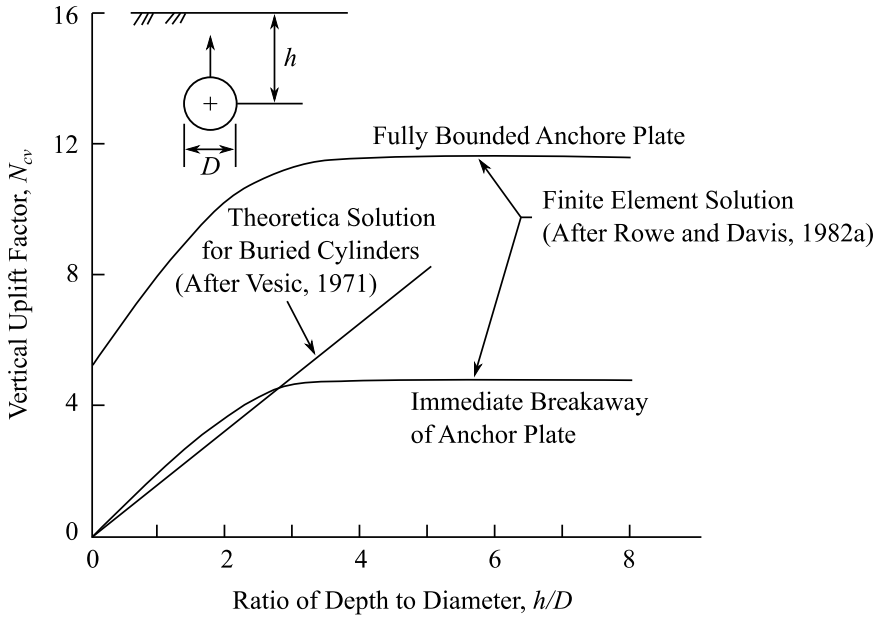

Figure B.1: Ranges for Values of N_{cv} and N_{qv} from Trautman and O'Rourke [134][3].

[3] R. K. Rowe and E. H. Davis, "The behaviour of anchor plates in sand," *Géotechnique*, vol. 32, no. 1, pp. 25-41, 1982.
R. K. Rowe and E. H. Davis, "The behaviour of anchor plates in clay," *Géotechnique*, vol. 32, no. 1, pp. 9-23, 1982a.

B.2 Vertical Bearing Soil Spring

As discussed in Chapter 4, the yield strength in bearing, q_{br}, may be calculated as follows:

$$q_{br} = cN_cD + \bar{\gamma}_s h N_q D + \frac{1}{2}\gamma_s D^2 N_\gamma \tag{B.2}$$

where h is depth of the lower end of the pipe below the ground surface; c is soil cohesion; and D is pipe outer diameter. γ_s and $\bar{\gamma}_s$ are total and effective soil unit weight, respectively. N_c, N_q, and N_γ are Meyerhof's bearing capacity factors for horizontal strip footing [109]. The Meyerhof's bearing capacity factors can be calculated from Eq. (B.3) to (B.5) or Figure B.2.

$$N_q = e^{\pi \tan\varphi} \tan^2\left(45 + \frac{\varphi}{2}\right) \tag{B.3}$$

$$N_c = \begin{cases} 5.14, & \varphi = 0 \\ (N_q - 1)\cot\varphi, & otherwise \end{cases} \tag{B.4}$$

$$N_\gamma = (N_q - 1)\tan(1.4\varphi) \tag{B.5}$$

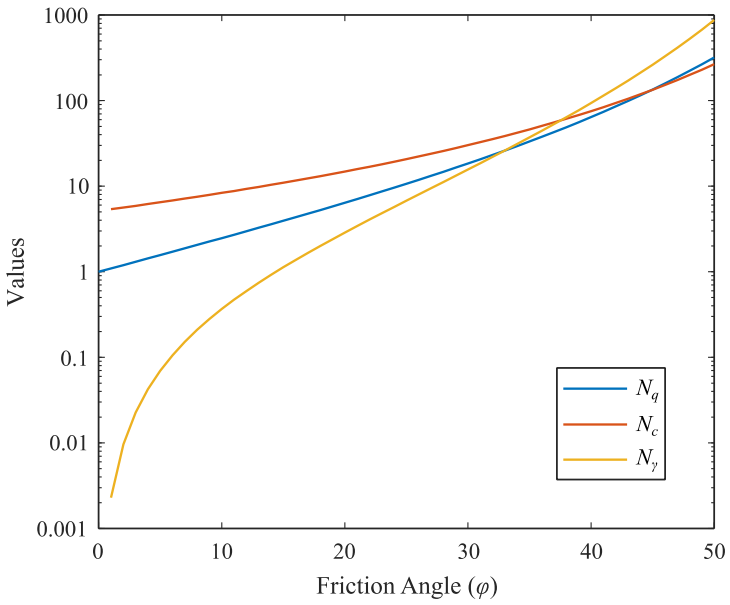

Figure B.2: Meyerhof bearing capacity factors

Appendix C
Analytical Model Formulation

The beam deformation profile within the transition zone, i.e., the segment ABC, (see Figure 4.7 of Chapter 4) can be obtained using the double integration method. However, this requires additional consideration because the response over the transition zone depends on the length of the pipe over which the soil has been yielded. Four types of responses are possible which are defined next along with the solution approach.

Case 1: soil yielding on both sides of the moist-dry boundary, surrounding the free bending zone.

$L_{free} > 0$

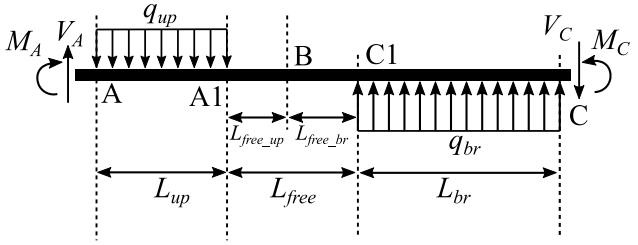

Figure C.1: Pipe segment ABC for load case 1 with a positive L_{free}

Force balance

$$V_A - V_C - q_{up}L_{up} + q_{br}L_{br} = 0 \tag{C.1}$$

Moment balance about point B

$$M_A - M_C + V_A\left(L_{up} + L_{free\_up}\right) + V_C\left(L_{br} + L_{free\_br}\right) - q_{up}L_{up}\left(L_{free\_up} + \frac{L_{up}}{2}\right) - q_{br}L_{br}\left(L_{free\_br} + \frac{L_{br}}{2}\right) = 0 \quad \text{(C.2)}$$

Writing the moment at any arbitrary point

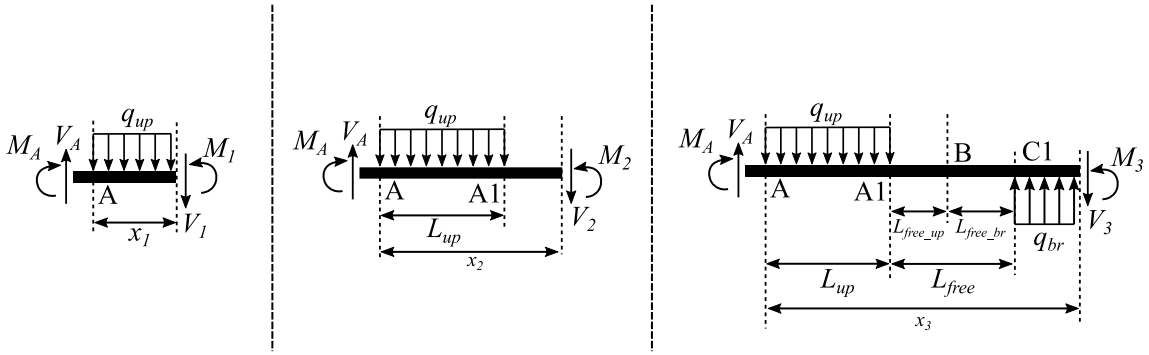

Figure C.2: Arbitrary section of the segment ABC for load case 1 with positive L_{free}

$$M_1 = M_A + V_A x_1 - \frac{q_{up}}{2} {x_1}^2$$

$$M_2 = M_A + V_A x_2 - q_{up}L_{up}\left(x_2 - \frac{L_{up}}{2}\right) \quad \text{(C.3)}$$

$$M_3 = M_A + V_A x_3 - q_{up}L_{up}\left(x_3 - \frac{L_{up}}{2}\right) + \frac{q_{br}}{2}\left(x_3 - L_{up} - L_{free}\right)^2$$

$L_{free} = 0$

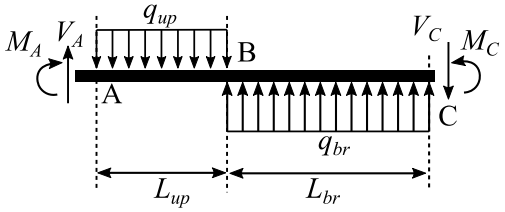

Figure C.3: Pipe segment ABC for load case 1 without L_{free}

Force balance

$$V_A - V_C - q_{up}L_{up} + q_{br}L_{br} = 0 \tag{C.4}$$

Moment balance about point B

$$M_A - M_C + V_A L_{up} + V_C L_{br} - \frac{q_{up}}{2}{L_{up}}^2 - \frac{q_{br}}{2}{L_{br}}^2 = 0 \tag{C.5}$$

Writing moment at any arbitrary point

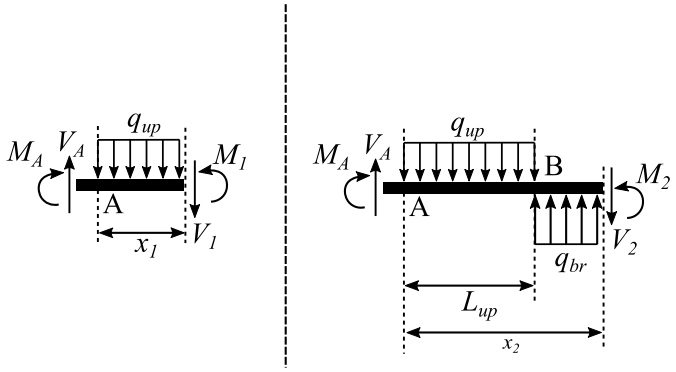

Figure C.4: Pipe segment ABC for load case 1 without L_{free}

$$\begin{aligned} M_1 &= M_A + V_A x_1 - \frac{q_{up}}{2}{x_1}^2 \\ M_2 &= M_A + V_A x_2 - q_{up}L_{up}\left(x_2 - \frac{L_{up}}{2}\right) + \frac{q_{br}}{2}\left(x_2 - L_{up}\right)^2 \end{aligned} \tag{C.6}$$

Case 2: soil yielding on both sides of the moist-dry boundary, surrounding the free bending zone.

$L_{free} > 0$

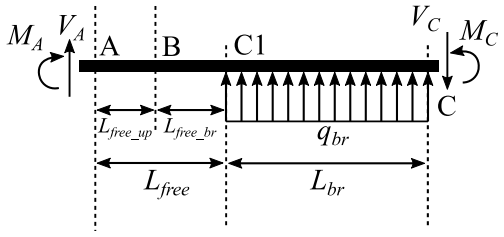

Figure C.5: Pipe segment ABC for load case 2 with a positive L_{free}

Force balance

$$V_A - V_C + q_{br}L_{br} = 0 \tag{C.7}$$

Moment balance about point B

$$M_A - M_C + V_A L_{free\_up} + V_C\left(L_{br} + L_{free\_br}\right) - q_{br}L_{br}\left(L_{free\_br} + \frac{L_{br}}{2}\right) = 0 \tag{C.8}$$

Writing moment at any arbitrary point

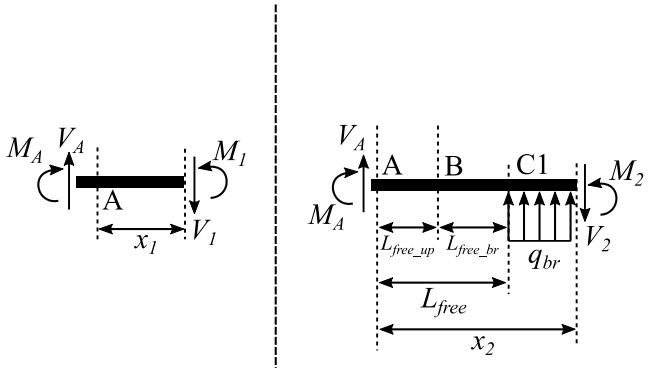

Figure C.6: Arbitrary sections of the segment ABC for load case 2 with positive L_{free}

$$M_1 = M_A + V_A x_1$$
$$M_2 = M_A + V_A x_2 + \frac{q_{br}}{2}\left(x_2 - L_{free}\right)^2 \tag{C.9}$$

$L_{free} = 0$

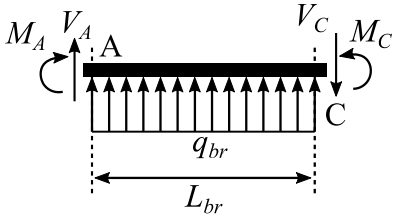

Figure C.7: Pipe segment ABC for load case 2 without L_{free}

Force balance

$$V_A - V_C + q_{br}L_{br} = 0 \tag{C.10}$$

Moment balance about point A

$$M_A - M_C + V_C L_{br} - \frac{q_{br}}{2}{L_{br}}^2 = 0 \tag{C.11}$$

Writing moment at any arbitrary point

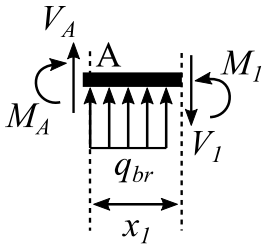

Figure C.8: Pipe segment ABC for load case 2 without L_{free}

$$M_1 = M_A + V_A x_1 + \frac{q_{br}}{2}{x_1}^2 \tag{C.12}$$

Case 3: soil yielding on both sides of the moist-dry boundary, surrounding the free bending zone.

$L_{free} > 0$

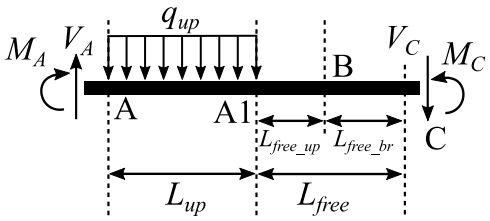

Figure C.9: Pipe segment ABC for load case 3 with a positive L_{free}

Force balance

$$V_A - V_C - q_{up}L_{up} = 0 \tag{C.13}$$

Moment balance about point B

$$M_A - M_C + V_A\left(L_{up} + L_{free\_up}\right) + V_C L_{free\_br} - q_{up} L_{up}\left(\frac{L_{up}}{2} + L_{free\_up}\right) = 0 \tag{C.14}$$

Writing moment at any arbitrary point

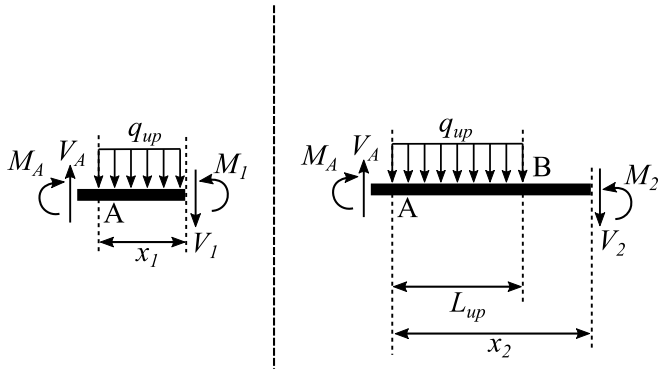

Figure C.10: Arbitrary sections of the segment ABC for load case 3 with positive L_{free}

$$M = M_A + V_A x - \frac{q_{up}}{2} x^2$$
$$M = M_A + V_A x - q_{up} L_{up}\left(x - \frac{L_{up}}{2}\right) \tag{C.15}$$

$L_{free} = 0$

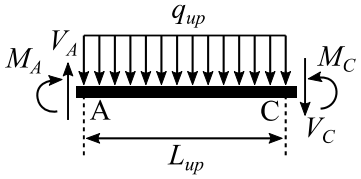

Figure C.11: Pipe segment ABC for load case 3 without L_{free}

Force balance

$$V_A - V_C - q_{up} L_{up} = 0 \tag{C.16}$$

Moment balance about point B

$$M_A - M_C + V_A L_{up} - \frac{q_{up}}{2} {L_{up}}^2 = 0 \tag{C.17}$$

Writing moment at any arbitrary point

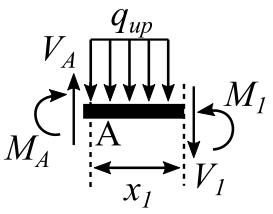

Figure C.12: Pipe segment ABC for load case 2 without L_{free}

$$M_1 = M_A + V_A x_1 - \frac{q_{up}}{2} {x_1}^2 \tag{C.18}$$

Case 4: soil yielding on both sides of the moist-dry boundary, surrounding the free bending zone.

$L_{free} > 0$

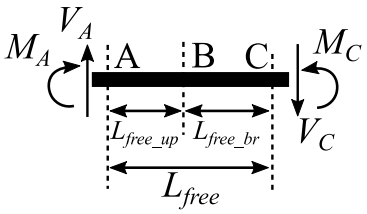

Figure C.13: Pipe segment ABC for load case 4 with a positive L_{free}

Force balance

$$V_A - V_C = 0 \tag{C.19}$$

Moment balance about point B

$$M_A - M_C + V_A L_{free\_up} + V_C L_{free\_br} = 0 \tag{C.20}$$

Writing moment at any arbitrary point

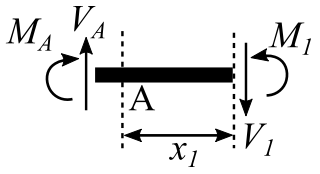

Figure C.14: Arbitrary sections of the segment ABC for load case 4 with positive L_{free}

$$M_1 = M_A + V_A x_1 \tag{C.21}$$

$L_{free} = 0$

This case represents elastic solution of beam on elastic foundation.

Appendix D
MATLAB Implementation Scripts

The following scripts are used to compute the pipe response. All these scripts are MATLAB custom functions whose role is outlined.

case1_upPbrP – analytic formulation when soil has been yielded in uplift as well as bearing

case2_upEbrP – analytic formulation when soil has been yielded in bearing only

case3_upPbrE – analytic formulation when soil has been yielded in uplift only

case4_upPbrP – analytic formulation when soil has not been yielded either in uplift or in bearing

dpit_AWWA – computes the corrosion pit depth as per AWWA corrosion model

dpit_pow – computes the corrosion pit depth as per power law corrosion model

raju_newman – computes the stress intensity factor for external crack in pipes

semi_inf_beam_def – computes the response of a semi-infinite beam on elastic foundation

soil_prop – computes the spring constants of soil in bearing and uplift

```
function [y_case1,x_range1,L_up,L_br,d_A,d_C,flag] =
case1_upPbrP(EI,d_up,q_up,d_br,q_br,dT,L_free_up,L_free_br)

%case1_brPupP - case1 of analytical formulation bearing-plastic-uplift-
plastic
%This function solves the analytic formulation of pipe-soil interaction
%
% Inputs:
%   EI - Modulus of rigidity (N-m2)
%   d_up - yieid displacement in uplift condition (m)
%   q_up - yield load in uplift condition (N/m)
%   d_br - yieid displacement in bearing condition (m)
%   q_br - yield load in bearing condition (N/m)
%   dT - total displacement at pipe level (m)
%   L_tr - length of load transition (m)
%
% Outputs:
%   y_case1 - deformation along length (m)
%   L_up - length of yield load in pulift (m)
%   L_br - length of yield load in bearing (m)
%   d_A - displacement at node A (m)
%   d_C - displacement at node C (m)
%   flag - fsolve exit flag
%
% See also:
% Author: Piyius Raj Singh
% PhD candidate
% University of Watrloo, CA
% email: prsingh@uwaterloo.ca
% Feb 2018; Last revision: 20-Feb-2019

%-------------------------- BEGIN CODE ------------------------------
% Variable defination
digits(6);
syms x M_Ar M_Cl V_Ar V_Cl
syms c1 c2 c3 c4 c5 c6 c7 c8
syms theta_Al theta_Cr L_up L_br

% numerical input values
L_free = L_free_up+L_free_br;
d_Al = d_up; % end deflection of pipe AA' at point A (at left side)
d_Cr = -d_br; % end deflection of pipe CC' at point C (at right side)
d_Ar = 0; % end deflection of pipe ABC at point A (at right side)
d_Cl = dT-abs(d_Al)-abs(d_Cr); % end deflection of pipe ABC at point C (at
left side)
k_up = q_up/d_up; % spring constant for soil uplift (N/m/m)
k_br = q_br/d_br; % spring constant for soil bearing (N/m/m)
Lbd_up = (0.25*k_up/EI)^0.25;
Lbd_br = (0.25*k_br/EI)^0.25;
```

```
% end moments and shear forces in semi-infinite beam on elastic foundation
M_Al = -2*Lbd_up*EI*(Lbd_up*d_Al+theta_Al);
V_Al = -2*Lbd_up^2*EI*(2*Lbd_up*d_Al+theta_Al);
M_Cr = -2*Lbd_br*EI*(Lbd_br*d_Cr+theta_Cr);
V_Cr = 2*Lbd_br^2*EI*(2*Lbd_br*d_Cr+theta_Cr);

% compatibility relations
M_Ar = M_Al;
V_Ar = V_Al;
M_Cl = M_Cr;
V_Cl = V_Cr;

% force balance and moment balance equation
eqF = V_Ar-V_Cl-q_up*L_up+q_br*L_br == 0;
eqM = M_Ar-M_Cl+V_Ar*(L_up+L_free_up)+V_Cl*(L_br+L_free_br)-q_up*L_up*...
    (L_free_up+L_up/2)-q_br*L_br*(L_free_br+L_br/2) == 0;

% solving for theta_Al and theta_Cr
eqns = [eqF, eqM];
vars = [theta_Al theta_Cr];
[Th] = solve(eqns, vars);
theta_Al(L_up,L_br) = simplify(Th.theta_Al);
theta_Cr(L_up,L_br) = simplify(Th.theta_Cr);

% redefining end moment and shear due to semi-infinite pipe sections
M_Al = -2*Lbd_up*EI*(Lbd_up*d_Al+theta_Al);
V_Al = -2*Lbd_up^2*EI*(2*Lbd_up*d_Al+theta_Al);

% calculating deflection
M_Ar = M_Al;
V_Ar = V_Al;
if L_free == 0
    M1(x,L_up,L_br) = M_Ar+V_Ar*x-q_up*x^2/2;  % from 0 to L_up
    M3(x,L_up,L_br) = M_Ar+V_Ar*x-q_up*L_up*(x-L_up/2)+q_br*(x-L_up)^2/2;
% from L_up to L

    y11 = int((int(M1, x)), x);
    y1(x) = (1/EI)*(y11 + c1*x + c2);
    theta1(x) = diff(y1, x);

    y33 = int((int(M3, x)), x);
    y3(x) = (1/EI)*(y33 + c3*x + c4);
    theta3(x) = diff(y3, x);

    eq1 = y1(0) == d_Ar;
    eq2 = y3(L_up+L_br) == d_Cl;
    eq3 = y1(L_up) == y3(L_up);
    eq4 = theta1(L_up) == theta3(L_up);

    eqns = [eq1, eq2, eq3, eq4];
    vars = [c1 c2 c3 c4];
    [c] = solve(eqns, vars);
    c11 = c.c1;
```

```
    c22 = c.c2;
    c33 = c.c3;
    c44 = c.c4;

    y1(x,L_up,L_br) = (1/EI)*(y11 + c11*x + c22);
    theta1(x,L_up,L_br) = diff(y1, x);

    y3(x,L_up,L_br) = (1/EI)*(y33 + c33*x + c44);
    theta3(x,L_up,L_br) = diff(y3, x);

else
    M1(x,L_up,L_br) = M_Ar+V_Ar*x-q_up*x^2/2;  % from 0 to L_up-l1
    M2(x,L_up,L_br) = M_Ar+V_Ar*x-q_up*L_up*(x-L_up/2);  % from L_up-l1 to
L_up
    M3(x,L_up,L_br) = M_Ar+V_Ar*x-q_up*L_up*(x-L_up/2)+q_br*(x-L_up-
L_free)^2/2;  % from L_up to L_up+l2

    y11 = int((int(M1, x)), x);
    y1(x) = (1/EI)*(y11 + c1*x + c2);
    theta1(x) = diff(y1, x);

    y22 = int((int(M2, x)), x);
    y2(x) = (1/EI)*(y22 + c3*x + c4);
    theta2(x) = diff(y2, x);

    y33 = int((int(M3, x)), x);
    y3(x) = (1/EI)*(y33 + c5*x + c6);
    theta3(x) = diff(y3, x);

    eq1 = y1(0) == d_Ar;
    eq2 = y3(L_up+L_free+L_br) == d_Cl;
    eq3 = y1(L_up) == y2(L_up);
    eq4 = y2(L_up+L_free) == y3(L_up+L_free);
    eq5 = theta1(L_up) == theta2(L_up);
    eq6 = theta2(L_up+L_free) == theta3(L_up+L_free);

    eqns = [eq1, eq2, eq3, eq4, eq5, eq6];
    vars = [c1 c2 c3 c4 c5 c6];
    [c] = solve(eqns, vars);
    c11 = c.c1;
    c22 = c.c2;
    c33 = c.c3;
    c44 = c.c4;
    c55 = c.c5;
    c66 = c.c6;

    y1(x,L_up,L_br) = (1/EI)*(y11 + c11*x + c22);
    y2(x,L_up,L_br) = (1/EI)*(y22 + c33*x + c44);
    y3(x,L_up,L_br) = (1/EI)*(y33 + c55*x + c66);
    theta1(x,L_up,L_br) = diff(y1, x);
    theta3(x,L_up,L_br) = diff(y3, x);
end
```

```
% solving for L_up and L_br
theta_Ar = theta1(0,L_up,L_br);
theta_Cl = theta3(L_up+L_free+L_br,L_up,L_br);
eq1 = simplify(theta_Ar+theta_Al);
eq2 = simplify(theta_Cr-theta_Cl);
eq11 = matlabFunction(eq1);
eq22 = matlabFunction(eq2);
eq = @(L_up,L_br) [eq11(L_up,L_br),eq22(L_up,L_br)];

% figure(15)
% fimplicit(eq1,[0 5 0 5],'-r')
% hold on
% fimplicit(eq2,[0 5 0 5],'-k')
% hold off

% for checking solution, vpasolve takes time but gives all the solution
% assume(L_up,'real')
% assume(L_up,'positive')
% assume(L_br,'real')
% assume(L_br,'positive')
% s = vpasolve([eq1 == 0,eq2 == 0],[L_up,L_br]);
% L_up = s.L_up
% L_br = s.L_br
% flag = 1;

z0 = [5,5];
[z,fval,exitflag,output] = fsolve(@(p) eq(p(1),p(2)),z0);
flag = exitflag;

L_up = z(1);
L_br = z(2);
L = L_up+L_free+L_br;
d_A = d_up;
d_C = d_br;
theta_A = theta1(0,L_up,L_br);
theta_C = theta3(L_up+L_free+L_br,L_up,L_br);
[y_AA,y_CC] =
semi_inf_beam_def(Lbd_up,Lbd_br,d_A,d_C,theta_A,theta_C,L,dT);

% solution for pipe deflection
if L_free == 0
    y1(x) = y1(x,L_up,L_br)+d_Al;
    y3(x) = y3(x,L_up,L_br)+d_Al;
    y_case1 = [y_AA y1 y3 y_CC];
    x_range1 = [-10 0 L_up L L+10];
else
    y1(x) = y1(x,L_up,L_br)+d_Al;
    y2(x) = y2(x,L_up,L_br)+d_Al;
    y3(x) = y3(x,L_up,L_br)+d_Al;
    y_case1 = [y_AA y1 y2 y3 y_CC];
    x_range1 = [-10 0 L_up L_up+L_free L L+10];
end
```

```
% figure(6)
% if L_free == 0
%     fplot(y_AA,[-10 0],'r')
%     hold on
%     fplot(y1,[0 L_up],'b')
%     fplot(y3,[L_up L],'k')
%     fplot(y_CC,[L L+10],'r')
%     hold off
% else
%     fplot(y_AA,[-10 0],'r')
%     hold on
%     fplot(y1,[0 L_up],'k')
%     fplot(y2,[L_up L_up+L_free],'r')
%     fplot(y3,[L_up+L_free L],'b')
%     fplot(y_CC,[L L+10],'k')
%     hold off
% end
end

%--------------------------- END CODE ----------------------------
```

```
function [y_case2,x_range2,L_up,L_br,d_A,d_C,flag] =
case2_upEbrP(EI,d_up,q_up,d_br,q_br,dT,L_free_up,L_free_br)
%case2_upEbrP - case1 of analytical formulation uplift-elastic-bearing-
plastic
%This function solves the analytic formulation of pipe-soil interaction
%
% Inputs:
%   EI - Modulus of rigidity (N-m2)
%   d_up - yieid displacement in uplift condition (m)
%   q_up - yield load in uplift condition (N/m)
%   d_br - yieid displacement in bearing condition (m)
%   q_br - yield load in bearing condition (N/m)
%   dT - total displacement at pipe level (m)
%   L_tr - length of load transition (m)
%
% Outputs:
%   y_case2 - deformation along length (m)
%   L_up - length of yield load in pulift (m)
%   L_br - length of yield load in bearing (m)
%   d_A - displacement at node A (m)
%   d_C - displacement at node C (m)
%   flag - fsolve exit flag
%
% See also:
% Author: Piyius Raj Singh
% PhD candidate
% University of Watrloo, CA
% email: prsingh@uwaterloo.ca
% Feb 2018; Last revision: 20-Feb-2019

%-------------------------- BEGIN CODE ----------------------------
```

```
% Variable defination
digits(6);
syms x M_Ar M_Cl V_Ar V_Cl
syms c1 c2 c3 c4 c5 c6 c7 c8
syms theta_Al theta_Cr L_br d_Al

% numerical input values
L_free = L_free_up+L_free_br;
d_Cr = -d_br; % end deflection of pipe CC' at point C (at right side)
d_Ar = 0; % end deflection of pipe ABC at point A (at right side)
d_Cl = dT-abs(d_Al)-abs(d_Cr); % end deflection of pipe ABC at point C (at
left side)
k_up = q_up/d_up; % spring constant for soil uplift (N/m/m)
k_br = q_br/d_br; % spring constant for soil bearing (N/m/m)
Lbd_up = (0.25*k_up/EI)^0.25;
Lbd_br = (0.25*k_br/EI)^0.25;

% end moments and shear forces in semi-infinite beam on elastic foundation
M_Al = -2*Lbd_up*EI*(Lbd_up*d_Al+theta_Al);
V_Al = -2*Lbd_up^2*EI*(2*Lbd_up*d_Al+theta_Al);
M_Cr = -2*Lbd_br*EI*(Lbd_br*d_Cr+theta_Cr);
V_Cr = 2*Lbd_br^2*EI*(2*Lbd_br*d_Cr+theta_Cr);

% compatibility relations
M_Ar = M_Al;
V_Ar = V_Al;
M_Cl = M_Cr;
V_Cl = V_Cr;

% force balance and moment balance equation
eqF = V_Ar-V_Cl+q_br*L_br == 0;
eqM = M_Ar-M_Cl+V_Ar*L_free_up+V_Cl*(L_br+L_free_br)-q_br*L_br*...
    (L_free_br+L_br/2) == 0;

% solving for theta_Al and theta_Cr
eqns = [eqF, eqM];
vars = [theta_Al theta_Cr];
[Th] = solve(eqns, vars);
theta_Al(d_Al,L_br) = simplify(Th.theta_Al);
theta_Cr(d_Al,L_br) = simplify(Th.theta_Cr);

% redefining end moment and shear due to semi-infinite pipe sections
M_Al = -2*Lbd_up*EI*(Lbd_up*d_Al+theta_Al);
V_Al = -2*Lbd_up^2*EI*(2*Lbd_up*d_Al+theta_Al);

% calculating deflection
M_Ar = M_Al;
V_Ar = V_Al;
if L_free == 0
    M3(x,d_Al,L_br) = M_Ar+V_Ar*x+q_br*x^2/2;  % from L_up+l2 to L

    y33 = int((int(M3, x)), x);
    y3(x) = (1/EI)*(y33 + c1*x + c2);
```

```
    eq1 = y3(0) == d_Ar;
    eq2 = y3(L_br) == d_Cl;

    eqns = [eq1, eq2];
    vars = [c1 c2];
    [c] = solve(eqns, vars);
    c11 = c.c1;
    c22 = c.c2;

    y3(x,d_Al,L_br) = (1/EI)*(y33 + c11*x + c22);
    theta1(x,d_Al,L_br) = diff(y3, x);
    theta3(x,d_Al,L_br) = diff(y3, x);

else
    M2(x,d_Al,L_br) = M_Ar+V_Ar*x;  % from L_up-l1 to L_up
    M3(x,d_Al,L_br) = M_Ar+V_Ar*x+q_br*(x-L_free)^2/2;  % from L_up-l1 to
L_up

    y22 = int((int(M2, x)), x);
    y2(x) = (1/EI)*(y22 + c1*x + c2);
    theta2(x) = diff(y2, x);

    y33 = int((int(M3, x)), x);
    y3(x) = (1/EI)*(y33 + c3*x + c4);
    theta3(x) = diff(y3, x);

    eq1 = y2(0) == d_Ar;
    eq2 = y3(L_free+L_br) == d_Cl;
    eq3 = y2(L_free) == y3(L_free);
    eq4 = theta2(L_free) == theta3(L_free);

    eqns = [eq1, eq2, eq3, eq4];
    vars = [c1 c2 c3 c4];
    [c] = solve(eqns, vars);
    c11 = c.c1;
    c22 = c.c2;
    c33 = c.c3;
    c44 = c.c4;

    y2(x,d_Al,L_br) = (1/EI)*(y22 + c11*x + c22);
    y3(x,d_Al,L_br) = (1/EI)*(y33 + c33*x + c44);
    theta1(x,d_Al,L_br) = diff(y2,x);
    theta3(x,d_Al,L_br) = diff(y3,x);
end

% solving for L_up and L_br
theta_Ar = theta1(0,d_Al,L_br);
theta_Cl = theta3(L_free+L_br,d_Al,L_br);
eq1 = simplify(theta_Ar+theta_Al);
eq2 = simplify(theta_Cr-theta_Cl);
eq11 = matlabFunction(eq1);
eq22 = matlabFunction(eq2);
```

```
eq = @(d_Al,L_br) [eq11(d_Al,L_br),eq22(d_Al,L_br)];

% figure(15)
% fimplicit(eq1,[0 .5 0 5],'-r')
% hold on
% fimplicit(eq2,[0 .5 0 5],'-k')
% hold off

% for checking solution, vpasolve takes time but gives all the solution
% assume(d_Al,'real')
% assume(d_Al,'positive')
% assume(L_br,'real')
% assume(L_br,'positive')
% s = vpasolve([eq1 == 0,eq2 == 0],[d_Al,L_br]);
% d_Al = s.d_Al
% L_br = s.L_br
% flag = 1;

z0 = [0.005,.05];
[z,fval,exitflag,output] = fsolve(@(p) eq(p(1),p(2)),z0);
flag = exitflag;

d_Al = z(1);
L_br = z(2);
L_up = 0;
L = L_up+L_free+L_br;
d_A = d_Al;
d_C = d_br;
theta_A = theta1(0,d_Al,L_br);
theta_C = theta3(L,d_Al,L_br);
[y_AA,y_CC] =
semi_inf_beam_def(Lbd_up,Lbd_br,d_A,d_C,theta_A,theta_C,L,dT);

% solution for pipe deflection
if L_free == 0
    y3(x) = y3(x,d_Al,L_br)+d_Al;
    y_case2 = [y_AA y3 y_CC];
    x_range2 = [-10 0 L L+10];
else
    y2(x) = y2(x,d_Al,L_br)+d_Al;
    y3(x) = y3(x,d_Al,L_br)+d_Al;
    y_case2 = [y_AA y2 y3 y_CC];
    x_range2 = [-10 0 L_free L L+10];
end

% figure(6)
% if L_free == 0
%     fplot(y_AA,[-10 0],'r')
%     hold on
%     fplot(y3,[0 L_br],'b')
%     fplot(y_CC,[L_br L_br+10],'r')
% %     hold off
% else
```

```
%     fplot(y_AA,[-10 0],'r')
%     hold on
%     fplot(y2,[0 L_free],'k')
%     fplot(y3,[L_free L],'r')
%     fplot(y_CC,[L L+10],'k')
% %     hold off
% end
end

%--------------------------- END CODE ----------------------------
```

```
function [y_case3,x_range3,L_up,L_br,d_A,d_C,flag] =
case3_upPbrE(EI,d_up,q_up,d_br,q_br,dT,L_free_up,L_free_br)
%case3_upPbrE - case1 of analytical formulation uplift-plastic-bearing-
elastic
%This function solves the analytic formulation of pipe-soil interaction
%
% Inputs:
%   EI - Modulus of rigidity (N-m2)
%   d_up - yieid displacement in uplift condition (m)
%   q_up - yield load in uplift condition (N/m)
%   d_br - yieid displacement in bearing condition (m)
%   q_br - yield load in bearing condition (N/m)
%   dT - total displacement at pipe level (m)
%   L_tr - length of load transition (m)
%
% Outputs:
%   y_case3 - deformation along length (m)
%   L_up - length of yield load in pulift (m)
%   L_br - length of yield load in bearing (m)
%   d_A - displacement at node A (m)
%   d_C - displacement at node C (m)
%   flag - fsolve exit flag
%
% See also:
% Author: Piyius Raj Singh
% PhD candidate
% University of Watrloo, CA
% email: prsingh@uwaterloo.ca
% Feb 2018; Last revision: 20-Feb-2019

%-------------------------- BEGIN CODE ----------------------------

% Variable defination
digits(6);
syms x M_Ar M_Cl V_Ar V_Cl
syms c1 c2 c3 c4 c5 c6 c7 c8
syms theta_Al theta_Cr L_up d_Cr

% numerical input values
L_free = L_free_up+L_free_br;
d_Al = d_up; % end deflection of pipe AA' at point A (at left side)
d_Ar = 0; % end deflection of pipe ABC at point A (at right side)
```

```
d_Cl = dT-abs(d_Al)-abs(d_Cr); % end deflection of pipe ABC at point C (at
left side)
k_up = q_up/d_up; % spring constant for soil uplift (N/m/m)
k_br = q_br/d_br; % spring constant for soil bearing (N/m/m)
Lbd_up = (0.25*k_up/EI)^0.25;
Lbd_br = (0.25*k_br/EI)^0.25;

% end moments and shear forces in semi-infinite beam on elastic foundation
M_Al = -2*Lbd_up*EI*(Lbd_up*d_Al+theta_Al);
V_Al = -2*Lbd_up^2*EI*(2*Lbd_up*d_Al+theta_Al);
M_Cr = -2*Lbd_br*EI*(Lbd_br*(-d_Cr)+theta_Cr);
V_Cr = 2*Lbd_br^2*EI*(2*Lbd_br*(-d_Cr)+theta_Cr);

% compatibility relations
M_Ar = M_Al;
V_Ar = V_Al;
M_Cl = M_Cr;
V_Cl = V_Cr;

% force balance and moment balance equation
eqF = V_Ar-V_Cl-q_up*L_up == 0;
eqM = M_Ar-M_Cl+V_Ar*(L_up+L_free_up)+V_Cl*L_free_br-q_up*L_up*...
    (L_free_up+L_up/2) == 0;

% solving for theta_Al and theta_Cr
eqns = [eqF, eqM];
vars = [theta_Al theta_Cr];
[Th] = solve(eqns, vars);
theta_Al(L_up,d_Cr) = simplify(Th.theta_Al);
theta_Cr(L_up,d_Cr) = simplify(Th.theta_Cr);

% redefining end moment and shear due to semi-infinite pipe sections
M_Al = -2*Lbd_up*EI*(Lbd_up*d_Al+theta_Al);
V_Al = -2*Lbd_up^2*EI*(2*Lbd_up*d_Al+theta_Al);

% calculating deflection
M_Ar = M_Al;
V_Ar = V_Al;
if L_free == 0
    M1(x,L_up,d_Cr) = M_Ar+V_Ar*x-q_up*x^2/2;  % from L_up+l2 to L

    y11 = int((int(M1, x)), x);
    y1(x) = (1/EI)*(y11 + c1*x + c2);
    theta1(x) = diff(y1, x);

    eq1 = y1(0) == d_Ar;
    eq2 = y1(L_up) == d_Cl;

    eqns = [eq1, eq2];
    vars = [c1 c2];
    [c] = solve(eqns, vars);
    c11 = c.c1;
    c22 = c.c2;
```

```
    y1(x,L_up,d_Cr) = (1/EI)*(y11 + c11*x + c22);
    theta1(x,L_up,d_Cr) = diff(y1, x);
    theta3(x,L_up,d_Cr) = diff(y1, x);

else
    M1(x,L_up,d_Cr) = M_Ar+V_Ar*x-q_up*x^2/2;  % from L_up-l1 to L_up
    M2(x,L_up,d_Cr) = M_Ar+V_Ar*x-q_up*L_up*(x-L_up/2);  % from L_up to
L_up+l2

    y11 = int((int(M1, x)), x);
    y1(x) = (1/EI)*(y11 + c1*x + c2);
    theta1(x) = diff(y1, x);

    y22 = int((int(M2, x)), x);
    y2(x) = (1/EI)*(y22 + c3*x + c4);
    theta2(x) = diff(y2, x);

    eq1 = y1(0) == d_Ar;
    eq2 = y2(L_up+L_free) == d_Cl;
    eq3 = y1(L_up) == y2(L_up);
    eq4 = theta2(L_up) == theta2(L_up);

    eqns = [eq1, eq2, eq3, eq4];
    vars = [c1 c2 c3 c4];
    [c] = solve(eqns, vars);
    c11 = c.c1;
    c22 = c.c2;
    c33 = c.c3;
    c44 = c.c4;

    y1(x,L_up,d_Cr) = (1/EI)*(y11 + c11*x + c22);
    y2(x,L_up,d_Cr) = (1/EI)*(y22 + c33*x + c44);
    theta1(x,L_up,d_Cr) = diff(y1, x);
    theta3(x,L_up,d_Cr) = diff(y2, x);
end

% solving for L_up and L_br
theta_Ar = theta1(0,L_up,d_Cr);
theta_Cl = theta3(L_up+L_free,L_up,d_Cr);
eq1 = simplify(theta_Ar+theta_Al);
eq2 = simplify(theta_Cr-theta_Cl);
eq11 = matlabFunction(eq1);
eq22 = matlabFunction(eq2);
eq = @(L_up,d_Cr) [eq11(L_up,d_Cr),eq22(L_up,d_Cr)];

% figure(14)
% fimplicit(eq11,[0 5 0 .5],'-r')
% hold on
% fimplicit(eq22,[0 5 0 .5],'-k')
% hold off

% for checking solution, vpasolve takes time but gives all the solution
```

```
% assume(d_Cr,'real')
% assume(d_Cr,'positive')
% assume(L_up,'real')
% assume(L_up,'positive')
% s = vpasolve([eq1 == 0,eq2 == 0],[L_up,d_Cr]);
% L_up = s.L_up
% d_Cr = s.d_Cr
% flag = 1;

z0 = [.05,0.005];
[z,fval,exitflag,output] = fsolve(@(p) eq(p(1),p(2)),z0);
flag = exitflag;

L_up = z(1);
d_Cr = z(2);
L_br = 0;
L = L_up+L_free+L_br;
d_A = d_up;
d_C = d_Cr;
theta_A = theta1(0,L_up,d_Cr);
theta_C = theta3(L,L_up,d_Cr);
[y_AA,y_CC] =
semi_inf_beam_def(Lbd_up,Lbd_br,d_A,d_C,theta_A,theta_C,L,dT);

% solution for pipe deflection
if L_free == 0
    y1(x) = y1(x,L_up,d_Cr)+d_Al;
    y_case3 = [y_AA y1 y_CC];
    x_range3 = [-10 0 L L+10];
else
    y1(x) = y1(x,L_up,d_Cr)+d_Al;
    y2(x) = y2(x,L_up,d_Cr)+d_Al;
    y_case3 = [y_AA y1 y2 y_CC];
    x_range3 = [-10 0 L_up L L+10];
end
% figure(6)
% if L_free == 0
%     fplot(y_AA,[-10 0],'r')
%     hold on
%     fplot(y1,[0 L],'b')
%     fplot(y_CC,[L L+10],'r')
% %     hold off
% else
%     fplot(y_AA,[-10 0],'r')
%     hold on
%     fplot(y1,[0 L_up],'k')
%     fplot(y2,[L_up L],'r')
%     fplot(y_CC,[L L+10],'k')
% %     hold off
% end
end

%--------------------------- END CODE ----------------------------
```

```
function [y_case4,x_range4,L_up,L_br,d_A,d_C,flag] =
case4_upEbrE(EI,d_up,q_up,d_br,q_br,dT,L_free_up,L_free_br)
%case4_upEbrE - case1 of analytical formulation uplift-elastic-bearing-
elastic
%This function solves the analytic formulation of pipe-soil interaction
%
% Inputs:
%   EI - Modulus of rigidity (N-m2)
%   d_up - yieid displacement in uplift condition (m)
%   q_up - yield load in uplift condition (N/m)
%   d_br - yieid displacement in bearing condition (m)
%   q_br - yield load in bearing condition (N/m)
%   dT - total displacement at pipe level (m)
%   L_tr - length of load transition (m)
%
% Outputs:
%   y_case4 - deformation along length (m)
%   L_up - length of yield load in pulift (m)
%   L_br - length of yield load in bearing (m)
%   d_A - displacement at node A (m)
%   d_C - displacement at node C (m)
%   flag - fsolve exit flag
%
% See also:
% Author: Piyius Raj Singh
% PhD candidate
% University of Watrloo, CA
% email: prsingh@uwaterloo.ca
% Feb 2018; Last revision: 20-Feb-2019

%-------------------------- BEGIN CODE ------------------------------

% Variable defination
digits(6);
syms x M_Ar M_Cl V_Ar V_Cl
syms c1 c2 c3 c4 c5 c6 c7 c8
syms theta_Al theta_Cr d_Cr d_Al

% numerical input values
L_free = L_free_up+L_free_br;
d_Ar = 0; % end deflection of pipe ABC at point A (at right side)
d_Cl = dT-abs(d_Al)-abs(d_Cr); % end deflection of pipe ABC at point C (at
left side)
k_up = q_up/d_up; % spring constant for soil uplift (N/m/m)
k_br = q_br/d_br; % spring constant for soil bearing (N/m/m)
Lbd_up = (0.25*k_up/EI)^0.25;
Lbd_br = (0.25*k_br/EI)^0.25;

% end moments and shear forces in semi-infinite beam on elastic foundation
M_Al = -2*Lbd_up*EI*(Lbd_up*d_Al+theta_Al);
```

```
V_Al = -2*Lbd_up^2*EI*(2*Lbd_up*d_Al+theta_Al);
M_Cr = -2*Lbd_br*EI*(Lbd_br*(-d_Cr)+theta_Cr);
V_Cr = 2*Lbd_br^2*EI*(2*Lbd_br*(-d_Cr)+theta_Cr);

% compatibility relations
M_Ar = M_Al;
V_Ar = V_Al;
M_Cl = M_Cr;
V_Cl = V_Cr;

% force balance and moment balance equation
eqF = V_Ar-V_Cl == 0;
eqM = M_Ar-M_Cl+V_Ar*L_free_up+V_Cl*L_free_br == 0;

% solving for theta_Al and theta_Cr
eqns = [eqF, eqM];
vars = [theta_Al theta_Cr];
[Th] = solve(eqns, vars);
theta_Al(d_Al,d_Cr) = simplify(Th.theta_Al);
theta_Cr(d_Al,d_Cr) = simplify(Th.theta_Cr);

% redefining end moment and shear due to semi-infinite pipe sections
M_Al = -2*Lbd_up*EI*(Lbd_up*d_Al+theta_Al);
V_Al = -2*Lbd_up^2*EI*(2*Lbd_up*d_Al+theta_Al);

% calculating deflection
M_Ar = M_Al;
V_Ar = V_Al;
if L_free == 0
    eq1 = simplify(theta_Al+theta_Cr);
    eq2 = simplify(d_Cl);
    eqn = [eq1, eq2];
    var = [d_Al d_Cr];
    [def] = solve(eqn, var);
    d_Al = def.d_Al;
    d_Cr = def.d_Cr;

%     figure(15)
%     fimplicit(eq1,[0 .5 0 .5],'-r')
%     hold on
%     fimplicit(eq2,[0 .5 0 .5],'-k')
%     hold off
else
    M1(x,d_Al,d_Cr) = M_Ar+V_Ar*x;  % from L_up to L_up+l2

    y11 = int((int(M1, x)), x);
    y1(x) = (1/EI)*(y11 + c1*x + c2);
    theta1(x) = diff(y1, x);

    eq1 = y1(0) == d_Ar;
    eq2 = y1(L_free) == d_Cl;

    eqns = [eq1, eq2];
```

```
    vars = [c1 c2];
    [c] = solve(eqns, vars);
    c11 = c.c1;
    c22 = c.c2;

    y1(x,d_Al,d_Cr) = (1/EI)*(y11 + c11*x + c22);
    theta1(x,d_Al,d_Cr) = diff(y1, x);
    theta3(x,d_Al,d_Cr) = diff(y1, x);

    % solving for L_up and L_br
    theta_Ar = theta1(0,d_Al,d_Cr);
    theta_Cl = theta3(L_free,d_Al,d_Cr);
    eq1 = simplify(theta_Ar+theta_Al);
    eq2 = simplify(theta_Cr-theta_Cl);

%     figure(15)
%     fimplicit(eq1,[0 .5 0 .5],'-r')
%     hold on
%     fimplicit(eq2,[0 .5 0 .5],'-k')
%     hold off

    eqn = [eq1, eq2];
    var = [d_Al d_Cr];
    [def] = solve(eqn, var);
    d_Al = def.d_Al;
    d_Cr = def.d_Cr;
end

d_A = double(d_Al);
d_C = double(d_Cr);
L_up = 0;
L_br = 0;
L = L_up+L_free+L_br;
theta_A = -theta_Al(d_Al,d_Cr);
theta_C = theta_Cr(d_Al,d_Cr);

[y_AA,y_CC] =
semi_inf_beam_def(Lbd_up,Lbd_br,d_A,d_C,theta_A,theta_C,L,dT);

% solution for pipe deflection
if L_free == 0
    y_case4 = [y_AA y_CC];
    x_range4 = [-10 0 10];
else
    y1(x) = y1(x,d_Al,d_Cr)+d_Al;
    y_case4 = [y_AA y1 y_CC];
    x_range4 = [-10 0 L L+10];
end
flag = 1;

% figure(6)
% if L_free == 0
%     fplot(y_AA,[-10 0],'r')
```

```
%     hold on
%     fplot(y_CC,[0 10],'r')
% %     hold off
% else
%     fplot(y_AA,[-10 0],'r')
%     hold on
%     fplot(y1,[0 L],'k')
%     fplot(y_CC,[L L+10],'k')
% %     hold off
% end
end

%---------------------------- END CODE ----------------------------
```

```
function d_pit_ndata = dpit_AWWA(age,t,n)

if age == 0
    d_pit_ndata = zeros(1,n);
    return
end
d_pit_mu = (0.0125*age+5.85*(1-exp(-0.058*age)))/1000;

% % COVs are calculated from AWWA corrosion data
if age >= 0 && age < 20
    d_pit_COV = 10;
elseif age >= 20 && age < 40
    d_pit_COV = 61.35141441;
elseif age >= 40 && age < 60
    d_pit_COV = 40.74398059;
elseif age >= 60 && age < 80
    d_pit_COV = 51.8342249;
elseif age >= 80 && age < 100
    d_pit_COV = 33.20680636;
elseif age >= 100 && age < 120
    d_pit_COV = 41.88911625;
else
    d_pit_COV = 41.88911625;
end

% d_pit_COV = 20;
d_pit_sig = d_pit_COV*d_pit_mu/100;
pd = makedist('Normal','mu',d_pit_mu,'sigma',d_pit_sig);

if length(t) == 1
    tpd = truncate(pd,0,t);
    d_pit_ndata = random(tpd,1,n);
    return
end

for i=1:n
    if t(i) == 0
        d_pit_ndata1 = zeros(1,10000);
    else
```

```
        tpd = truncate(pd,0,t(i));
        d_pit_ndata1 = random(tpd,1,10000);
    end
    ind = randi(n);
    d_pit_ndata(i) = d_pit_ndata1(ind);
end

% x = linspace(-.01,.02,1000);
% figure
% plot(x,pdf(pd,x))
% hold on
% plot(x,pdf(tpd,x),'LineStyle','--')
% histogram(d_pit_ndata,'Normalization','pdf')
% legend('Normal','Truncated','Truncated bar')
% hold off

end
```

```
function d_pit_ndata = dpit_pow(age,kk,nn,n)

if age == 0
    d_pit_ndata = zeros(1,n);
    return
end
d_pit_ndata = (kk.*age.^nn)/1000;

end
```

```
function SIF = raju_newman(thk,OD,a)

ID = OD-2*thk;
R = (1/2)*ID;

%ratios corresponding to the discrete solutions presented by Raju-Newman
rbyt = [1, 2, 4, 10];
abyt = [0.2, 0.5, 0.8];

%array containing discrete solutions; rows = r/t ratio, columns = a/t
ratio
F = [1.136, 1.162, 1.233;
     1.137, 1.188, 1.287;
     1.133, 1.204, 1.327;
     1.131, 1.212, 1.348];

% interpolation in r/t
rbyt_given = R./thk;
SIF_rbyt = interp1(rbyt,F,rbyt_given,'linear','extrap');

% interpolation in a/t
abyt_given = a./thk;
SIF_abyt = interp1(abyt,SIF_rbyt',abyt_given,'linear','extrap');

% extracting diagonal emelemts
```

```
SIF = (diag(SIF_abyt))';
end
```

```
function [y_AA,y_CC] =
semi_inf_beam_def(Lbd_up,Lbd_br,d_A,d_C,theta_A,theta_C,L,dT)

syms x
ALxAA(x) = exp(Lbd_up*x)*(cos(-Lbd_up*x)+sin(-Lbd_up*x));
BLxAA(x) = exp(Lbd_up*x)*sin(-Lbd_up*x);
y_AA(x) = d_A*ALxAA-theta_A*BLxAA/Lbd_up;

ALxCC(x) = exp(-Lbd_br*(x-L))*(cos(Lbd_br*(x-L))+sin(Lbd_br*(x-L)));
BLxCC(x) = exp(-Lbd_br*(x-L))*sin(Lbd_br*(x-L));
y_CC(x) = -d_C*ALxCC+theta_C*BLxCC/Lbd_br+dT;

end
```

```
function [d_uplift,q_uplift,d_bearing,q_bearing] =
soil_prop(h,d_out,c,phi,s_w)

%% Bearing condition
phi_r = deg2rad(phi);
Nq = (tan(deg2rad(45+phi/2))).^2.*exp(pi().*tan(phi_r));
Nc = (Nq-1).*cot(phi_r);
Ny = (Nq-1).*tan(1.4.*phi_r);
s_wsub = s_w-9.81; % submerg unit weight of soil
q_bearing = (Nc.*c.*d_out+Nq.*s_wsub.*h.*d_out+Ny.*s_w.*d_out.^2/2).*1000;
d_bearing = 0.125.*d_out;

%% Uplift condition (undrained condition)
% calculation of Nqv
hd31 = [1.5454036 4.1033297 9.05801];
Nqv31 = [1.3060464 2.0334957 2.2705045];
hd36 = [1.5664417 4.1416807 9.112489];
Nqv36 = [1.3152703 3.267367 5.5664773];
hd44 = [1.5688227 4.0994987 9.155496];
Nqv44 = [1.580675 3.6778355 7.7600737];
phi_all=[31, 36, 44];

hd = h./d_out;
Nqv_phi = [interp1(hd31,Nqv31,hd,'linear','extrap');...
           interp1(hd36,Nqv36,hd,'linear','extrap'); ...
           interp1(hd44,Nqv44,hd,'linear','extrap')];

Nqv1 = interp1(phi_all,Nqv_phi,phi,'linear','extrap');
Nqv = (diag(Nqv1))';
Nqv(Nqv < 0) = 0;

% calculation of Ncv
hd_iv = [0 0.44524476 1.0638145 1.6903391 2.0341692 2.223592 2.4663835 ...
    2.6910095 3.021809 3.432474 3.9133573 4.3232703 4.786364 5.231104 ...
    6.014599 6.7437844 7.464264 7.962373];
Ncv_iv = [0 0.88609236 2.1811411 3.385324 3.931787 4.1771083 4.420135 ...
```

```
    4.627733 4.776452 4.903632 4.9372687 4.992062 5.026464 5.0073404 ...
    5.04607 4.9966116 4.965632 4.944214];
hd_fb = [0 0.43179867 0.7623509 1.0369025 1.3019954 1.5576295 1.794722 ...
   2.0759125 2.31908 2.5620596 2.7953923 3.1627111 3.5465035 3.8137236 ...
   4.107816 4.5260596 4.9531984 5.816182 6.519436 7.365006 7.8896112];
Ncv_fb = [5.3034697 6.4448276 7.4263754 8.156864 8.8334465 9.4561205 ...
  10.007173 10.52012 10.799339 11.060463 11.249582 11.487254 11.597486 ...
  11.622205 11.663873 11.663994 11.663733 11.64473 11.668805 11.686761 ...
  11.646098];
Ncv =
(interp1(hd_iv,Ncv_iv,hd,'linear','extrap')+interp1(hd_fb,Ncv_fb,hd,'linea
r','extrap'))/2;
Ncv(Ncv < 0) = 0;

q_uplift = (c.*Ncv.*d_out+s_wsub.*h.*Nqv.*d_out).*1000;
d_uplift = ones(1,length(h))*0.005;
% d_uplift = min(0.15*h,0.2*d_out);

end
```

Appendix E
ABAQUS Implementation Scripts

The following script is used to simulate the pipe-soil interactions in ABAQUS. Note that the script provided here only contains material, interaction, and boundary conditions. Due to limited space, model description and discretization are not given.

```
** MATERIALS
**
*Material, name=CastIron
*Density
7850.,
*Elastic
 1.1e+11, 0.22
*Material, name=Soil
*Density
1900.,
*Drucker Prager
 36.2,1.,0.
*Drucker Prager Hardening, type=SHEAR
55000.,  0.
60000., 0.5
*Elastic
 1.329e+07, 0.4
*Expansion, type=ORTHO
0.,  0., 0.1
**
** INTERACTION PROPERTIES
**
*Surface Interaction, name=IntProp-1
1.,
*Friction, slip tolerance=0.005
 0.3,
*Surface Behavior, pressure-overclosure=HARD
```

```
**
** BOUNDARY CONDITIONS
**
** Name: BCxdir Type: Symmetry/Antisymmetry/Encastre
*Boundary
_PickedSet120, XSYMM
** Name: BCydir Type: Symmetry/Antisymmetry/Encastre
*Boundary
_PickedSet71, YSYMM
** Name: BCzdir Type: Symmetry/Antisymmetry/Encastre
*Boundary
_PickedSet72, ZSYMM
**
** PREDEFINED FIELDS
**
** Name: Predefined Field-1   Type: Temperature
*Initial Conditions, type=TEMPERATURE
_PickedSet83, 0.
**
** INTERACTIONS
**
** Interaction: Int-1
*Contact Pair, interaction=IntProp-1, type=SURFACE TO SURFACE
_PickedSurf85, _PickedSurf86
** ----------------------------------------------------------------
**
** STEP: Step-1
**
*Step, name=Step-1, nlgeom=YES, inc=1000000, unsymm=YES
*Static
0.001, 1., 1e-05, 1.
**
** LOADS
**
** Name: Load-1   Type: Gravity
*Dload
, GRAV, 9.81, 0., 0., -1.
**
** OUTPUT REQUESTS
**
*Restart, write, frequency=0
**
** FIELD OUTPUT: F-Output-1
**
*Output, field
*Node Output
CF, RF, U
*Element Output, directions=YES
LE, NFORC, PE, PEEQ, PEMAG, S
*Contact Output
CDISP, CFORCE, CNAREA, CSTATUS, CSTRESS
**
** HISTORY OUTPUT: H-Output-1
```

```
**
*Output, history, variable=PRESELECT
*End Step
** ----------------------------------------------------------------
**
** STEP: Step-2
**
*Step, name=Step-2, nlgeom=YES, inc=1000000, unsymm=YES
*Static
0.001, 1., 1e-05, 1.
**
** PREDEFINED FIELDS
**
** Name: Predefined Field-2   Type: Temperature
*Temperature
_PickedSet98, 1.
**
** OUTPUT REQUESTS
**
*Restart, write, frequency=0
**
** FIELD OUTPUT: F-Output-1
**
*Output, field, time interval=0.01
*Node Output
CF, RF, U
*Element Output, directions=YES
LE, NFORC, PE, PEEQ, PEMAG, S
*Contact Output
CDISP, CFORCE, CNAREA, CSTATUS, CSTRESS
**
** HISTORY OUTPUT: H-Output-1
**
*Output, history, variable=PRESELECT
*End Step
```